U.S. Department
of Transportation

**Federal Railroad
Administration**

Experimental 3-D Residual Stress Measurement in Rails with Thermal Annealing

Office of Research and
Development
Washington, D.C. 20590

Baishi Wang
Tieyu Zheng
Shiyi Wu
Fu-Peng Chiang

U.S. Department of Transportation
Research and Special Programs Administration
Volpe National Transportation Systems Center
Cambridge, MA 02142-1093

DOT/FRA/ORD-99/04
DOT-VNTSC-FRA-99-8

July 1999
Final Report

REPORT DOCUMENTATION PAGE

Form Approved
OMB No. 0704-0188

1. AGENCY USE ONLY (Leave blank)	2. REPORT DATE	3. REPORT TYPE & DATES COVERED
	July 1999	Final Report - January 1997

4. TITLE AND SUBTITLE
Experimental 3-D Residual Stress Measurement in Rails via Thermal Annealing

5. FUNDING NUMBERS
R-9052/RR-919

6. AUTHOR(S)
Baishi Wang*, Tieyu Zheng*, Shiyi Wu*, and Fu-Pen Chiang*

7. PERFORMING ORGANIZATION NAME(S) AND ADDRESS(ES)
Lab for Experimental Mechanics Research
Department of Mechanical Engineering
State University of New York at Stony Brook
Stony Brook, NY 11794-2300

8. PERFORMING ORGANIZATION REPORT NUMBER
DOT-VNTSC-FRA-99-8

9. SPONSORING/MONITORING AGENCY NAME(S) AND ADDRESS(ES)
U.S. Department of Transportation
Federal Railroad Administration
Office of Research and Development
Washington, D.C. 20590

10.SPONSORING OR MONITORING AGENCY REPORT NUMBER
DOT/FRA/ORD-99/04

11. SUPPLEMENTARY NOTES
*under contract to: U.S. Department of Transportation
Research and Special Programs Administration
John A. Volpe National Transportation Systems Center
Cambridge, MA 02142-1093

12a. DISTRIBUTION/AVAILABILITY
This document is available to the public through the National Technical Information Service, Springfield, VA 22161

12b. DISTRIBUTION CODE

13. ABSTRACT (Maximum 200 words)
This report describes a novel method to determine three-dimensional (3-D) residual stresses in railroad rails. The method uses Moire and Twyman/Green interferometry to measure the deformation of rail slices during a stress relief process which is accomplished by thermal annealing (heat treatment). The rail slices are approximately ¼ inch thick. Two slices from the same general location on a rail are used in this method. One splice is cut in the transverse plane and another in a 45° oblique plane. The 3-D residual stresses are then reconstructed from the deformation measurements by applying basic engineering assumptions and principles. In this report, the thermal annealing method was applied to five different rails to examine the effect of rail grinding on rail performance. Residual stress was used as a measure of performance because it is known to have a strong affect on the occurrence and growth of rail defects. One rail sample was naturally worn. A second rail sample had conformal grinding. Two rails were ground at periodic intervals for two-point contact up to a total accumulation of 178 million gross tons (MGT); one rail was ground at 12.5 MGT intervals and another every 25 MGT. The final rail sample was a brand new rail. Traffic accumulation and rail grinding were performed on the High Tonnage Loop at the Facility for Accelerated Service Testing (FAST) which is located at the Transportation Technology Center (TTC) in Pueblo, Colorado. The results from the residual stress reconstruction indicate that the horizontal tensile stress, which is the stress component most closely related to rail failures, was highest for the naturally worn rail. In the rails with two-point contact, the horizontal tensile stress was found be relatively small, although these rails also had the largest compressive stresses. The horizontal tensile stress component was found to be the smallest in the brand new rail.

14. SUBJECT TERMS
heat treatment, interferometry, rail grinding, residual stress, stress relief, thermal annealing

15. NUMBER OF PAGES
166

16. PRICE CODE

17. SECURITY CLASSIFICATION OF REPORT	18.SECURITY CLASSIFICATION OF THIS PAGE	19. SECURITY CLASSIFICATION OF ABSTRACT	20. LIMITATION OF ABSTRACT
Unclassified	Unclassified	Unclassified	

PREFACE

This report describes a novel method to determine residual stresses in railroad rails. The method uses thermal annealing to relieve the internal stresses in rail slices while advanced techniques (Moire and Twyman/Green interferometry) are applied to measure the deformations associated with the stress relief. Numerical engineering methods are then used to reconstruct the entire three-dimensional residual stress field from the deformation measurements. This method was applied to rail sections from five different grinding conditions. The rails were obtained from rail grinding experiments performed at the Transportation Technology Center.

The work described in this report was performed by the State University of New York at Stony Brook under contract to the John A. Volpe National Transportation Systems Center (Volpe Center). The Volpe Center is managing and conducting research to develop technical information which can be used to support rational criteria for safe operations on railroad tracks. This research is sponsored by the Track Research Division, Office of Research and Development, Federal Railroad Administration (FRA).

The support of the Department of Transportation is gratefully acknowledged. Beneficial information and suggestions from Dr. O. Orringer, Dr. D. Y. Jeong, and Mr. J. E. Gordon of DOT/Volpe National Transportation Systems Center and Dr. Roger Steele of the Association of American Railroads are greatly appreciated.

METRIC/ENGLISH CONVERSION FACTORS

ENGLISH TO METRIC	METRIC TO ENGLISH
LENGTH (APPROXIMATE)	**LENGTH (APPROXIMATE)**
1 inch (in) = 2.5 centimeters (cm)	1 millimeter (mm) = 0.04 inch (in)
1 foot (ft) = 30 centimeters (cm)	1 centimeter (cm) = 0.4 inch (in)
1 yard (yd) = 0.9 meter (m)	1 meter (m) = 3.3 feet (ft)
1 mile (mi) = 1.6 kilometers (km)	1 meter (m) = 1.1 yards (yd)
	1 kilometer (km) = 0.6 mile (mi)
AREA (APPROXIMATE)	**AREA (APPROXIMATE)**
1 square inch (sq in, in^2) = 6.5 square centimeters (cm^2)	1 square centimeter (cm^2) = 0.16 square inch (sq in, in^2)
1 square foot (sq ft, ft^2) = 0.09 square meter (m^2)	1 square meter (m^2) = 1.2 square yards (sq yd, yd^2)
1 square yard (sq yd, yd^2) = 0.8 square meter (m^2)	1 square kilometer (km^2) = 0.4 square mile (sq mi, mi^2)
1 square mile (sq mi, mi^2) = 2.6 square kilometers (km^2)	10,000 square meters (m^2) = 1 hectare (ha) = 2.5 acres
1 acre = 0.4 hectare (he) = 4,000 square meters (m^2)	
MASS - WEIGHT (APPROXIMATE)	**MASS - WEIGHT (APPROXIMATE)**
1 ounce (oz) = 28 grams (gm)	1 gram (gm) = 0.036 ounce (oz)
1 pound (lb) = 0.45 kilogram (kg)	1 kilogram (kg) = 2.2 pounds (lb)
1 short ton = 2,000 pounds (lb) = 0.9 tonne (t)	1 tonne (t) = 1,000 kilograms (kg) = 1.1 short tons
VOLUME (APPROXIMATE)	**VOLUME (APPROXIMATE)**
1 teaspoon (tsp) = 5 milliliters (ml)	1 milliliter (ml) = 0.03 fluid ounce (fl oz)
1 tablespoon (tbsp) = 15 milliliters (ml)	1 liter (l) = 2.1 pints (pt)
1 fluid ounce (fl oz) = 30 milliliters (ml)	1 liter (l) = 1.06 quarts (qt)
1 cup (c) = 0.24 liter (l)	1 liter (l) = 0.26 gallon (gal)
1 pint (pt) = 0.47 liter (l)	
1 quart (qt) = 0.96 liter (l)	
1 gallon (gal) = 3.8 liters (l)	
1 cubic foot (cu ft, ft^3) = 0.03 cubic meter (m^3)	1 cubic meter (m^3) = 36 cubic feet (cu ft, ft^3)
1 cubic yard (cu yd, yd^3) = 0.76 cubic meter (m^3)	1 cubic meter (m^3) = 1.3 cubic yards (cu yd, yd^3)
TEMPERATURE (EXACT)	**TEMPERATURE (EXACT)**
[(x-32)(5/9)] °F = y °C	[(9/5) y + 32] °C = x °F

QUICK INCH - CENTIMETER LENGTH CONVERSION

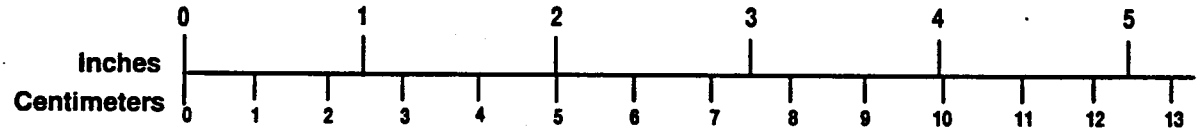

QUICK FAHRENHEIT - CELSIUS TEMPERATURE CONVERSION

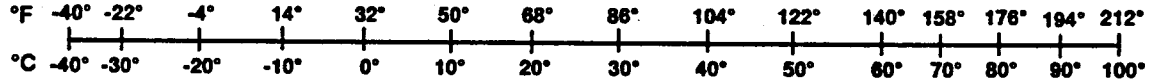

For more exact and or other conversion factors, see NIST Miscellaneous Publication 286, Units of Weights and Measures. Price $2.50 SD Catalog No. C13 10286

Updated 6/17/98

TABLE OF CONTENTS

LIST OF FIGURES

Figure **Page**

LIST OF FIGURES (cont.)

Figure **Page**

LIST OF FIGURES (cont.)

Figure **Page**

LIST OF TABLES

Table **Page**

EXECUTIVE SUMMARY

Residual stresses in railroad rail are known to have a significant effect on the formation and growth of internal rail defects. The development of residual stresses in rail, however, is difficult to determine as well as to control in service. The conventional method to determine residual (internal) stresses is destructive in nature. The rail is cut into slices and rods to relieve the internal stresses while the strains associated with the stress relief are measured using strain gages. The accuracy of this cutting or sectioning method depends on the size of the elements cut from the rail. Higher accuracy can be achieved by cutting smaller elements, but the machining costs increase if more cuts are made. Moreover, cutting may introduce additional stresses that may distort the actual residual distribution. An alternative method to relieve internal stresses, which is also destructive in nature, is to apply subcritical thermal annealing or heat treatment. The deformations associated with the stress relief are measured by two advanced measurement techniques known as Moiré and Twyman/Green interferometry.

Several railroads in North America have been conducting scheduled rail grinding programs to control wear and shelling on heavy haul freight lines. Generally speaking, grinding refers to methods of controlling and maintaining the shape of the rail head profile. On the whole, grinding programs appear to achieve their wear and fatigue objectives. However, each program appears to involve a unique combination of variables such as grinding frequency, depth of material removed, etc.

The work described in this report applies the thermal annealing method for determining residual stresses to rails obtained from rail grinding experiments conducted on the High Tonnage Loop at the Facility for Accelerated Service Testing, which is located at the Transportation Technology Center. Residual stresses in rails with different types of grinding are compared. The various grinding conditions included: a naturally worn rail (i.e., no grinding), conformal grinding, grinding for two-point contact, and a brand new rail. Conformal grinding is used to alter the rail head profile to broaden the wheel/rail contact area. Two-point contact is intended to alleviate gage corner loading of the rail by splitting the wheel/rail contact into two regions.

The results of this work show that the tensile component of residual stress most relevant to rail failures was highest for the naturally worn rail. This suggests that rail grinding is useful to control the occurrence and growth of internal rail defects.

1. Introduction

It is well known that residual stresses exist in rails because of rail manufacturing processes and periodic wheel contact load when the rails are in service. The determination of the residual stress field is essential for predicting the possible failure modes of rails, such as initiation and propagation of fatigue cracks.

Several techniques have been proposed to measure residual stresses in rails. The essence of the available methods is to section the rail into rudimentary stress-free elements and to measure the strain changes generated by the residual stress relaxation. The Battelle 3-D technique[1] is one of such destructive methods whereby the 3-D residual stress state in a rail is determined upon consecutive sectioning of the rail, first into longitudinal and transverse slices and then into stress-free dices and rods. The 3-D residual stresses are calculated from strains obtained by the strain gage method. An alternative approach[2] is to reconstruct the 3-D stress in a rail by an iterative approach from pointwise measurements made on vertical and oblique slices by assuming independence of the residual stress components on the axial direction of the rail. More recently, moiré interferometry[3, 4] has been employed to measure the whole field deformation and strain field after sectioning the rail slices into small grid elements. The destructive sectioning techniques give the average strain value at the center of the grid element. Since the measurement accuracy is determined by the size of the grid element, in principle, the more the grid elements, the higher the accuracy. However, this will be compromised by the increase in the cost of machining and the susceptibility to machining stress produced by the cutting process.

A novel, whole-field approach has been developed in this research to measure the 3-D residual stress in rails by moiré and Twyman/Green interferometry coupled with thermal annealing. Compared with the destructive sectioning method, the advantages of the new technique are three-fold. First, the residual stress relief is achieved by thermal annealing without further machining. As a result, the machining cost is much reduced and, more importantly, the possibility of machining-induced stress is completely circumvented. Second, it is believed that the results are more accurate. Instead of the average strains over the grid elements, the entire strain field is obtained without discontinuity created by cutting. The resolution is limited only by the precision

of moiré interferometry, which is of submicron level. Third, by combining the in-plane and out-of-plane displacement measurement, coupled with certain assumptions, it is possible to reconstruct the 3-D residual stresses in a rail by only using the transverse slice, based on certain plausible assumptions of the residual stress distribution. The experimental procedures are much simpler and the experimental results are more reliable.

To perform the residual stress measurement by thermal annealing, the fabrication of gratings that can sustain a high temperature is a prerequisite. In this research, a refractory of 1200 lines/mm cross-grating which can sustain a temperature of up to 1100°F has been successfully made on the surface of rail slices. After the thermal annealing process, the whole-field three-dimensional displacement components (u, v, and w) are obtained through the application of moiré and Twyman/Green interferometries. In this report, the principle of the experimental technique, procedures for the fabrication of the high-temperature grating, and data analysis are described. The mechanism of the residual stress relief by thermal annealing is also discussed. Results of the 3-D strain and stress fields of five different types of rails are presented. The five different rails are Number 1, control wear (CFI 136 RE25-0357); Number 2, conformal grinding (CFI 136 RE25-0881); Number 3, two-point contact (CFI 136 RE03-1605); Number 4, two-point contact (CFI 136 RE25-1042); and Number 5, new CFI. Here, Number 3 and Number 4 are both two-point contact with a total of 178 MGT heavy axle load, but Number 3 rail was ground every 12.5 MGT and Number 4 rail was ground every 25 MGT. These rail samples were provided by the sponsor of the work, the DOT/Volpe National Transportation Systems Center.

It should be noted that the original plan was to use the results from both a transverse slice and a 45° oblique slice to reconstruct the 3-D residual stress field via a tensorial transformation. Thus, both transverse and oblique slices were provided. However, the experimental results will show that after thermal annealing, the oblique slices experience severe global deformation (warping) indicating that the strains obtained from the fringes are not the strains they are supposed to represent and they cannot be used for the stress reconstruction. As a result, the one-slice approach is proposed. Although it involves a number of assumptions, we believe the basis for these assumptions is sound and the resulting stress data are more accurate.

2. EXPERIMENTAL TECHNIQUES AND PROCEDURES

The moiré and Twyman/Green interferometries are two advanced deformation measurement techniques based on wave-front interference. Moiré interferometry is used to measure the in-plane deformation (u, v) with a sensitivity of 0.417 μm/fringe for a 1200 lines/mm specimen grating, whereas the Twyman/Green interferometry is employed to obtain the out-of-plane deformation (w) with a sensitivity of 0.244 μm/fringe by using a 488 nm wavelength laser.

2.1 Moiré Interferometry

The set-up of the moiré interferometry is schematically shown in Figure 1, in which two symmetric, collimated incident waves (beams 1 and 2) are used. The interference of the two beams in the specimen plane generates a virtual grating with frequency f given by:

$$f = \frac{2\sin\alpha}{\lambda} \tag{1}$$

where α is the angle between the incident beam and the normal direction of the specimen surface, and λ is the wavelength of the laser beam. The specimen grating, with a frequency of 1200 lines/mm, one-half that of the virtual grating, is fabricated on the specimen surface beforehand. The superposition of the deformed specimen grating and the virtual grating yields moiré fringe patterns that represent the in-plane displacements u and (or) v fields in the direction perpendicular to the grating lines. The quantitative interpretation of the moiré fringes is given by the following equations:

$$u = \frac{N_x}{f}$$
$$v = \frac{N_y}{f} \tag{2}$$

where N_x and N_y are fringe orders (0, ±1, ±2, ...) of u-field moiré and v-field moiré, respectively, and f is the grating frequency. When both strains and rotations are small, the in-plane strains can be extracted from the displacement fields by the following equations:

$$\varepsilon_x = \frac{1}{f}\left(\frac{\partial N_x}{\partial x}\right)$$

$$\varepsilon_y = \frac{1}{f}\left(\frac{\partial N_y}{\partial y}\right) \qquad (3)$$

$$\varepsilon_{xy} = \frac{1}{2f}\left(\frac{\partial N_x}{\partial y} + \frac{\partial N_y}{\partial x}\right)$$

When a 1200 lines/mm specimen grating is used, two adjacent fringes represent a 0.417 μm difference in displacement.

2.2 Twyman/Green Interferometry

A schematic of the Twyman/Green interferometry is also shown in Figure 1, in which beam 3 is used while blocking out beams 1 and 2. It consists of a plane mirror and a flat specimen oriented perpendicular to each other and a beamsplitter bisecting the angle between the mirror and the specimen. A carefully adjusted plane incident wave is divided into two waves by the beamsplitter. The two beams travel separate paths -- one to the plane mirror and the other to the specimen. They are then recombined at the output of the interferometer. The beam from the mirror is the reference wave and the beam from the specimen is the object wave. The complex amplitude of the object and the reference waves in the recorded plane are $\mathbf{U}_1(x,y)$ and $\mathbf{U}_2(x,y)$, respectively, and they can be expressed as follows:

$$\mathbf{U}_1(x,y) = a(x,y) \cdot e^{-i\,\phi_1(x,y)}$$

$$\mathbf{U}_2(x,y) = a(x,y) \cdot e^{-i\,\phi_2(x,y)} \qquad (4)$$

The light intensity at the recorded plane is proportional to:

$$I(x,y) = |\,\mathbf{U}_1(x,y) + \mathbf{U}_2(x,y)\,|^2 \qquad (5)$$

When both the mirror and the specimen surfaces are optically flat, the initial phase difference between the two waves at the recorded plane can be adjusted to zero. Therefore, $\phi_1(x,y) = \phi_2(x,y) = \phi(x,y)$. When the specimen is deformed, a phase change, denoted by $\Delta\phi(x,y)$, is experienced by the object beam. The intensity at the recorded plane is then:

$$I(x,y) = | a(x,y)\cdot e^{-i\,\phi(x,y)} + a(x,y)\cdot e^{-i\,[\phi(x,y)+\Delta\phi(x,y)]} |^2$$

$$= 4a^2(x,y)\cos^2[\Delta\phi(x,y)/2] \qquad (6)$$

Thus, dark fringes are observed whenever $\Delta\phi(x,y) = 2k\pi$, whereas bright fringes are observed whenever $\Delta\phi(x,y) = (2k+1)\pi$, $k = 0, \pm1, \pm2 \ldots$. The phase change $\Delta\phi(x,y)$ can be related to the out-of-plane displacement w by the following equation when the wave is normally incident to the specimen:

$$\Delta\phi(x,y) = \frac{2\pi}{\lambda} 2w \qquad (7)$$

Hence, the out-of-plane displacement can be obtained from the following equation by simply counting the fringe order k at the given location:

$$w = \frac{k\lambda}{2} \qquad k = 0, \pm1, \pm2 \ldots \qquad (8)$$

For a thin slice specimen, if the out-of-plane deformation w is symmetric with respect to its mid-plane, the through thickness average strain ε_z can be obtained from the following equation:

$$\varepsilon_z = \frac{w}{t} \qquad (9)$$

where t is the half-thickness of the slice.

2.3 Fabrication of the High Temperature Resistant Grating and Heat Treatment

To fabricate the high-temperature resistant cross-grating, the surface of the rail slice is first carefully lapped to become optically flat with approximate $\lambda/2$ surface finish. Next, the specimen surface is coated with a thin layer of diluted photoresist. Uniformity of the coating thickness is achieved by spinning the slice at high speed. The thickness of the photoresist coating is approximately 0.1 μm. The photoresist is then exposed to two interfering beams in the moiré interferometry set-up with an argon laser operating at 488 nm wavelength as shown in Figure 1.

The angle between the two symmetrically collimated incident beams is 34° resulting in a 1200 lines/mm "virtual" grating. For a 500 mw argon laser, a typical exposure time is about 4 minutes. A cross-grating is produced by rotating the specimen through a 90° angle with a stepping motor after the initial exposure. Afterwards, the photoresist is properly developed and dried. A heat resistant, anti-oxidizing metal thin layer is then coated onto the photoresist grating. The coating is applied by vacuum evaporation and a typical coating thickness is about 0.1μm. The experiments show that a grating made in this way can sustain temperatures of up to 1100°F.

During the process of the stress relief by thermal annealing, the specimen with the coated grating is slowly heated to a temperature of 900°F and soaked for 20 hours (see Appendix for details) to allow sufficient relaxation of the residual stresses. It is then slowly cooled inside the oven to the ambient temperature. Finally, the specimen is repositioned in the moiré and Twyman/Green interferometry set-up as shown in Figure 1. Because of the deformation of the cross-grating due to the relaxation of the residual stresses, u and v moiré fringes are generated by the moiré interferometry. And because of the thickness change of the specimen due to the relief of the in-plane as well as the out-of-plane stresses, a w fringe pattern is created by the Twyman/Green interferometer.

3. THE MECHANISM OF THE RESIDUAL STRESS RELIEF BY THERMAL ANNEALING

Residual stresses in rails are caused in part by mechanical shakedown in cold-working. A large amount of internal strain energy is accumulated in the rail. To relieve the residual stress, subcritical annealing is employed whereby the mechanical shakedown and work-hardening will be removed through inelastic deformation known as creep relaxation.

Microstructurally, the generation and relaxation of the residual stress is quite complex. However, it is known that residual stress is associated with dislocations, including edge dislocation, screw dislocation and dislocation pile-up[5]. A strong internal stress field will be created by heavy cold-working because of the generation and accumulation of these dislocations. Sufficient activation energy is needed to make the dislocations move to relieve the residual stress. At the high temperature during the annealing process, the grain boundaries become glissile (atom conserving) so that grains can slide over one another, and a large enough thermal agitation also allows the dislocations to move. Therefore, the internal stress is relieved due to the elimination of the dislocations by climb and cross-slip resulting in an inelastic strain. It is this strain field that we measure and that is used to reconstruct the residual stress field.

4. 3-D RESIDUAL STRESS RECONSTRUCTION IN RAILS

To increase the lifetime of rail service, several alternative rail grinding programs for controlling the wear and shelling of heavy haul freight lines had been carried out and the results were compared with natural wear in tests of 300HB standard carbon rails on the High Tonnage Loop at the Transportation Technology Center (TTC). In some cases, a ground contour was established to relieve the gage corner from loading by splitting wheel/rail contact into two regions as schematically shown in Figure 2. Earlier theoretical work [6] and numerical analysis [7] have suggested that the change of the wheel running location caused by different grinding patterns might significantly change the residual stress distributions, possibly affecting fatigue life. The aim of the study is to provide some experimental evidence to the residual stress distributions in samples of the rails that were tested at the TTC.

In order to reconstruct the 3-D residual stresses in rails, the following assumptions are made:

- the residual stress components σ_x, σ_{xy}, σ_y, and σ_z are independent of the z axis; i. e., the axis along the longitudinal direction of the rail, and there are no out-of-plane shear stresses; i.e., $\sigma_{xz} = \sigma_{yz} = 0$;

- the rail material is isotropic and homogeneous;

- stress relief is attained via a purely elastic process and Hooke's law applies with the effective modulus and Poisson's ratio being that at the annealing temperature of the material;

- the interior residual stresses are not affected by the cutting and polishing of the slice.

As shown in Figure 3, a transverse slice with thickness of 1/4" was cut from the processed rail. The slice was lapped into a mirror-like surface. For the convenience of fabricating the grating, the rail head and base were cut along the web of the slice. Because the residual stress is very small in the web, the separation of the head and base from the web has negligible influence on

the residual stress state in the rail head and base. This fact was established in a previous study[8] (see Appendix).

It should be noted that the thickness change due to the relaxation of in-plane residual stresses only gives rise to part of resulting strain ε_z. The remaining part is due to the relief of out-of-plane normal stress σ_z. It is assumed that σ_z within the slice has a distribution shown in Figure 4; i.e., there is a thin layer at the boundary where σ_z drops to zero (to satisfy the free surface boundary condition) drastically. The magnitude of σ_z in the interior region remains essentially the same as that in the original rail. We had calculated the thickness change of the slice due to the relaxation of the in-plane strains and found that the value and distribution were completely different from what were actually measured. We were convinced that there existed a substantial amount of σ_z remaining in the slice. Hence, the proposed model of the stress distribution assumes that the remaining σ_z makes the dominant contribution to the thickness change of the slice after annealing. Based on these assumptions, the 3-D residual stresses in the rails can be reconstructed from a single transverse slice by the following equations, with E and ν being the Young's modulus and Poisson's ratio, respectively of the rail material at the annealing temperature:

$$\begin{aligned}
\sigma_x &= \frac{E(1-\nu)}{(1+\nu)(1-2\nu)}\left[\varepsilon_x + \frac{\nu}{1-\nu}(\varepsilon_y+\varepsilon_z)\right] \\
\sigma_y &= \frac{E(1-\nu)}{(1+\nu)(1-2\nu)}\left[\varepsilon_y + \frac{\nu}{1-\nu}(\varepsilon_x+\varepsilon_z)\right] \\
\sigma_{xy} &= \frac{E}{1+\nu}\varepsilon_{xy} \\
\sigma_z &= \frac{E(1-\nu)}{(1+\nu)(1-2\nu)}\left[\varepsilon_z + \frac{\nu}{1-\nu}(\varepsilon_x+\varepsilon_y)\right]
\end{aligned} \tag{10}$$

where ε_x , ε_{xy}, and ε_y are the in-plane strains obtained by moiré interferometry, and ε_z is the average through thickness out-of-plane strain deduced via Twyman/Green interferometry.

In the experiments for measuring 3-D deformation, the proper repositioning of the specimen and the determination of the fringe signs are crucial for the accurate calculation of the strains. The guide for the proper repositioning of the slice is through the realization that the residual stress in

the web area is negligible compared to that in the crown area. In ordering the fringes, the zeroth order fringe is at the bottom of the slice, i.e., the web area. The sign of the fringes in the slice is determined by the carrier (or mismatch) fringe technique. In moiré interferometry, a pattern of carrier fringes is introduced by changing the virtual grating pitch. If the number of moiré fringes increases with the increase of the virtual grating pitch, the fringe order is negative. Conversely, if the number of moiré fringes decreases, the fringe order is positive. In the Twyman/Green interferometry, in a similar way, the fringe sign is determined by introducing a fictitious phase change. Because of the known zero stress state in the web, the possible surface tilting error can be eliminated by minimizing the fringes in the web area.

For rail #3, two-point contact (CFI 136 RE 03-1605), the in-plane u and v deformation fringe patterns of the rail head by moiré interferometry are shown in Figures 5 and 6. The w fringe pattern of the rail head by Twyman/Green interferometry is shown in Figure 7. The in-plane strains and the average out-of-plane strain were computed using equation (3) after digitizing the fringes. The strain contours ε_x, ε_y, ε_{xy}, and ε_z of the rail head are shown in Figures 8, 9, 10, and 11, respectively. The corresponding residual stresses were calculated using equation (10). In the calculations, Young's modulus and Poisson's ratio at the annealing temperature (E=172GPa, ν=0.32, kindly provided by Mr. Jeff Gordon of DOT/Volpe Center) were used. The contours of the residual stresses in the rail head are shown in Figures 12, 13, 14, 15, and 16, respectively, together with the contours of Von Mises effective stress σ_e defined by the following equation.

$$\sigma_e = \sqrt{\frac{1}{2}[(\sigma_x-\sigma_y)^2+(\sigma_y-\sigma_z)^2+(\sigma_x-\sigma_z)^2]+3[(\sigma_{xy})^2+(\sigma_{yz})^2+(\sigma_{xz})^2]}$$

The same approach was used for the reconstruction of the 3-D residual stresses of the other four rails. The results for rail #1 are shown in Figures 17-28. Figures 17-19 are the fringe patterns for u, v, and w displacement components. Figures 20-23 are strain contours of ε_x, ε_y, ε_z, and ε_{xy}, respectively. Figures 24-28 are the reconstructed stress contours of σ_x, σ_y, σ_z, σ_{xy}, and σ_e, respectively. The results of rail #2 are shown in Figures 29-47. Because of the relatively poor quality of the fringe patterns, they are not shown. Instead, the digitized contours of displacement components u, v, and w are depicted in Figures 29-31. The strain contours of ε_x, ε_y, ε_z and ε_{xy} are

shown in Figures 32-35 and the stress contours of σ_x, σ_y, σ_z, σ_{xy}, and σ_e are shown in Figures 36-40, respectively. For rail #2, the results for a 45° oblique slice were also obtained. The digitized displacement contours of u, v, and w are shown, respectively, in Figures 41-43. Figures 44-47 depict the strain contours of $\varepsilon_{x'}$, $\varepsilon_{y'}$, $\varepsilon_{z,}$ and $\varepsilon_{xy'}$, respectively. From the contour plot of w in Figure 43 and ε_z plot in Figure 46, it is very clear that the slice had experienced a large warpage (roughly along the vertical axis) after annealing. We believe this is due to the fact that $\sigma_{x'z'}$ and $\sigma_{y'z'}$ (where x'-y'-z' is the rotated coordinate system of the oblique slice) is not negligible and inherently asymmetric. As a result, the calculated ε_z is not reliable at all. Without $\varepsilon_{z,}$ the corresponding 3-D stress components cannot be reconstructed.

The displacement fringe patterns of u, v, and w of a transverse slice of rail #4 after stress relief are shown in Figures 48, 49, and 50, respectively. The strain contours of ε_x, ε_y, $\varepsilon_{z,}$ and ε_{xy} are given in Figures 51-54 and the corresponding stress plots are depicted in Figures 55-59. The strain contours of $\varepsilon_{x'}$, $\varepsilon_{y'}$, $\varepsilon_{z,}$ and $\varepsilon_{x'y'}$ of a 45° oblique slice of rail #4 are shown in Figures 60-63. From the pattern of $\varepsilon_{z'}$ contours depicted in Figure 62, it is also evident that a warpage along roughly the vertical axis was experienced by the slice after annealing. Hence the corresponding stress values were not calculated.

The u, v, and w fringe patterns of an oblique slice of rail #5 are depicted in Figures 64-66, respectively. The strain contour plots of $\varepsilon_{x'}$, $\varepsilon_{y'}$, $\varepsilon_{z'}$ and $\varepsilon_{x'y'}$ are shown in Figures 67-70, respectively. This is a new rail without too many residual stresses (or strains). The resulting slice warpage is relatively small as evidenced by the pattern shown in Figure 66. We felt that the effect on stress calculation is probably modest. Hence, the 3-D stress fields were reconstructed and plotted as shown in Figures 71-74 for stresses of $\sigma_{x'}$, $\sigma_{y'}$, $\sigma_{z'}$ and $\sigma_{x'y'}$, respectively. This is offered as a mean for relative and qualitative comparison with the rest of the rail slices. (Note: the transverse slice of rail #5 and oblique slice of rail #3 were rendered useless by the fact that the gratings were severely damaged after the annealing.)

5. RESULTS AND DISCUSSIONS

The 3-D residual stress measurement results for rail #3 two-point contact (CFI 136 RE 03-1605) show that the largest residual stresses are confined within the rail crown contact zone. The maximum absolute magnitudes of all normal stress components σ_x, σ_y, and σ_z are of the same order of magnitude. The maximum Von-Mises effective stress is the same as the yield stress of the rail material (400 MPa). The shear stress value is relatively small (less than 40 MPa) compared with that of the normal stress components. Therefore, the normal residual stresses are dominant in this rail. It might be inferred from this fact that the magnitude of out-of-plane shear stresses is also in the same range as that of the in-plane ones (we have assumed them to be zero at the outset). The influence of the flange contact zone on the local residual stress is shown in Figures 7 and 14 and its effect is confined to the local areas. The residual stress in the base is small compared with that in the head. Its magnitude is less than 100 MPa[6].

The magnitudes of the maximum/minimum normal, shear and effective stresses of different rail slices are listed in Table 1, and the corresponding values of the strain components are listed in Table 2.

Table 1: Comparisons of the Maximum/Minimum Stresses and Effective Residual Stress σ_E in Different Rail Slices

	#1 control wear	#2 conformal ground	#3 two-point contact (1)	#4 two-point contact (2)	#5 new rail (45° slice)
σ_x (MPa)	310/10	250/10	230/0	90/10	35/-80 ($\sigma_{x'}$)
σ_y (MPa)	110/-110	45/-260	50/-300	-10/-500	60/-160 ($\sigma_{y'}$)
σ_z (MPa)	170/-160	-30/-187	-20/-200	-20/-320	145/-200 ($\sigma_{z'}$)
σ_{xy} (MPa)	6/-1	110/-120	40/5	10/-70	5/-10 ($\sigma_{x'y'}$)
σ_e (MPa)	370/20	400/20	400/40	500/20	150/10

Table 2: Comparisons of the Maximum/Minimum Strains in Different Rail Slices

	#1 control wear	#2 conformal ground	#3 two-point contact (1)	#4 two-point contact (2)	#5 new rail (45° slice)
ε_x (10^{-3})	0/-2.0	0.0/-1.8	0.1/-2.0	0.2/-2.0	0.1/-0.2 ($\varepsilon_{x'}$)
ε_y (10^{-3})	1.0/-0.4	1.8/-0.2	1.5/-0.2	3.0/0.0	0.2/0.0 ($\varepsilon_{y'}$)
ε_z (10^{-3})	1.0/-0.7	1.0/0.1	1.4/0.0	1.6/0.0	1.1/-1.0 ($\varepsilon_{z'}$)
ε_{xy} (10^{-3})	0.0/0.0	1.3/-1.0	0.5/-0.7	0.6/-0.3	0.1/-0.1 ($\varepsilon_{x'y'}$)

It is seen from the comparison that in a control wear grinding scheme, the horizontal tensile stress, which is probably the main cause of the rail breakage, is the largest. In two-point contact (2) grinding, the horizontal tensile stress is small, however, the value of the compressive stress is the largest. The maximum magnitudes of Von-Mises effective stresses are fairly close for control wear, conformal ground, and two-point contact (1) rails. For the two-point contact (2), the maximum value of the Von-Mises effective stress is somewhat higher. For the new rail, it is seen that all the stress components are small in comparison with other (used) rails, except the longitudinal normal stress, $\sigma_{z'}$. This is what one would expect because the only cause for the existence of the residual stress is due to the cold-working process during rail manufacturing. The same conclusion could be drawn from the strain data as well, where $\varepsilon_{z'}$ is one order of magnitude higher than other components.

6. CONCLUSIONS

In this series of experiments, we have tried to measure the residual stresses in five sets of rail slices. We believe the results obtained are fairly close to the true residual stresses. Much more work is needed to verify some of the assumptions made and establish the thermal annealing test as a standard test whereby residual stress can be obtained routinely.

First, we have developed a technique whereby we can manufacture a fine (1200 lines/mm) moiré grating in a rail specimen which can sustain a high temperature up to 1100°F. With this capability we are able to thermal-anneal the rail slices (at 900°F for 20 hours) to relieve the locked-in residual stresses. This is a major advance over the grid-cutting approach previously employed by the principal investigator (Dr. F. P. Chiang) as well as others. Cutting a rail slice into grid elements not only is a time-consuming and labor-intensive process, it is also a process whose effect on residual stress distribution (or redistribution) is unknown. It was thought that cutting might only affect the moiré fringes at the edge of the grid element (similar to the boundary layer effect of a photoelasticity slice, for example). We find this is not the case in many situations. The evidence is the fact that, in a typical moiré fringe pattern produced by the grid-cutting method, the local fringes within a grid element can be drastically different from that of an adjacent element. So much so that they would not follow smooth curves if they were connected through the cut grooves. It is believed that since steel is a highly efficient heat-conducting material, the high temperature generated by the cutting process might have significantly altered the residual stress distribution. And if this is true, as we believe it is, because of the evidence at hand, it will bring all the previous results (those obtained by strain gage as well as by moiré interferometry) into question. The thermal annealing process has completely circumvented this concern.

When the project was initiated, it was thought that we could use the results from a transverse slice and a 45° oblique slice to reconstruct the 3-D state of the stress. Thus, both types of slices were provided. However, our experiments show that when an oblique slice is annealed, it experiences a large amount of global warpage, whereas a transverse slice maintains symmetry with respect to the mid-plane after annealing. (This actually should have been anticipated,

because the residual shear stress in the inclined slice is inherently asymmetric, since we have assumed that residual stress distribution is independent of the z-axis). As a result, the fringes obtained from an inclined slice do not lend themselves for a simple interpretation.

Hence, we make some assumptions and propose a new approach to reconstruct the 3-D residual stresses in rails using only a transverse slice. First, we obtain the in-plane u and v moiré fringes via moiré interferometry. Second, we modify the moiré interferometer so it acts as a Twyman/Green interferometer as well, whereby the fringes of the out-of-plane deformation w (i.e., the thickness change after annealing) are also obtained. We assume that the thickness change is largely due to the relaxation of σ_z (upon where we have to assume that σ_z has a distribution that it is uniform throughout the thickness, but drops drastically to zero in a thin boundary layer near the surface). Third, we assume that constitutive relation is that of Hooke's law with E and ν being the Young's modulus and Poisson's ratio at the annealing temperature. (The existence of σ_z within a thin transverse slice was discovered accidentally. When the data from moiré fringes were used to calculate ε_x and ε_y, the resulting thickness change due to Poisson's effect was completely different from the measured thickness change using Twyman/Green interferometry.)

Armed with all these assumptions, we were able to reconstruct the 3-D residual stress distribution of all the rails. Qualitatively, we believe they represent the actual residual stress distribution quite closely. Quantitatively, they should be about the same order of magnitude of the true residual stresses. Much more work is needed to test some of the assumptions made and to establish this approach to become a standard and a routine testing method for the determination of 3-D residual stresses in rails.

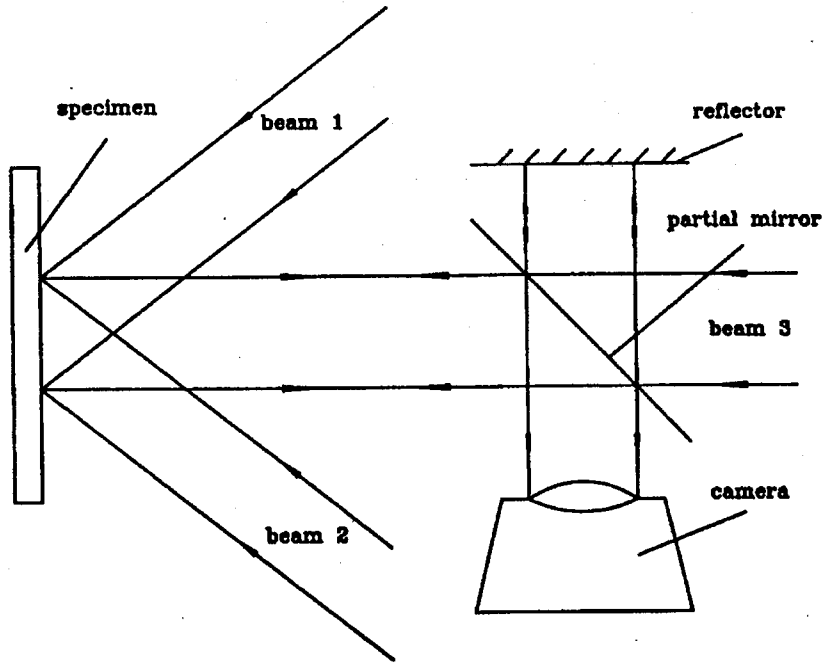

Fig. 1 a sketch of the moiré and Twyman/Green interferometry set-up

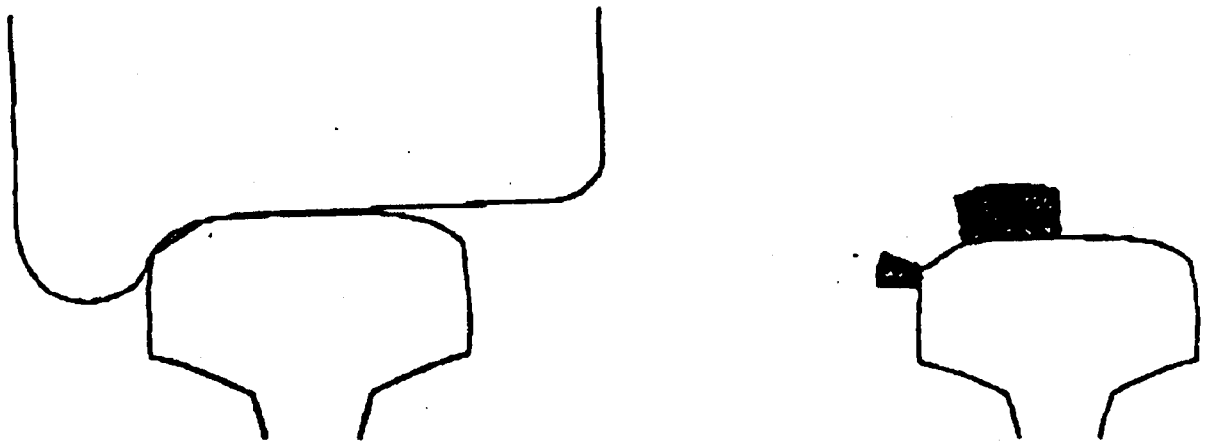

Fig. 2 rail ground for two-point contact

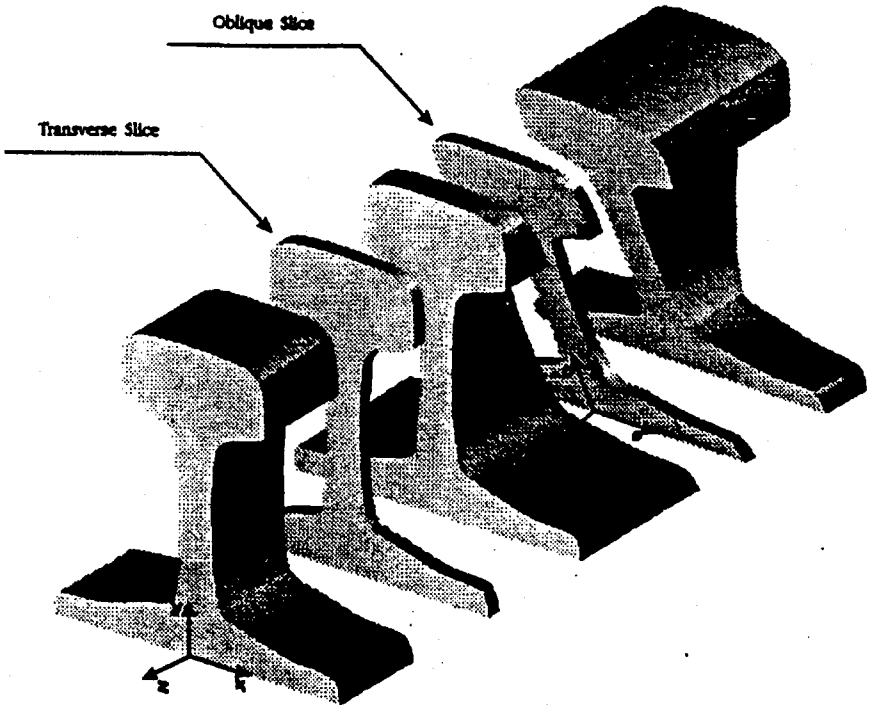

Fig. 3 the cutting scheme of the rail

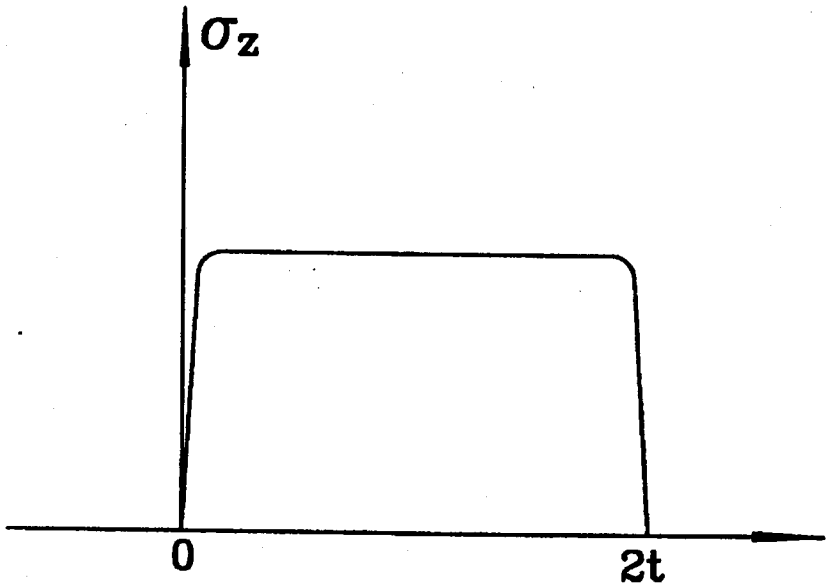

Fig. 4 the assumption of σ_{zz} distribution through the slice thickness

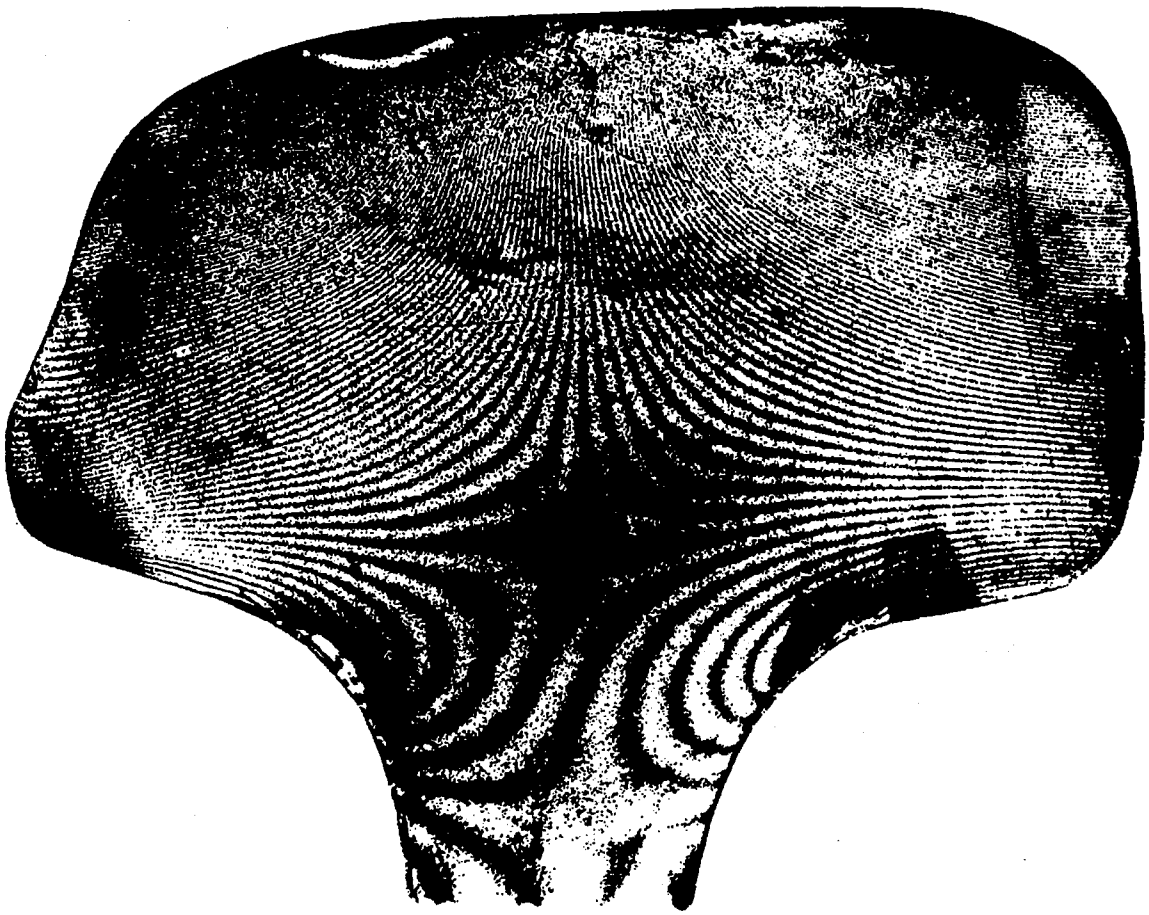

Fig. 5 u-field fringes by moire interferometry
(rail # 3, two-point contact -- CFI 136 RE03-1605)

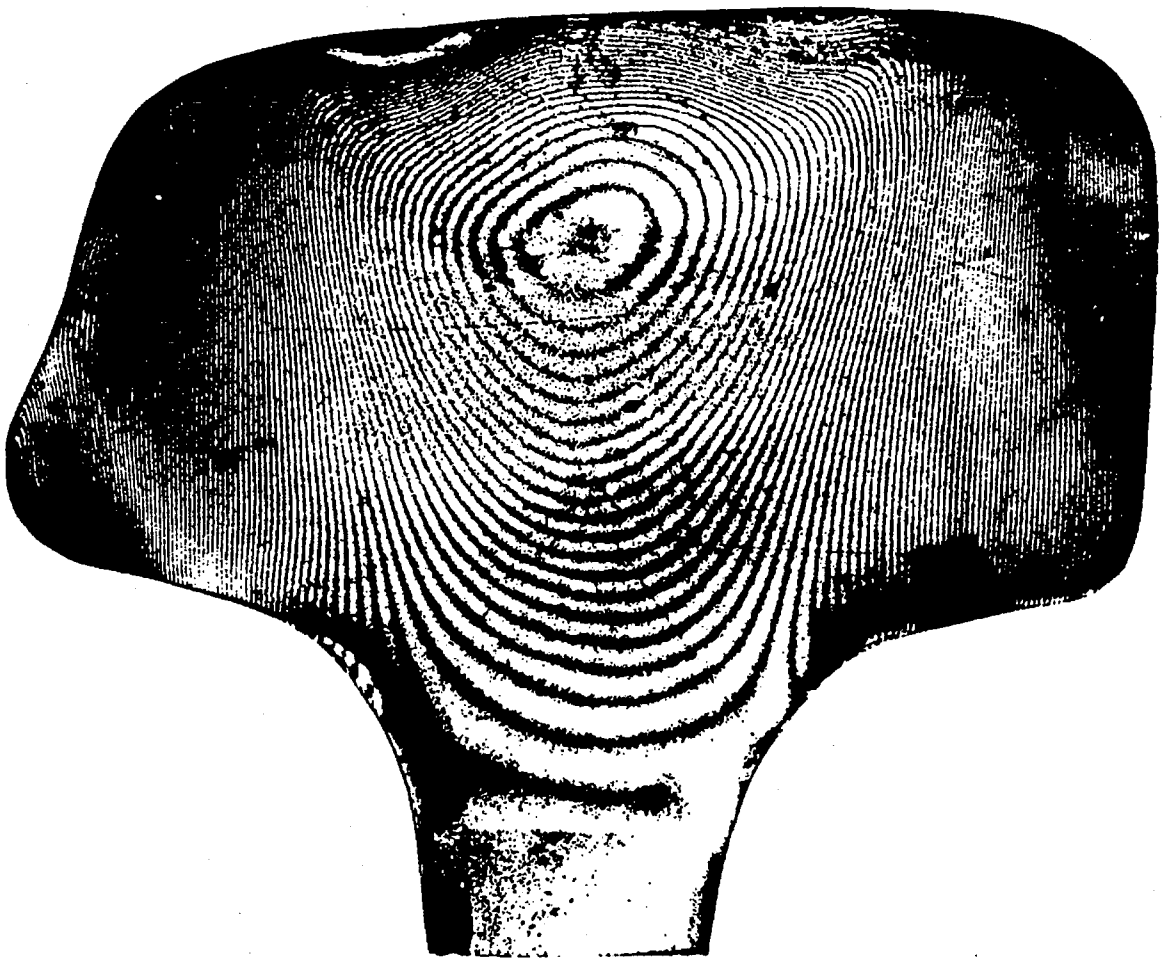

Fig. 6 v-field fringes by moire interferometry
(rail # 3, two-point contact -- CFI 136 RE03-1605)

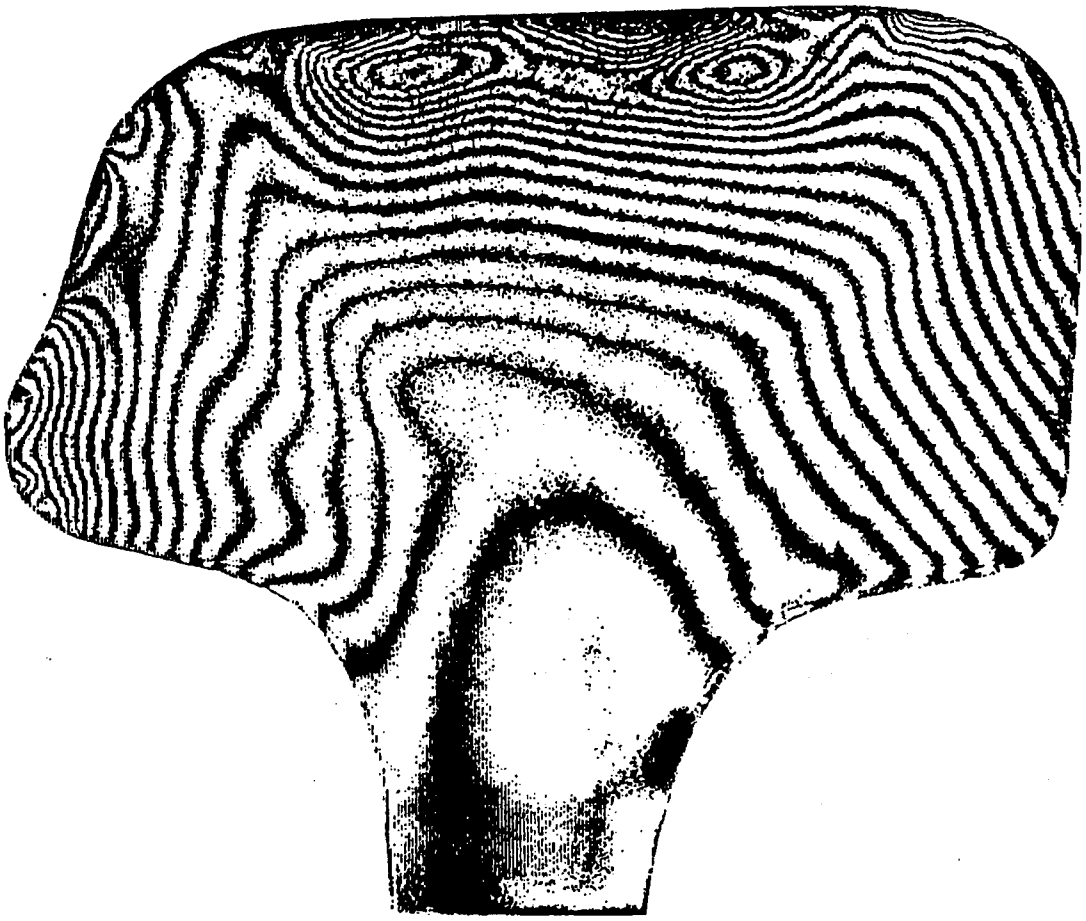

Fig. 7 w-field fringes by Twyman/Green interferometry
(rail # 3, two-point contact -- CFI 136 RE03-1605)

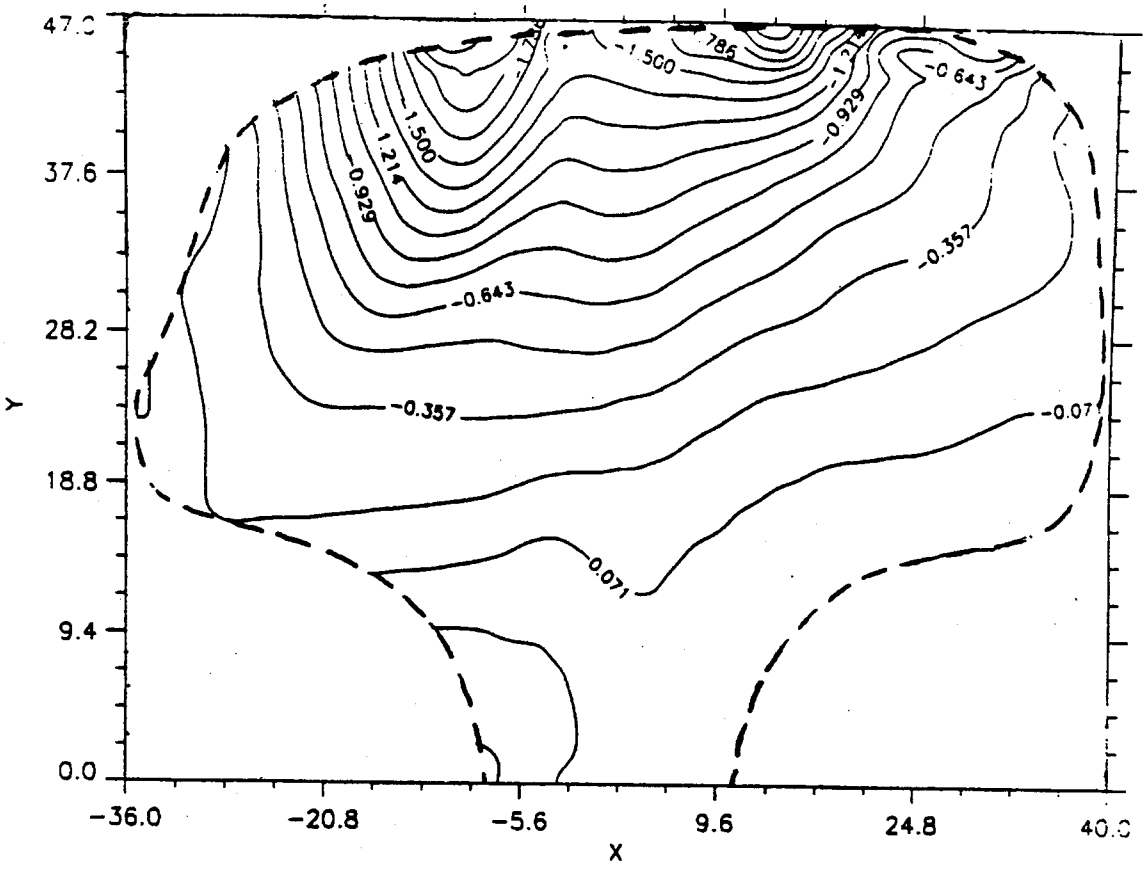

Fig. 8 ϵ_x (10^{-3})
(rail # 3, two-point contact -- CFI 136 RE03-1605)

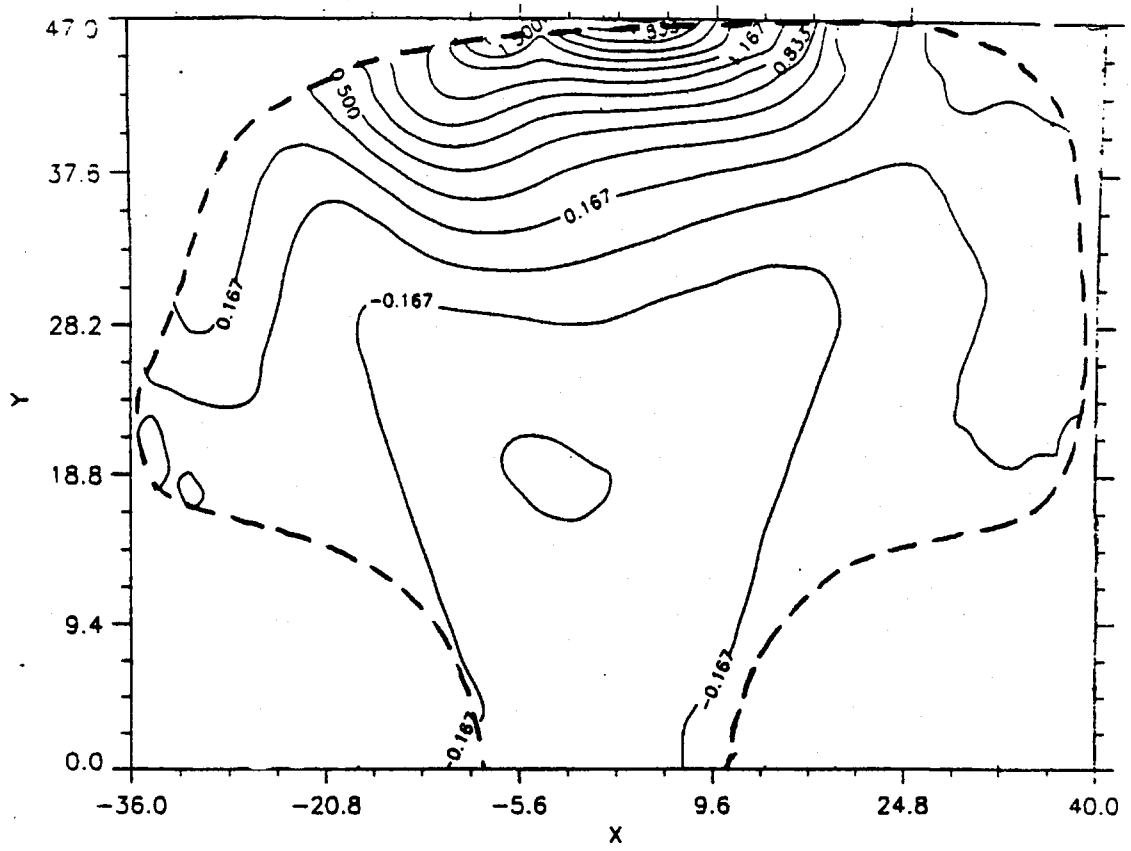

Fig. 9 ϵ_y (10^{-3})
(rail # 3, two-point contact -- CFI 136 RE03-1605)

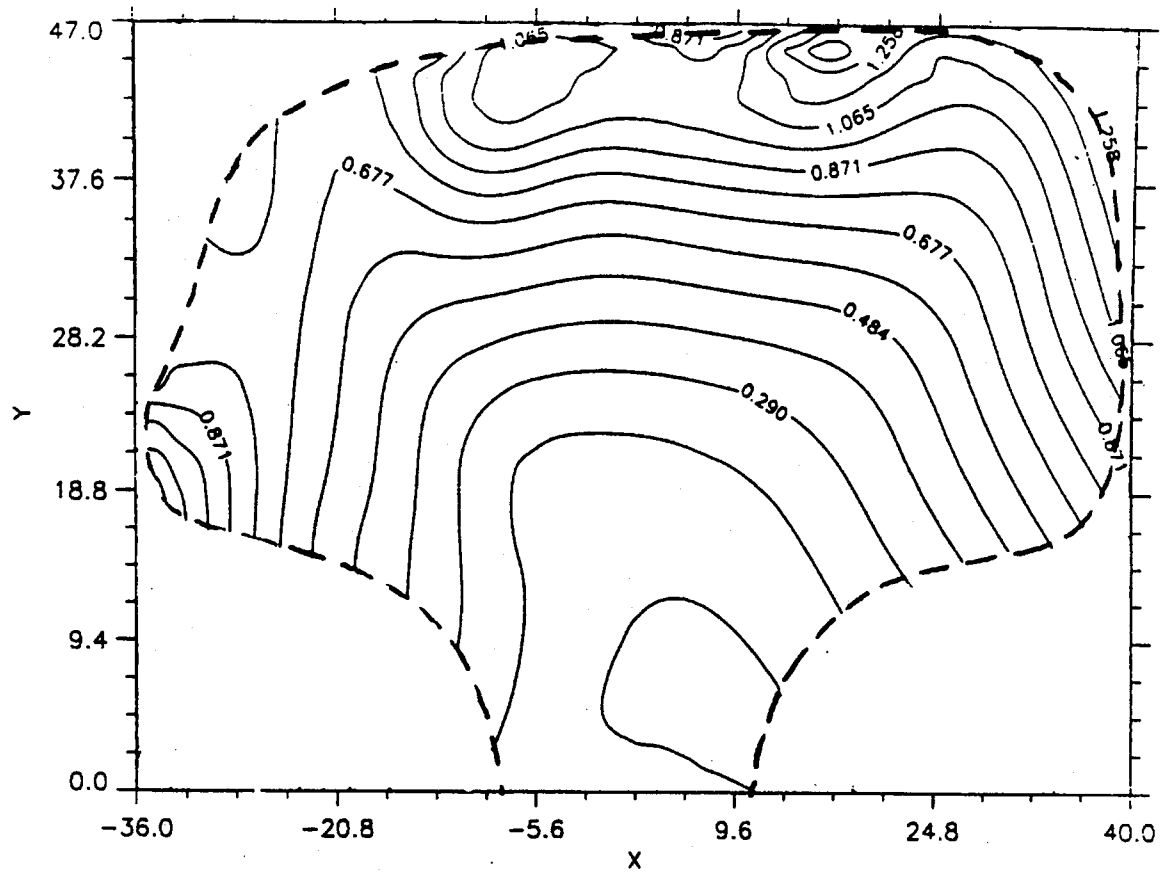

Fig. 10 ϵ_z (10^{-3})
(rail # 3, two-point contact -- CFI 136 RE03-1605)

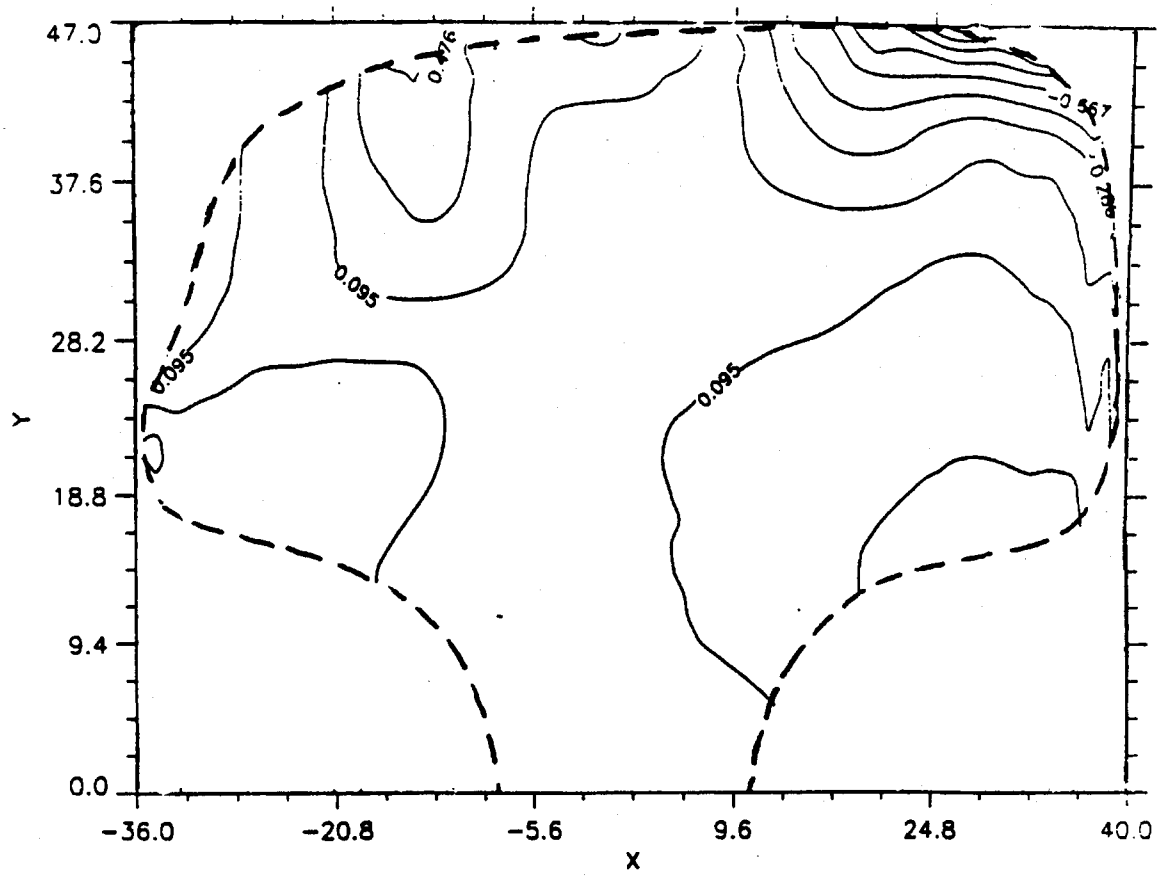

Fig. 11 ϵ_{xy} (10^{-3})
(rail # 3, two-point contact -- CFI 136 RE03-1605)

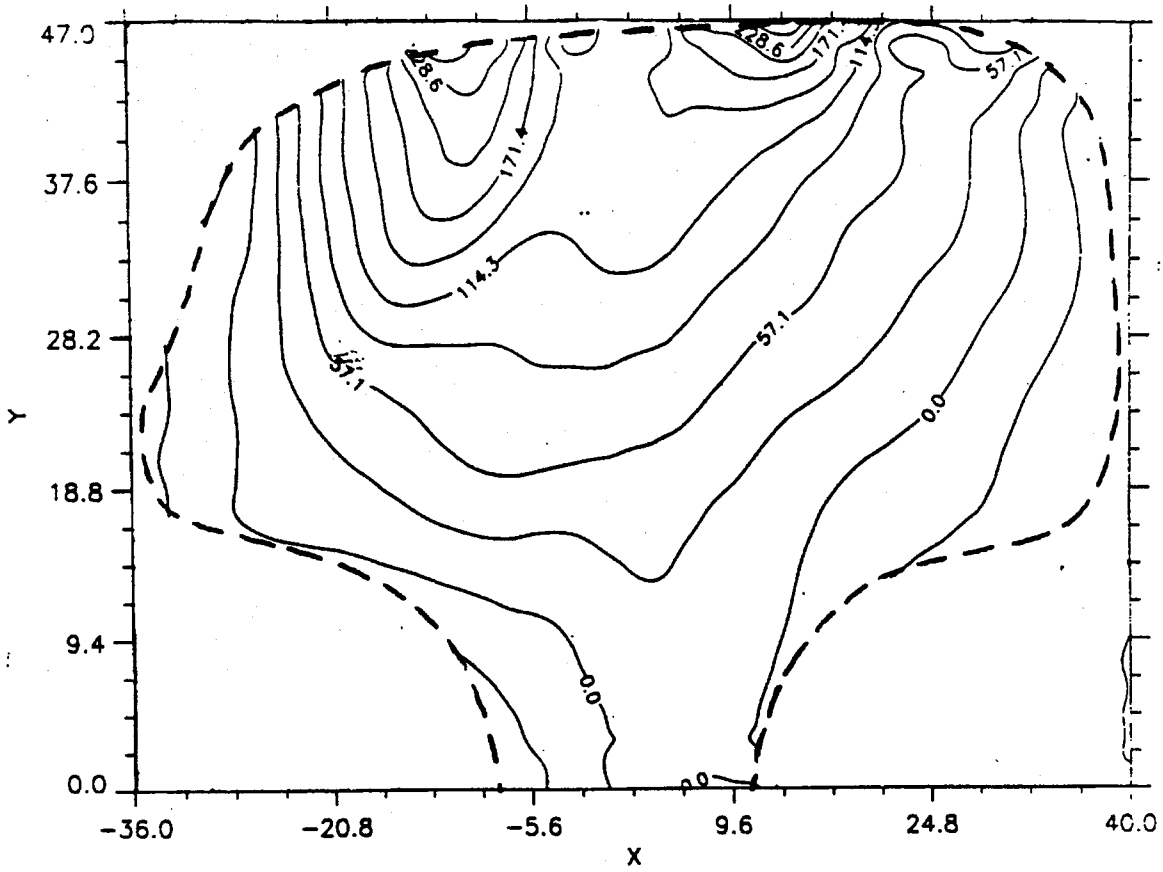

Fig. 12 σ_x (MPa)
(rail # 3, two-point contact -- CFI 136 RE03-1605)

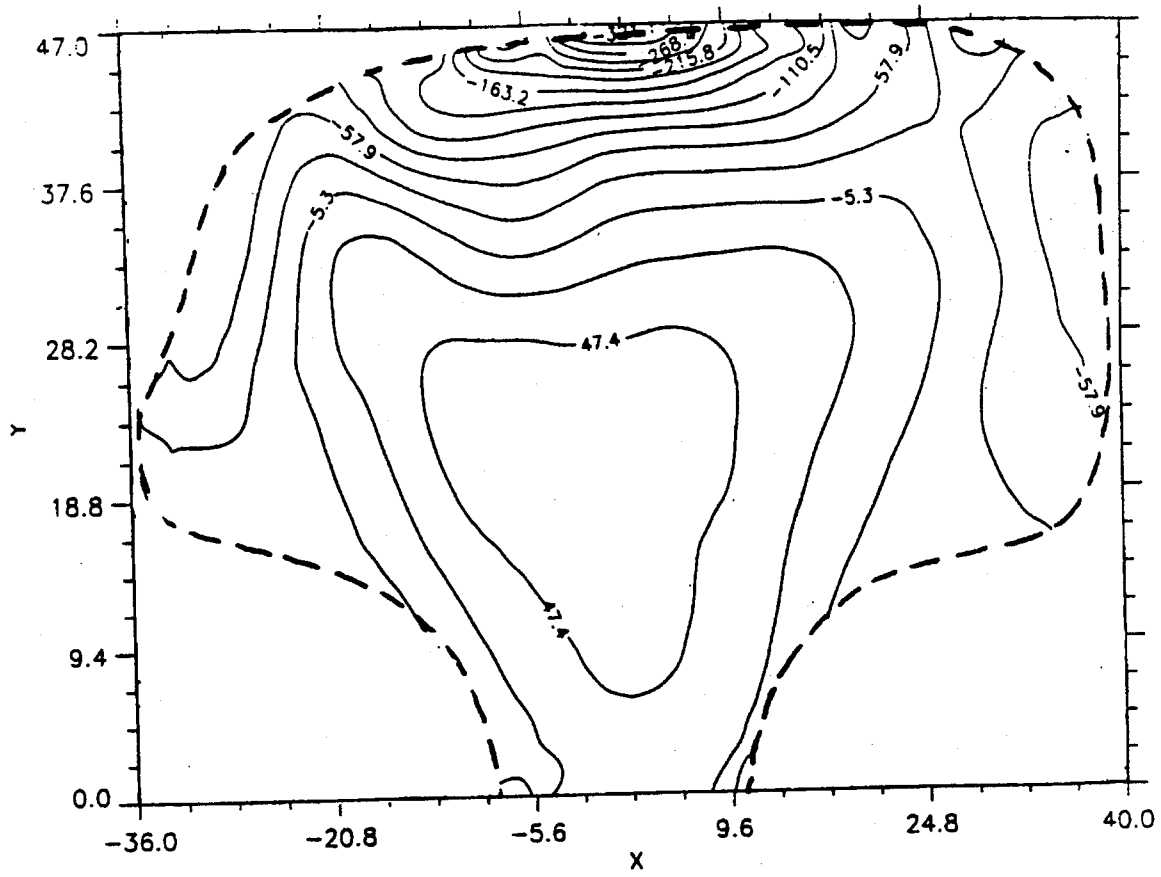

Fig. 13 σ_y (MPa)
(rail # 3, two-point contact -- CFI 136 RE03-1605)

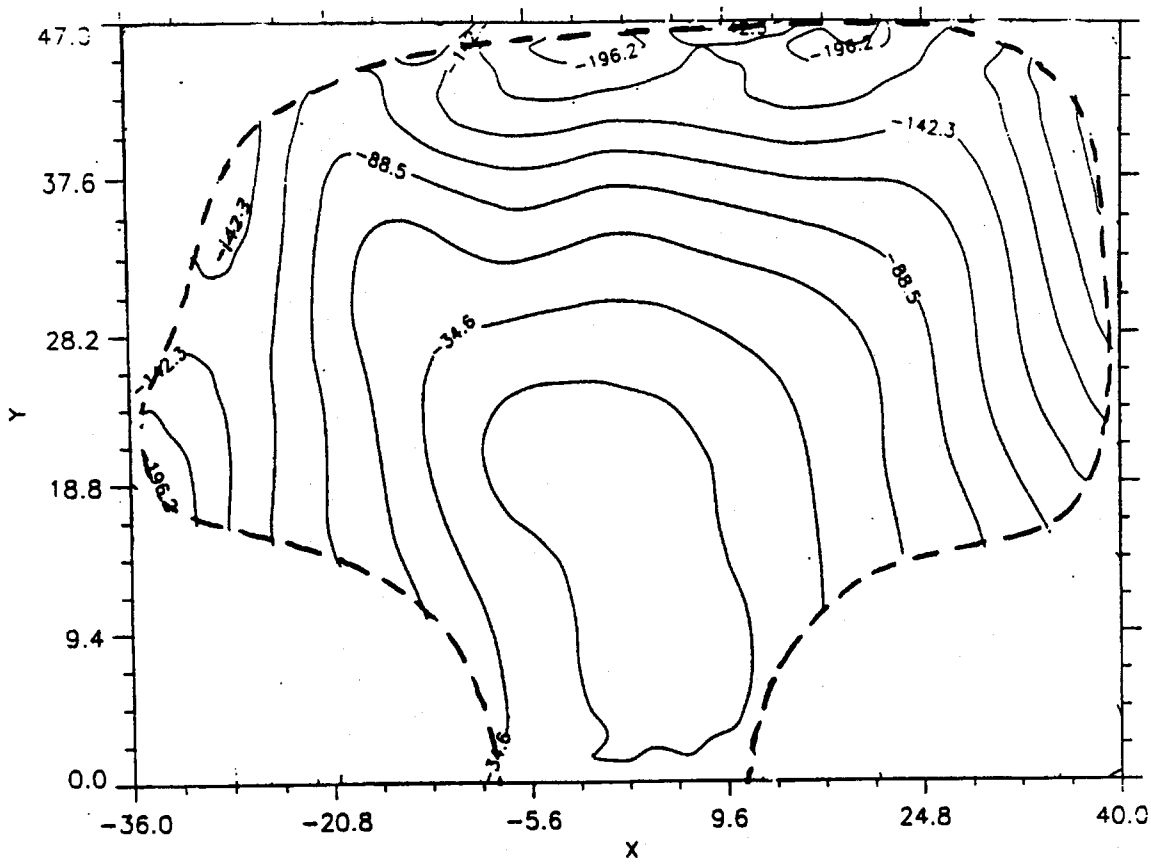

Fig. 14 σ_z (MPa)
(rail # 3, two-point contact -- CFI 136 RE03-1605)

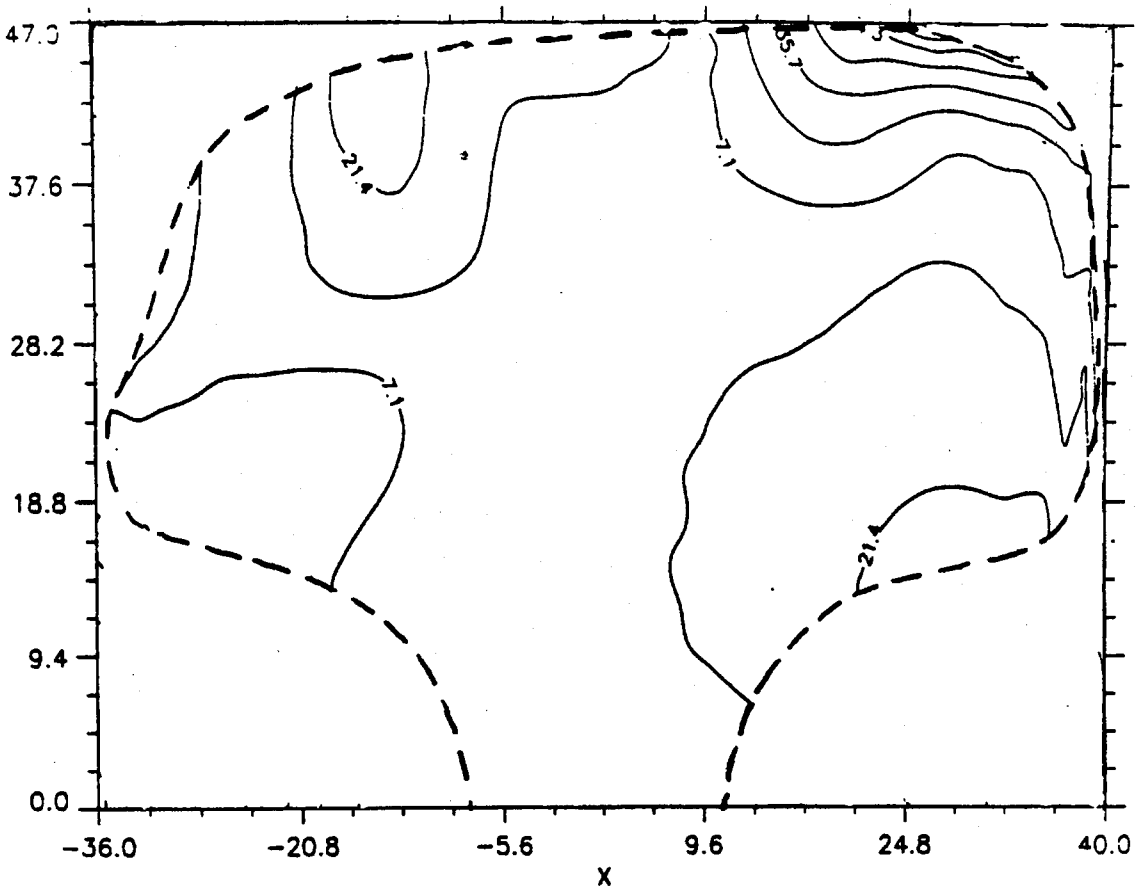

Fig. 15 σ_{xy} (MPa)
(rail # 3, two-point contact – CFI 136 RE03-1605)

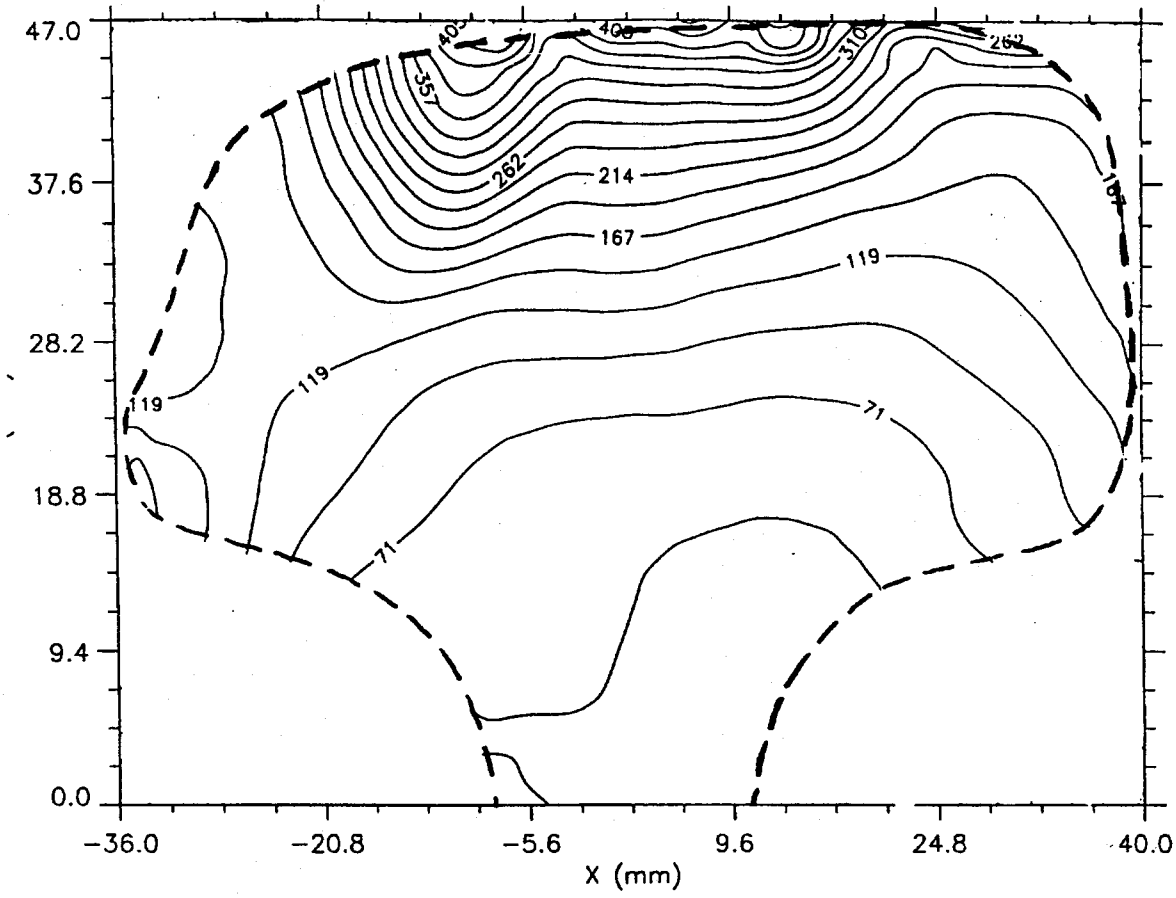

Fig. 16 effective stress σ_e (MPa)
(rail # 3, two-point contact -- CFI 136 RE03-1605)

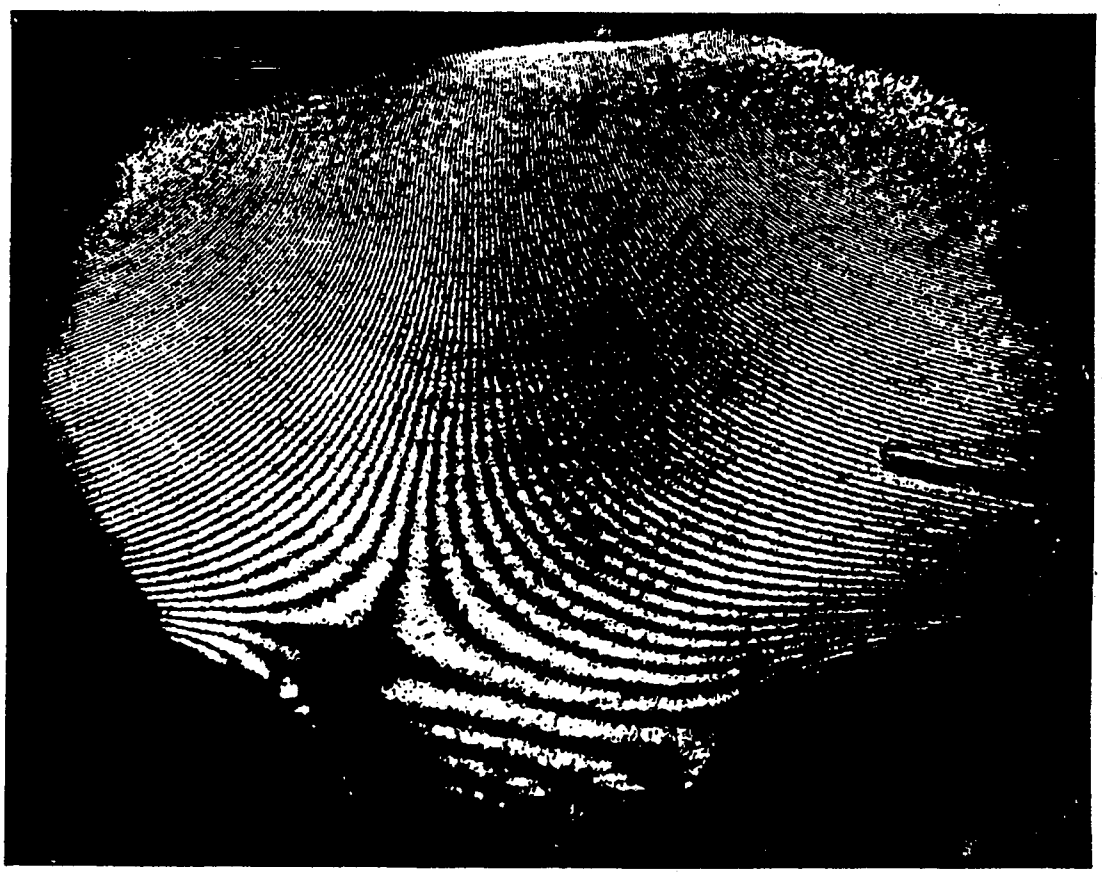

Fig. 17 u-field fringes by moire interferometry
(rail # 1, control wear -- CFI 136 RE25-0357)

Fig. 18 v-field fringes by moire interferometry
(rail # 1, control wear -- CFI 136 RE25-0357)

Fig. 19 w-field fringes by Twyman/Green interferometry
(rail # 1, control wear -- CFI 136 RE25-0357)

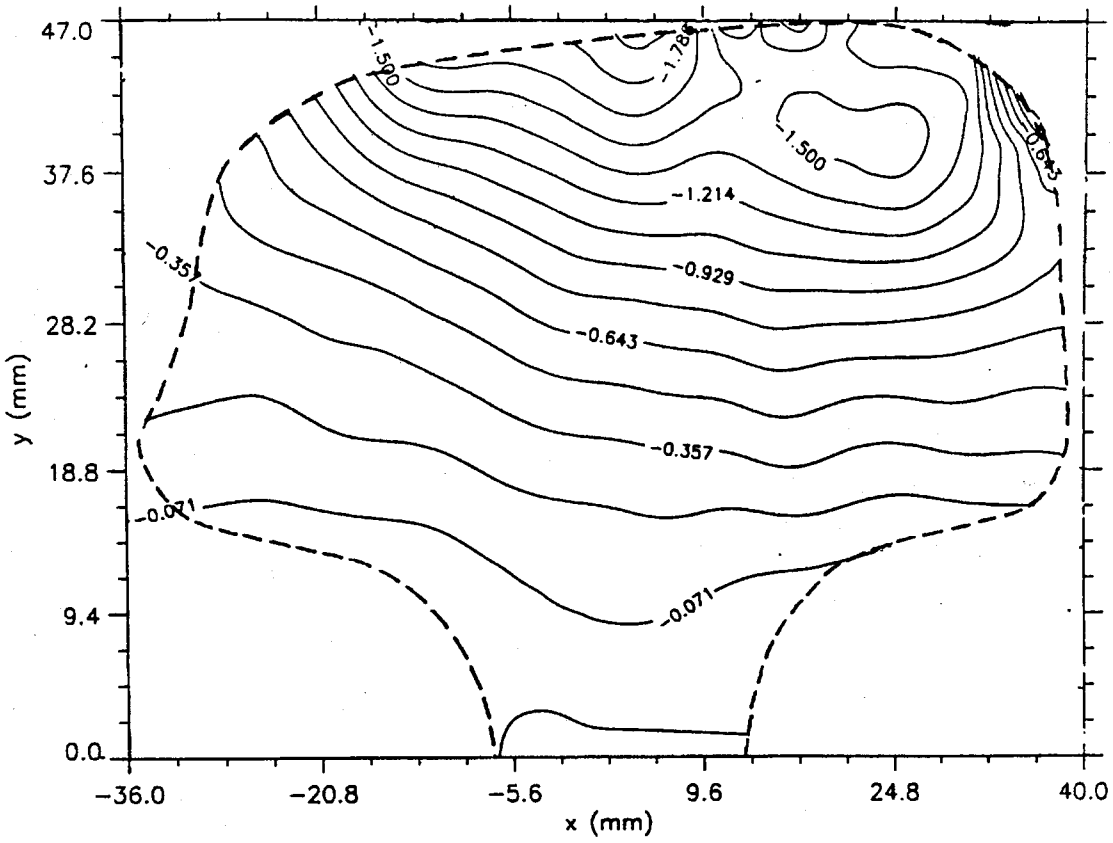

Fig. 20 ϵ_x (10^{-3})
(rail # 1, control wear -- CFI 136 RE25-0357)

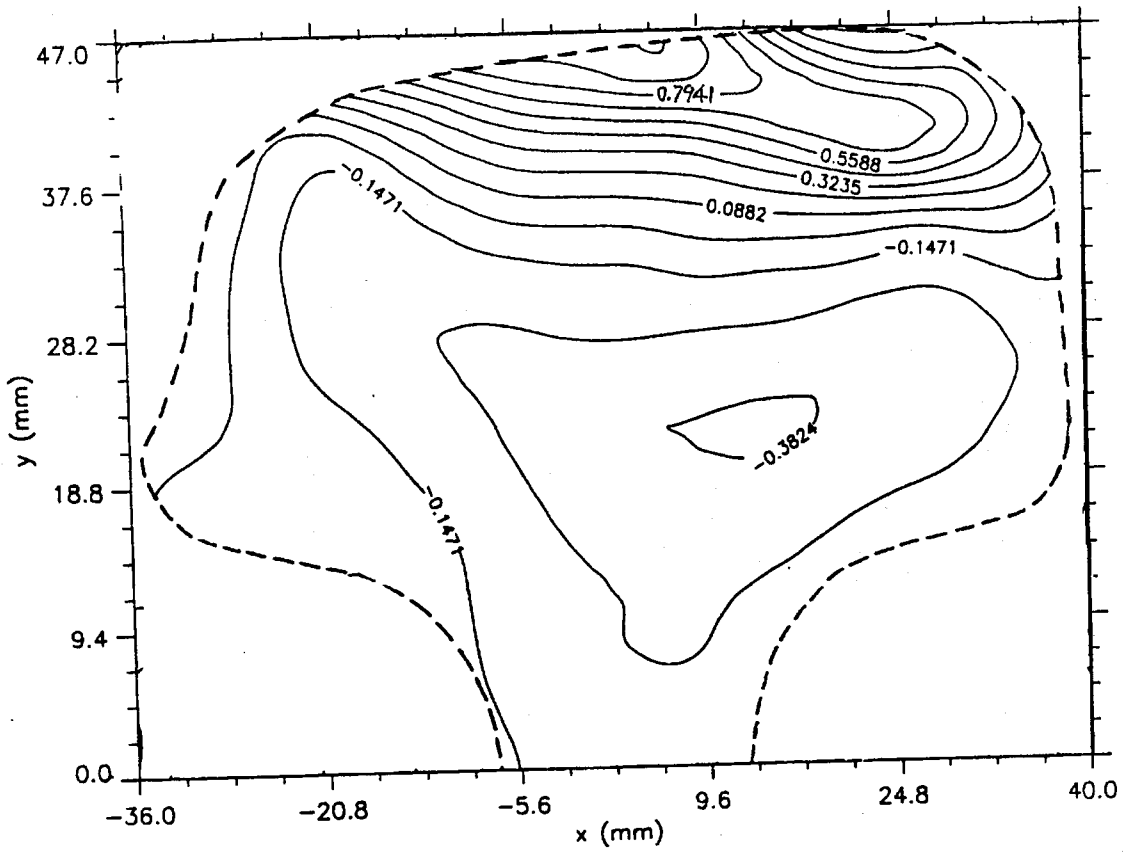

Fig. 21 ϵ_y (10^{-3})
(rail # 1, control wear -- CFI 136 RE25-0357)

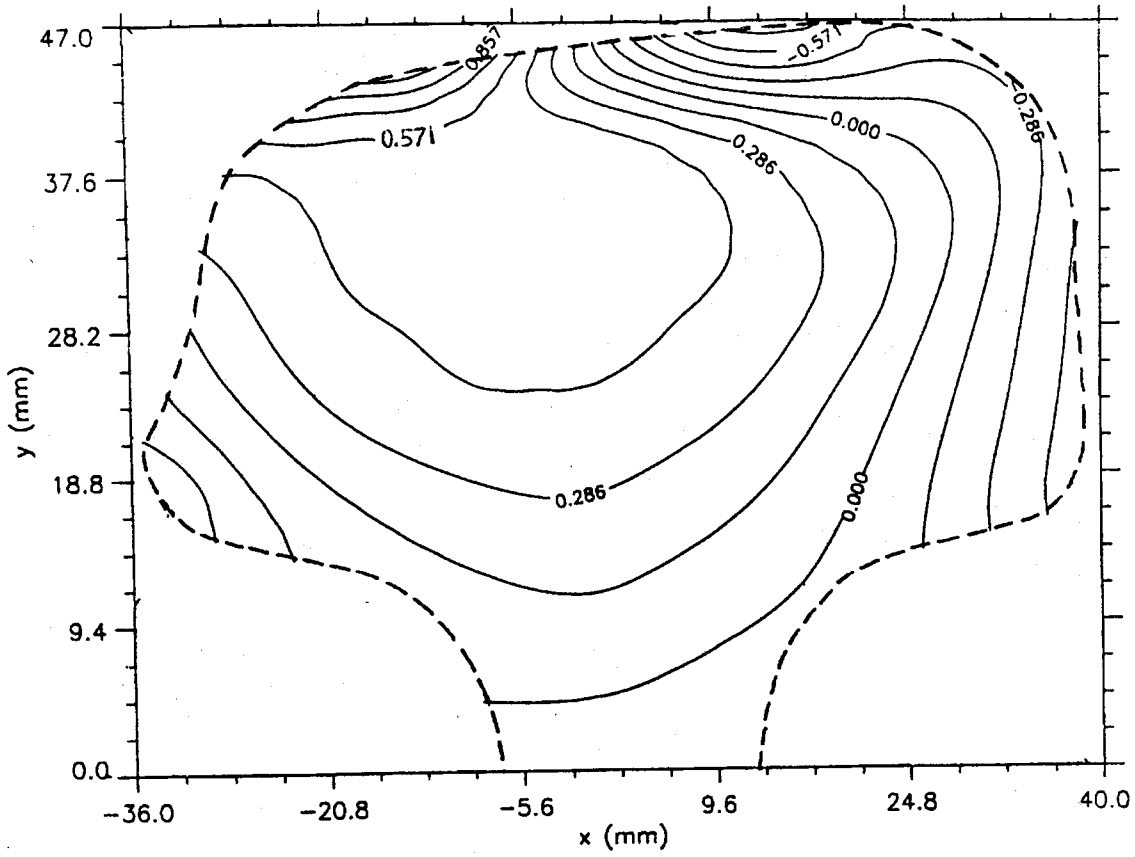

Fig. 22 ϵ_z (10^{-3})
(rail # 1, control wear -- CFI 136 RE25-0357)

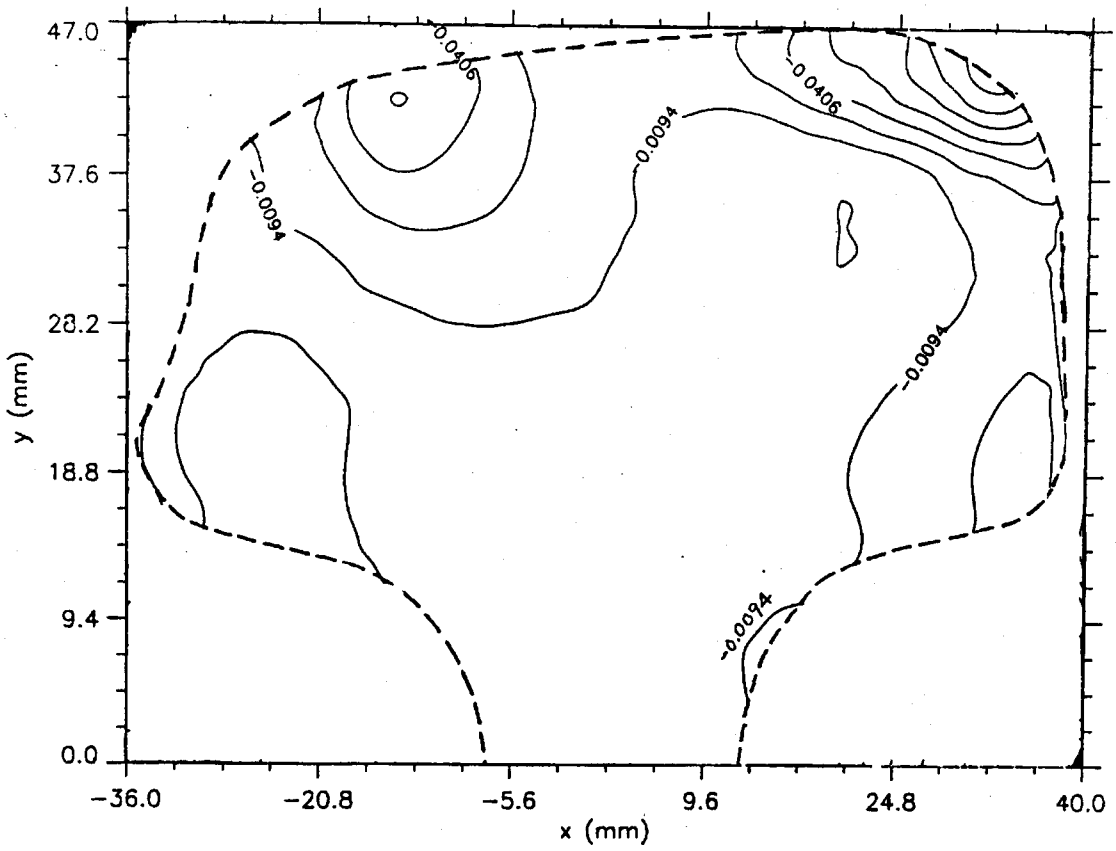

Fig. 23 ϵ_{xy} (10^{-3})
(rail # 1, control wear -- CFI 136 RE25-0357)

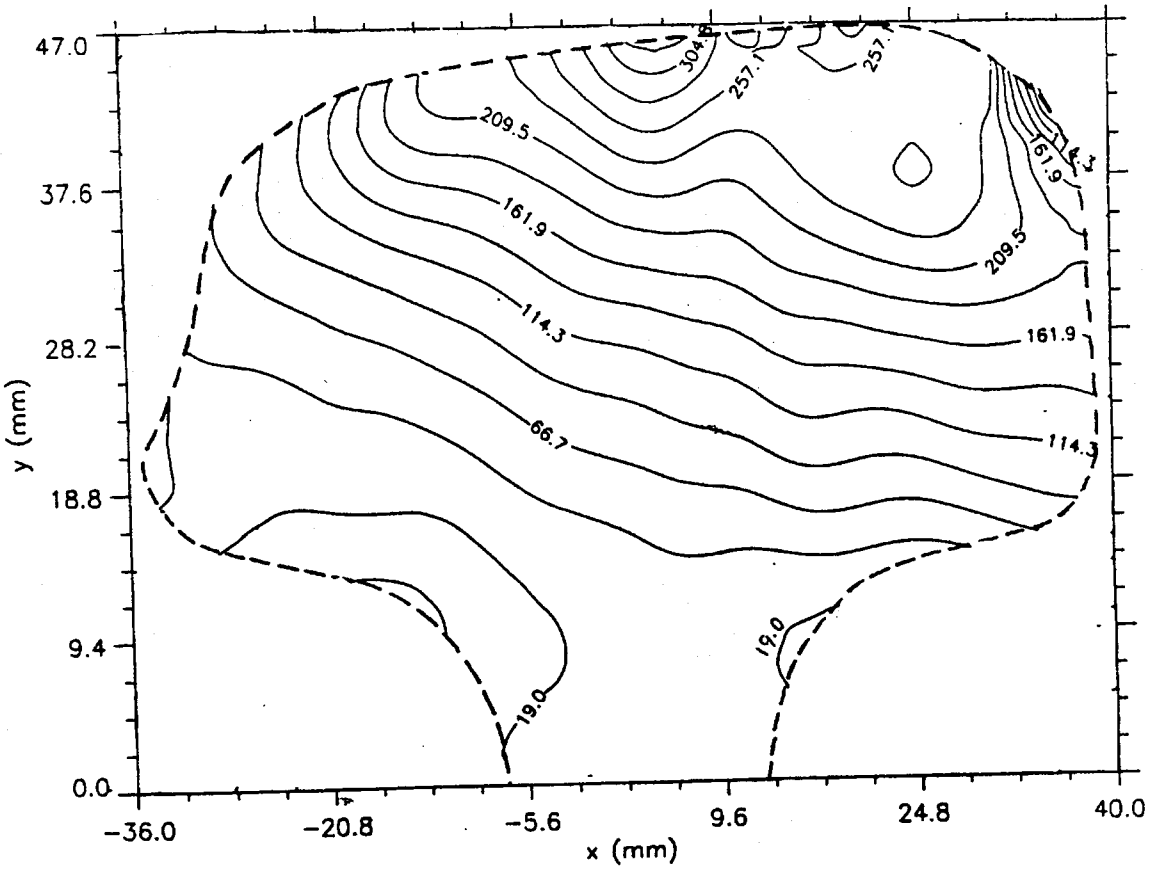

Fig. 24 σ_x (MPa)
(rail # 1, control wear -- CFI 136 RE25-0357)

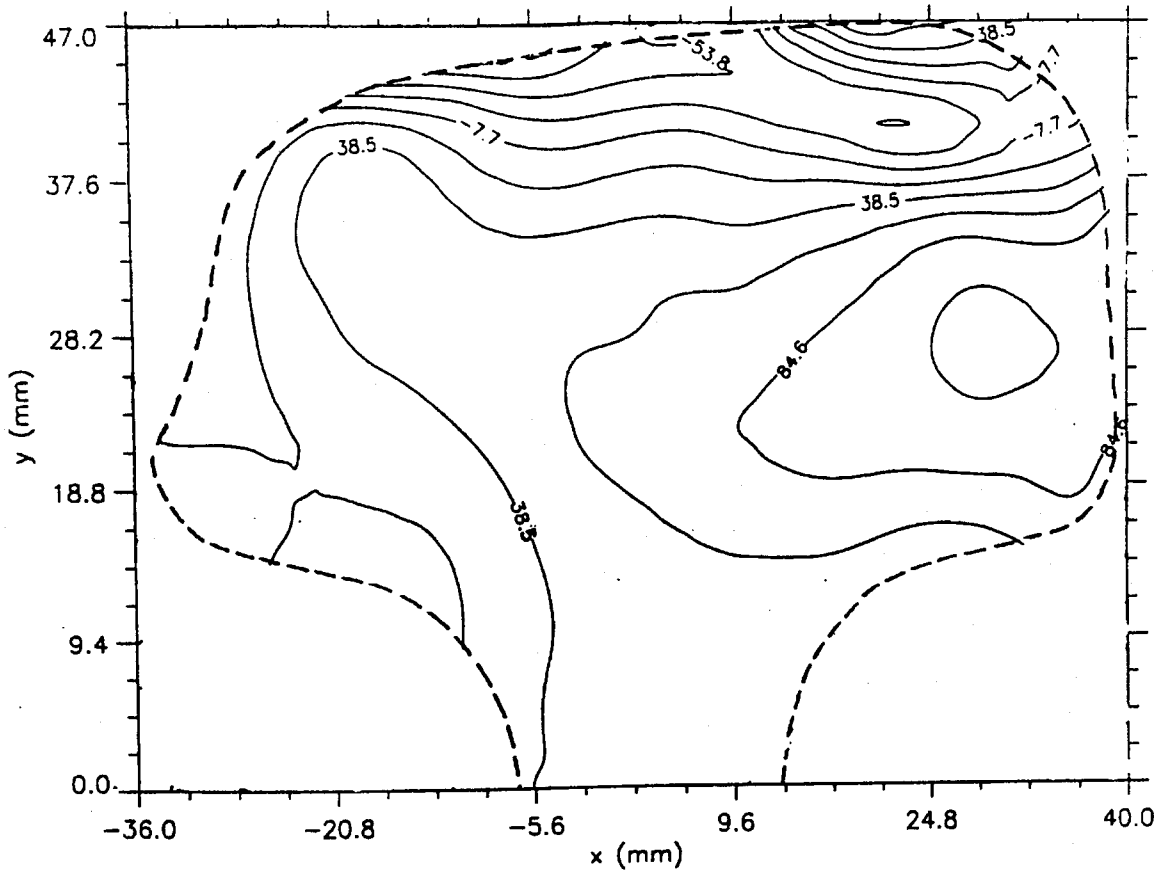

Fig. 25 σ_y (MPa)
(rail # 1, control wear -- CFI 136 RE25-0357)

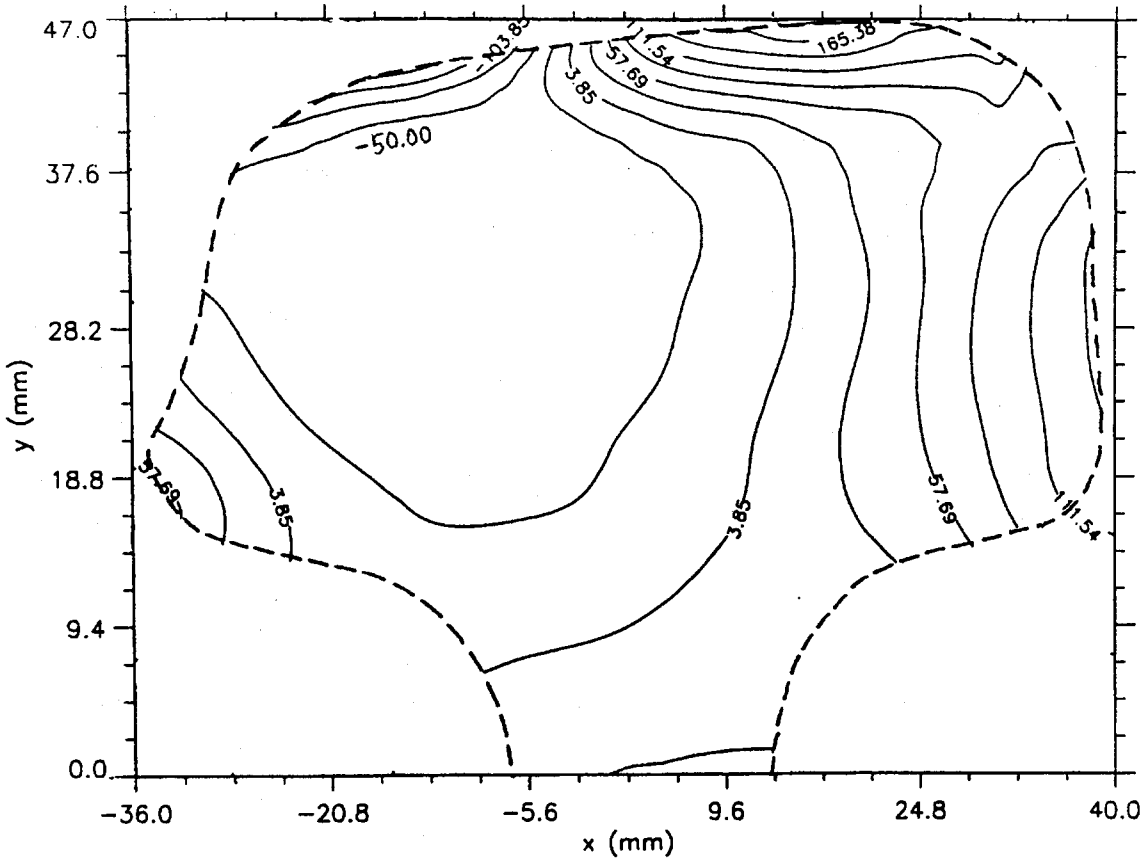

Fig. 26 σ_z (MPa)
(rail # 1, control wear -- CFI 136 RE25-0357)

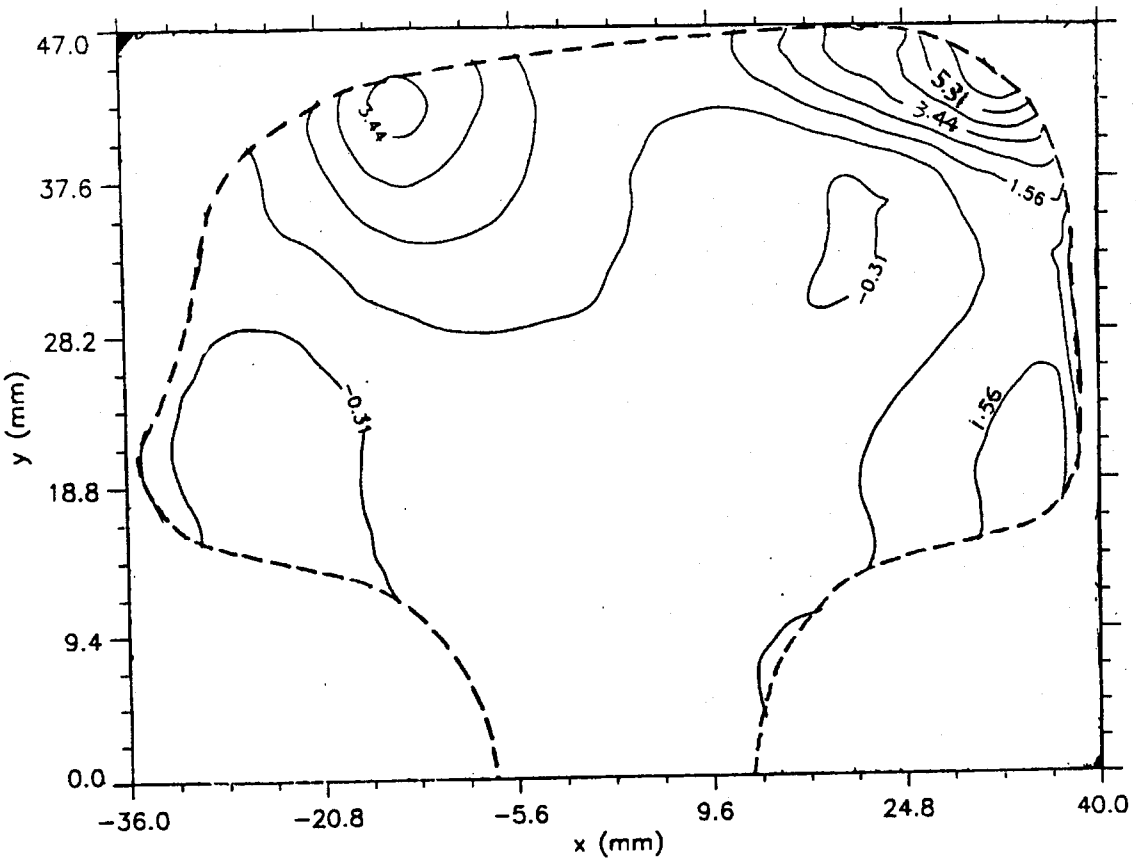

Fig. 27 σ_{xy} (MPa)
(rail # 1, control wear -- CFI 136 RE25-0357)

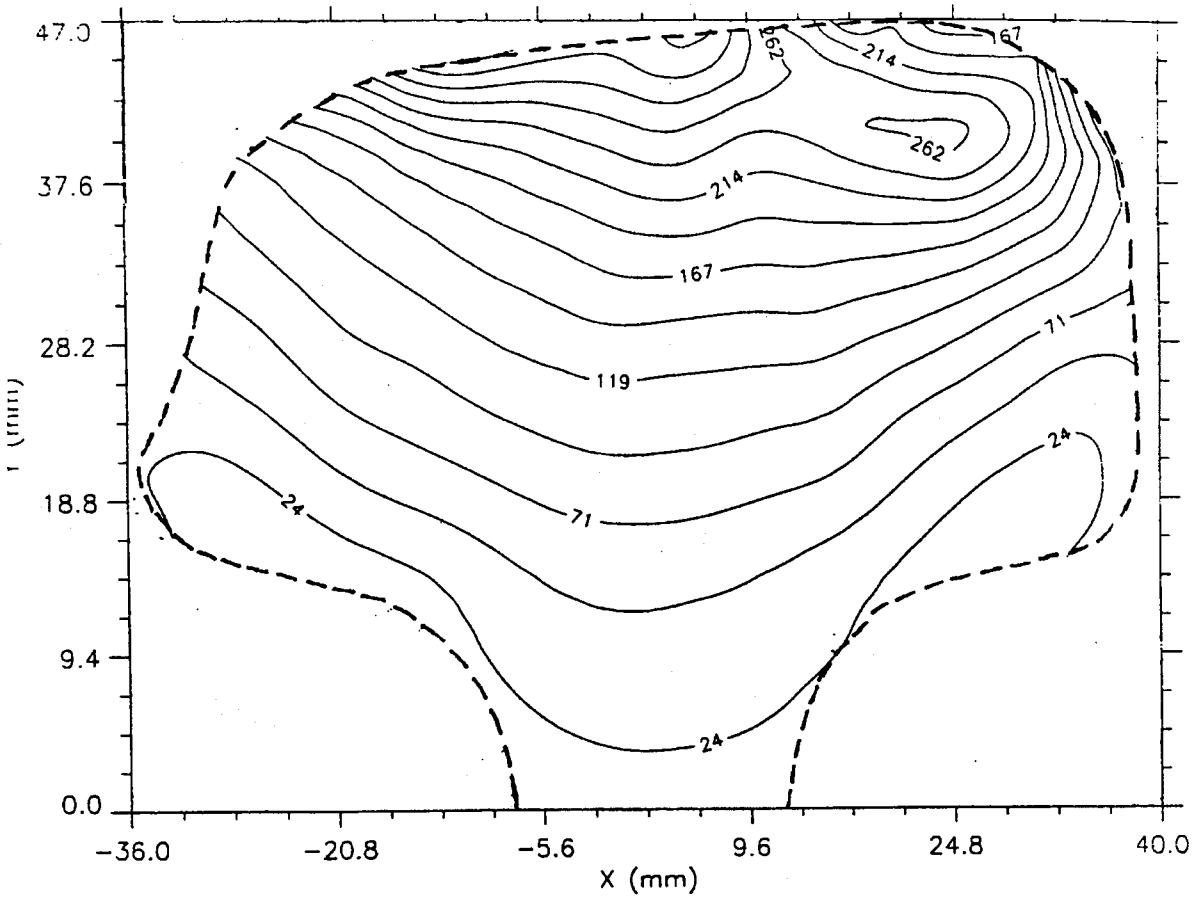

Fig. 28 effective stress σ_e (MPa)
(rail # 1, control wear -- CFI 136 RE25-0357)

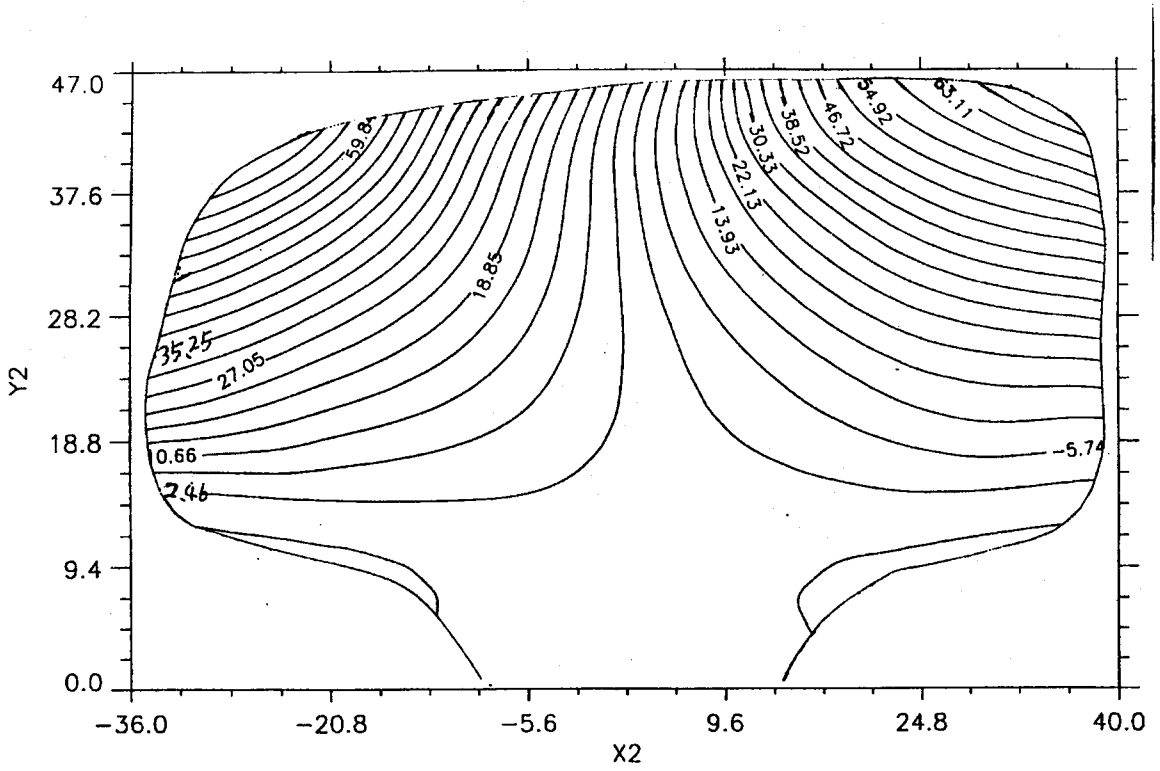

Fig. 29 u-field displacement contours (μm)
(rail # 2 conformal grinding -- CFI 136 RE25-0881)

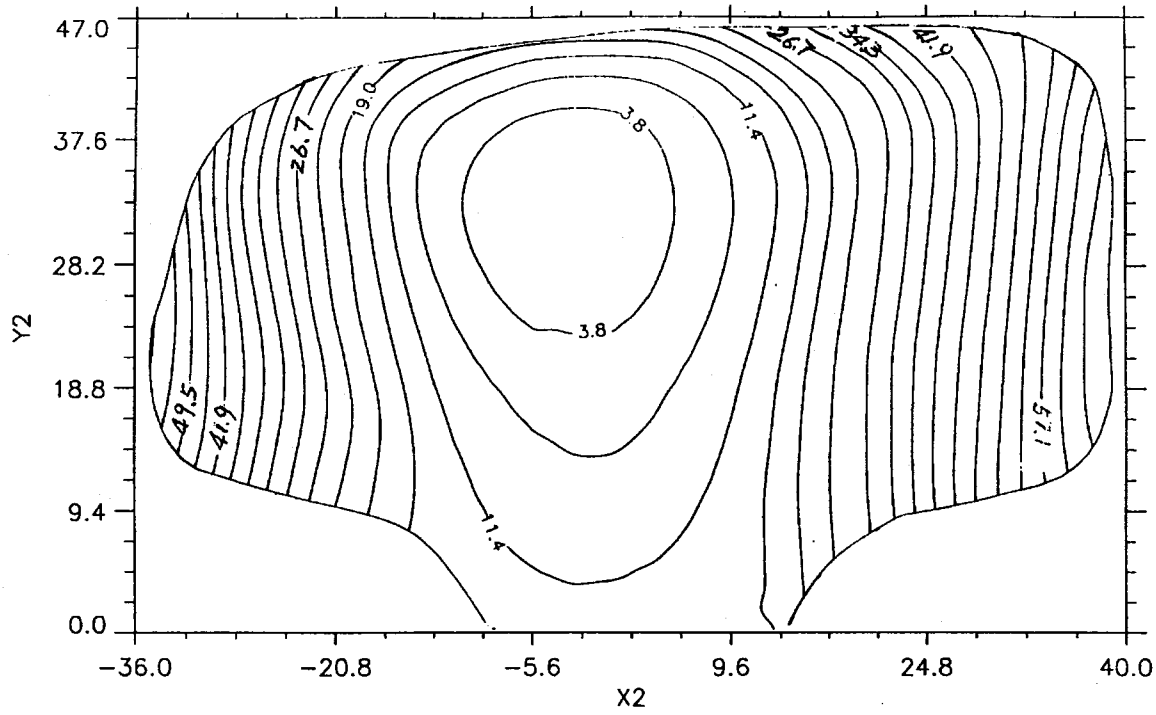

Fig. 30 v-field displacement contours (μm)
(rail # 2 conformal grinding -- CFI 136 RE25-0881)

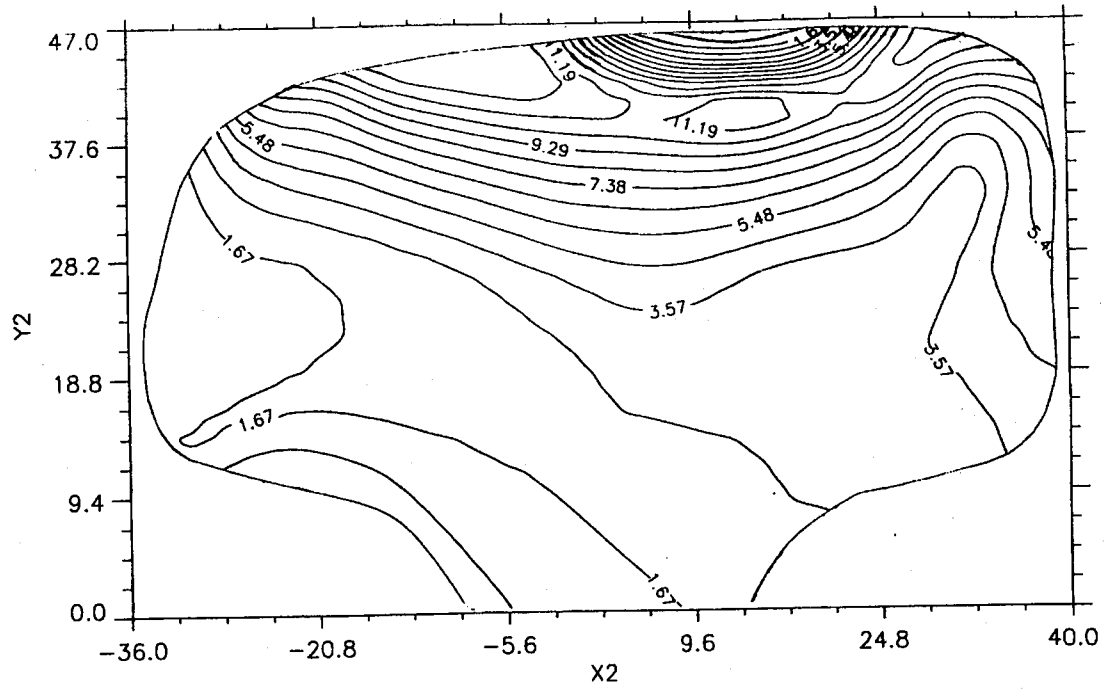

Fig. 31 w-field displacement contours (μm)
(rail # 2 conformal grinding -- CFI 136 RE25-0881)

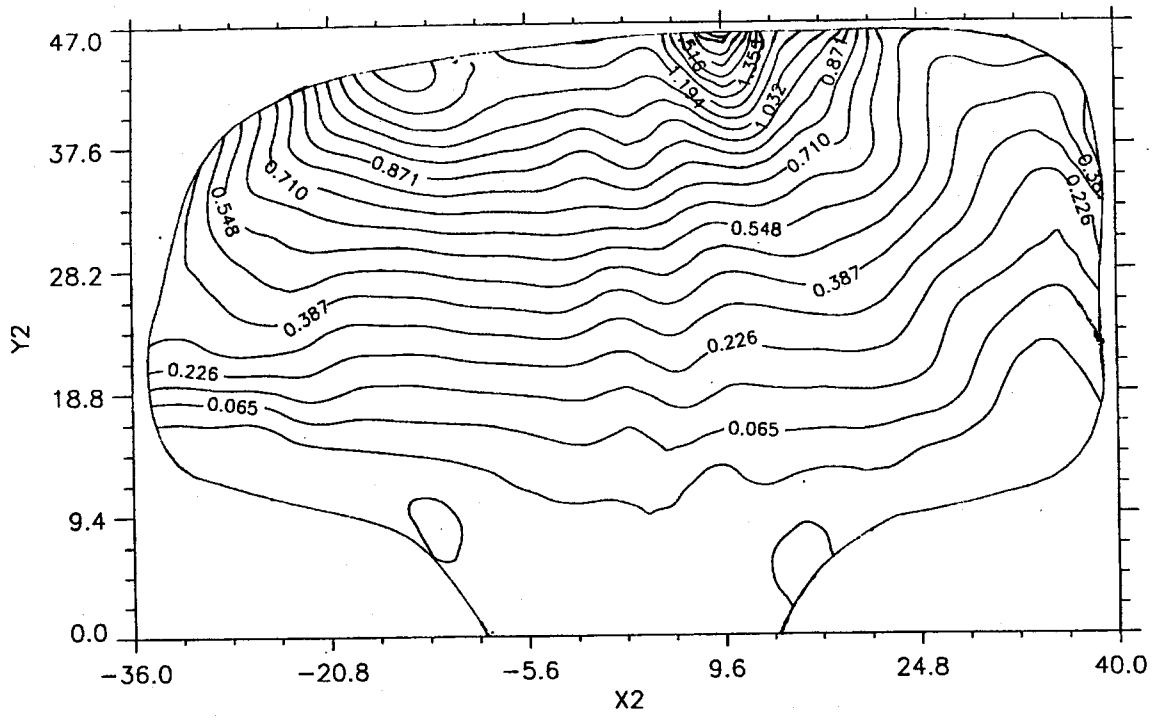

Fig. 32 ϵ_x (10^{-3})
(rail # 2 conformal grinding -- CFI 136 RE25-0881)

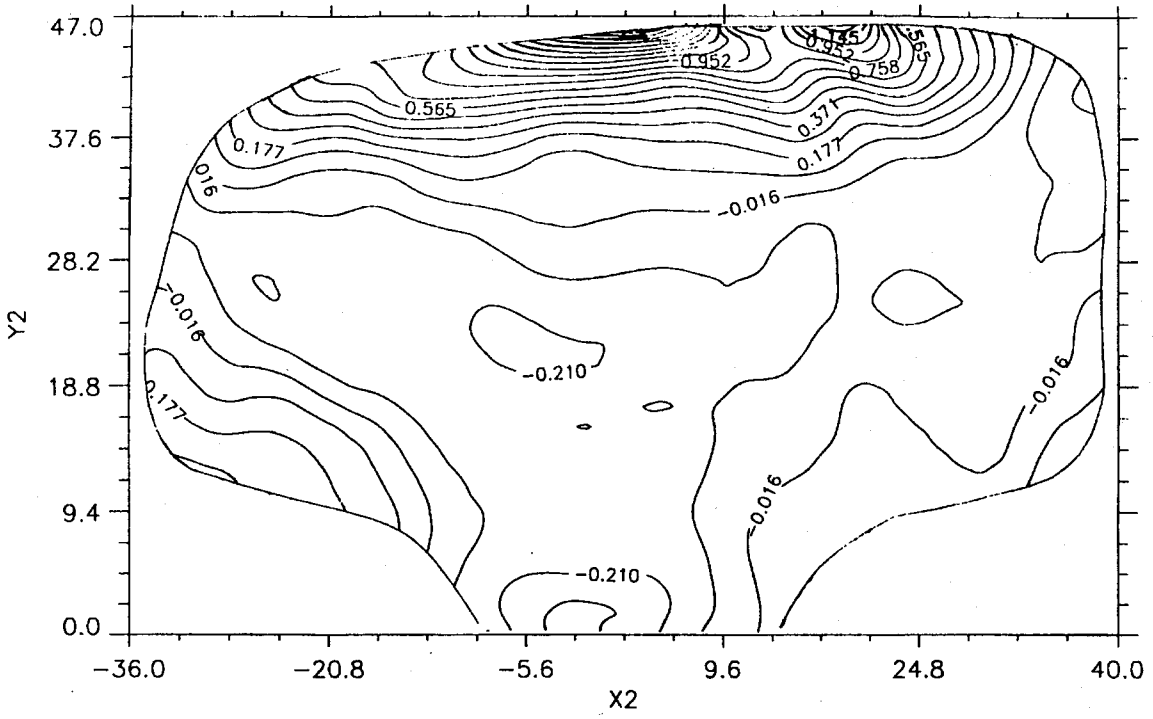

Fig. 33 ϵ_y (10^{-3})
(rail # 2 conformal grinding -- CFI 136 RE25-0881)

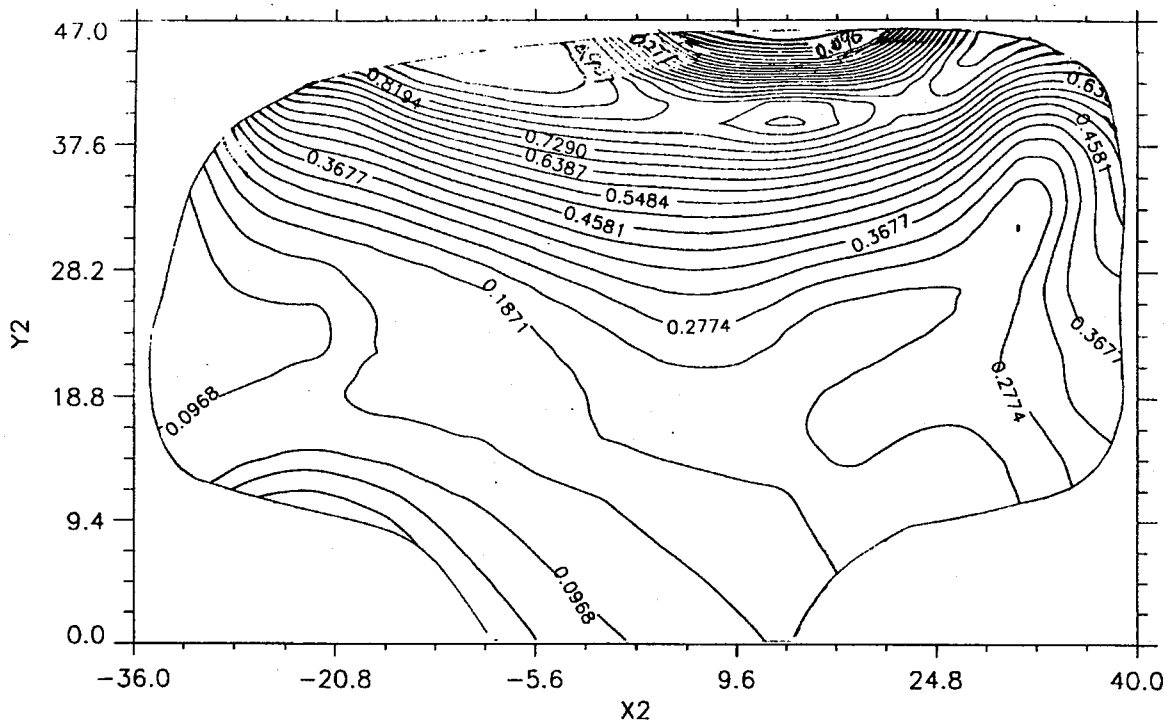

Fig. 34 ϵ_z (10^{-3})
(rail # 2 conformal grinding -- CFI 136 RE25-0881)

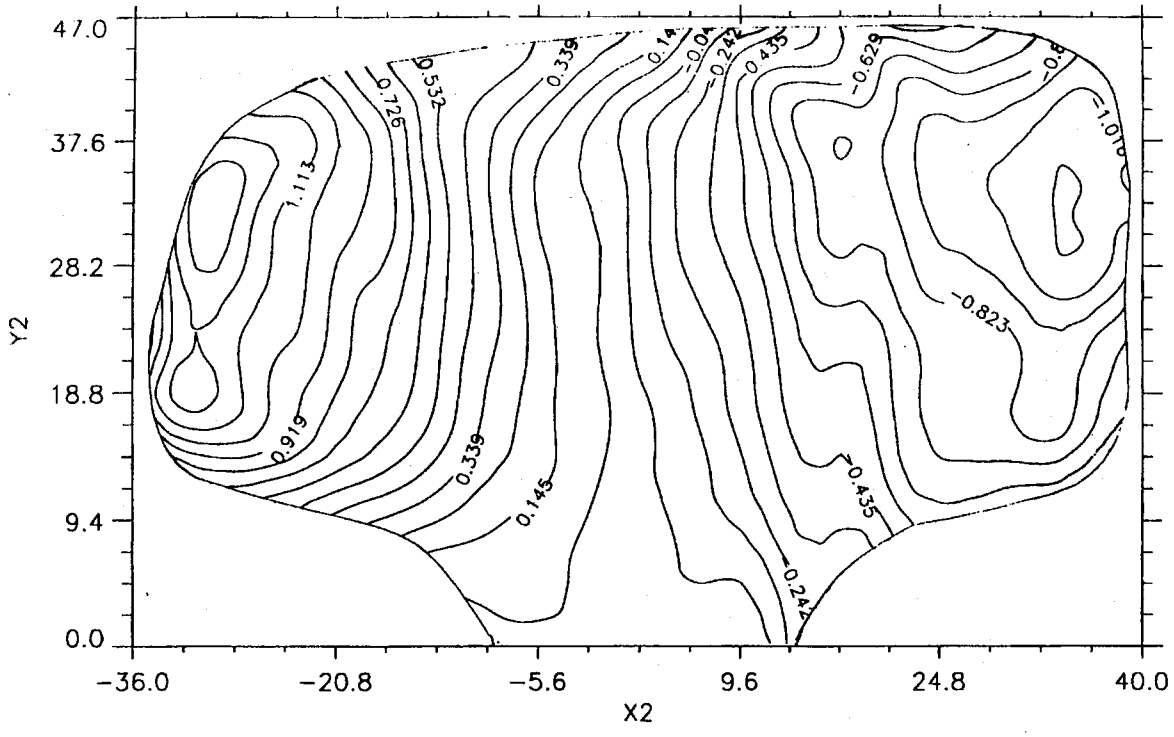

Fig. 35 ϵ_{xy} (10^{-3})
(rail # 2 conformal grinding -- CFI 136 RE25-0881)

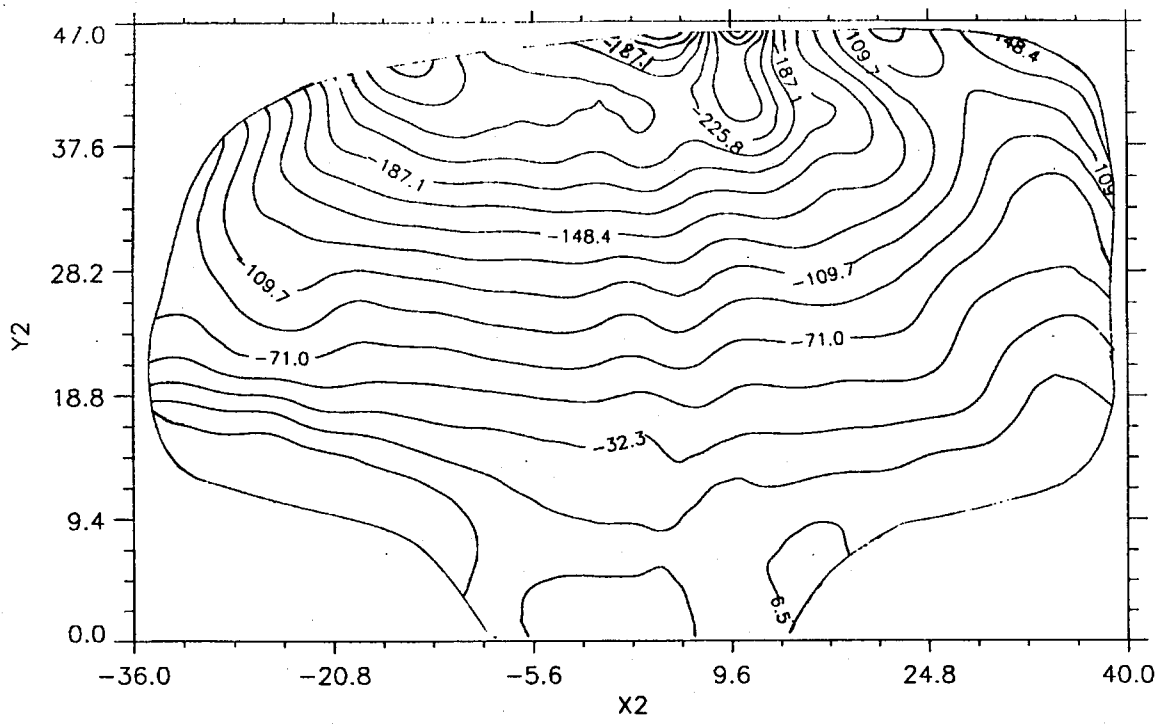

Fig. 36 σ_x (MPa)
(rail # 2 conformal grinding -- CFI 136 RE25-0881)

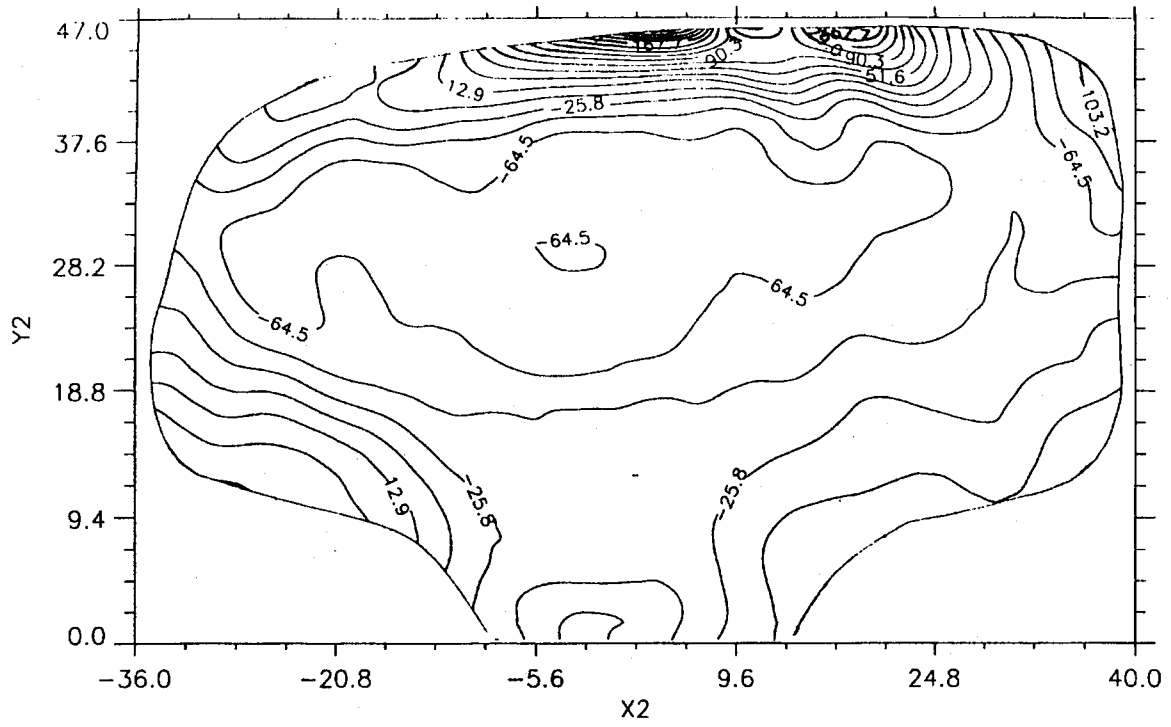

Fig. 37 σ_y (MPa)
(rail # 2 conformal grinding -- CFI 136 RE25-0881)

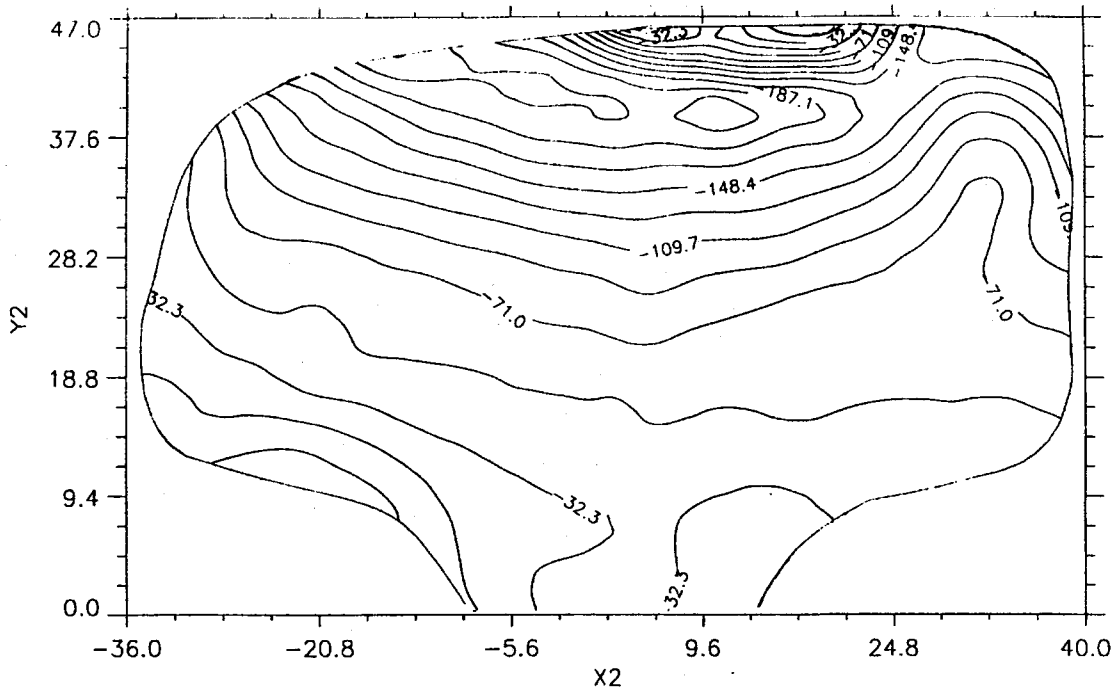

Fig. 38 σ_z (MPa)
(rail # 2 conformal grinding -- CFI 136 RE25-0881)

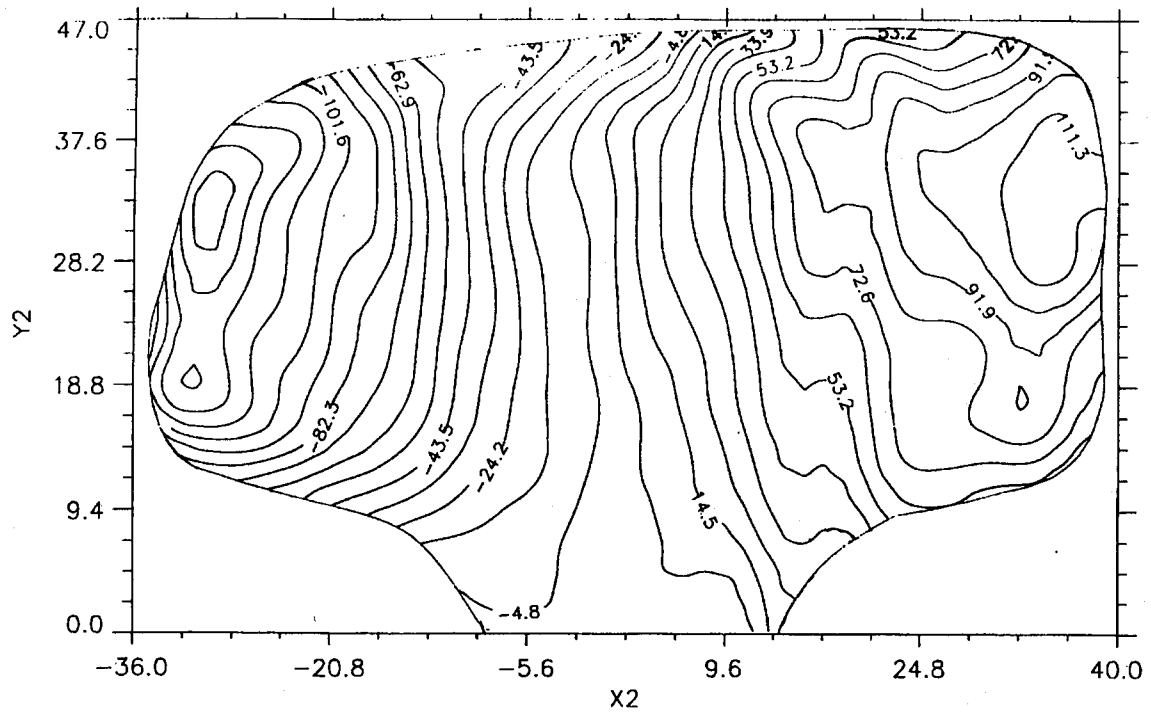

Fig. 39 σ_{xy} (MPa)
(rail # 2 conformal grinding -- CFI 136 RE25-0881)

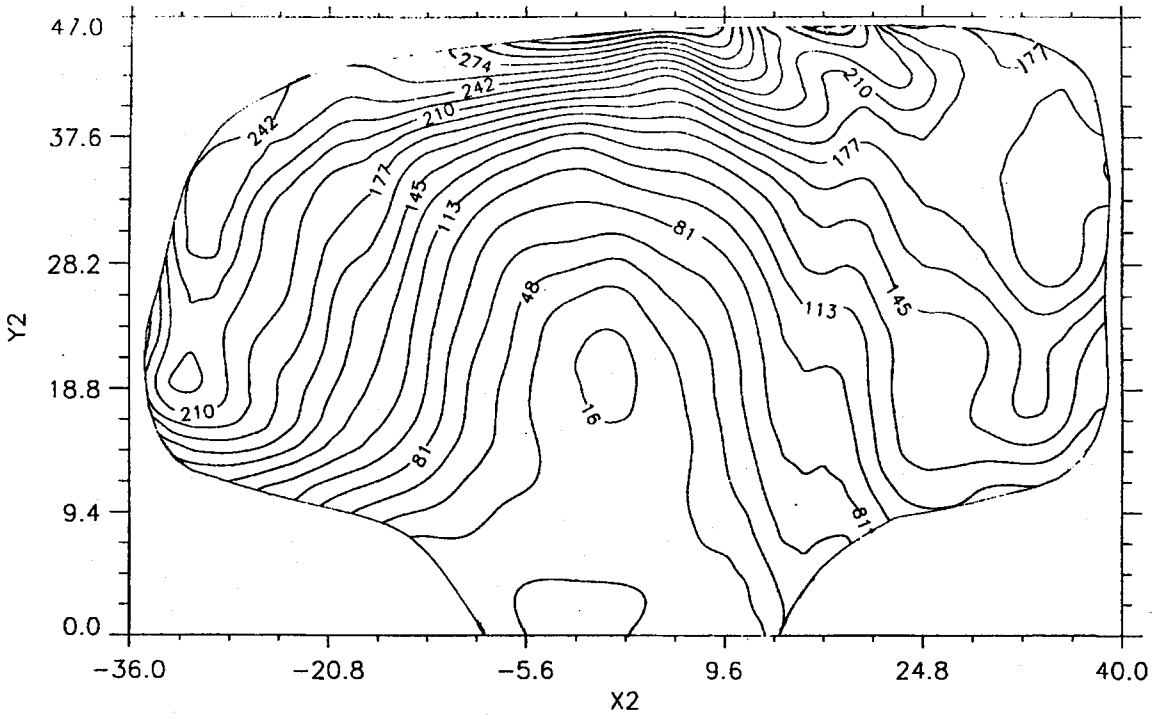

Fig. 40 σ_e (MPa)
(rail # 2 conformal grinding -- CFI 136 RE25-0881)

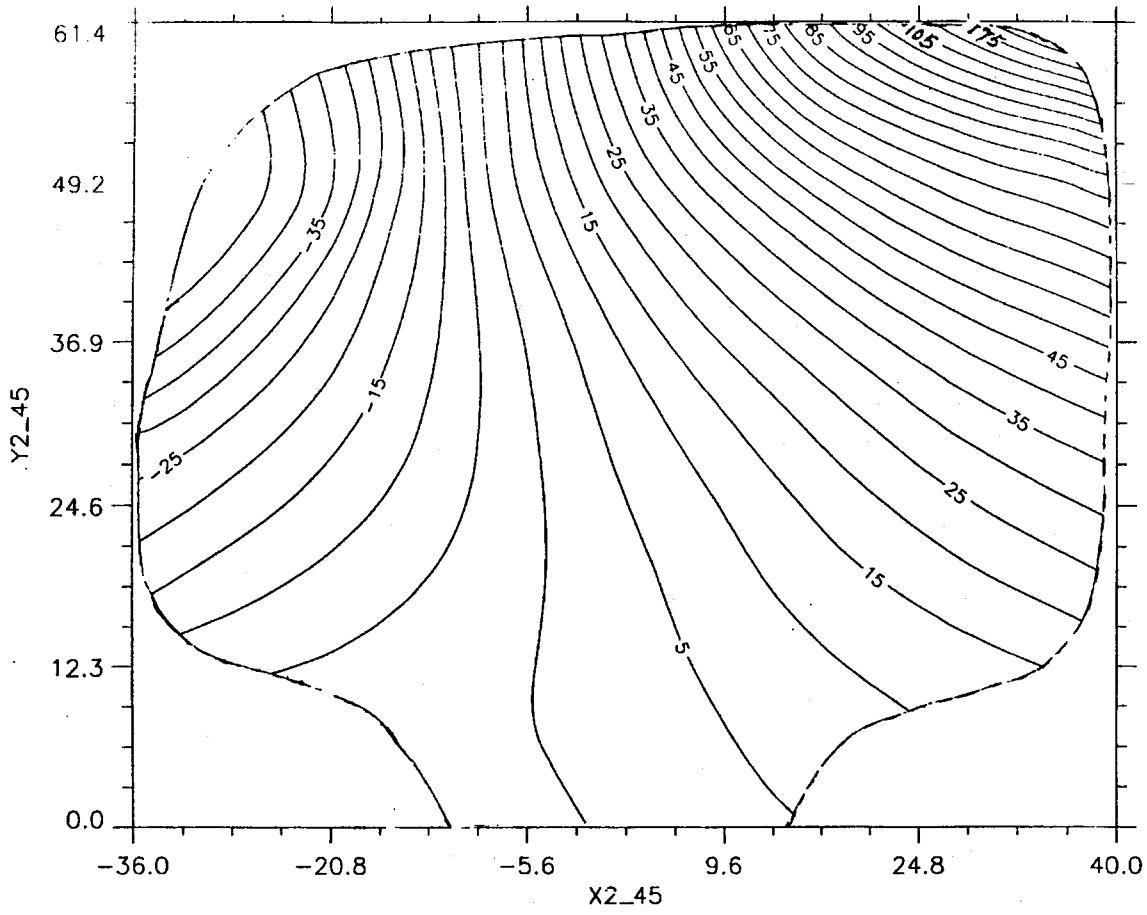

Fig. 41 u-field displacement contours (μm)
(rail # 2 conformal grinding, 45° oblique slice)

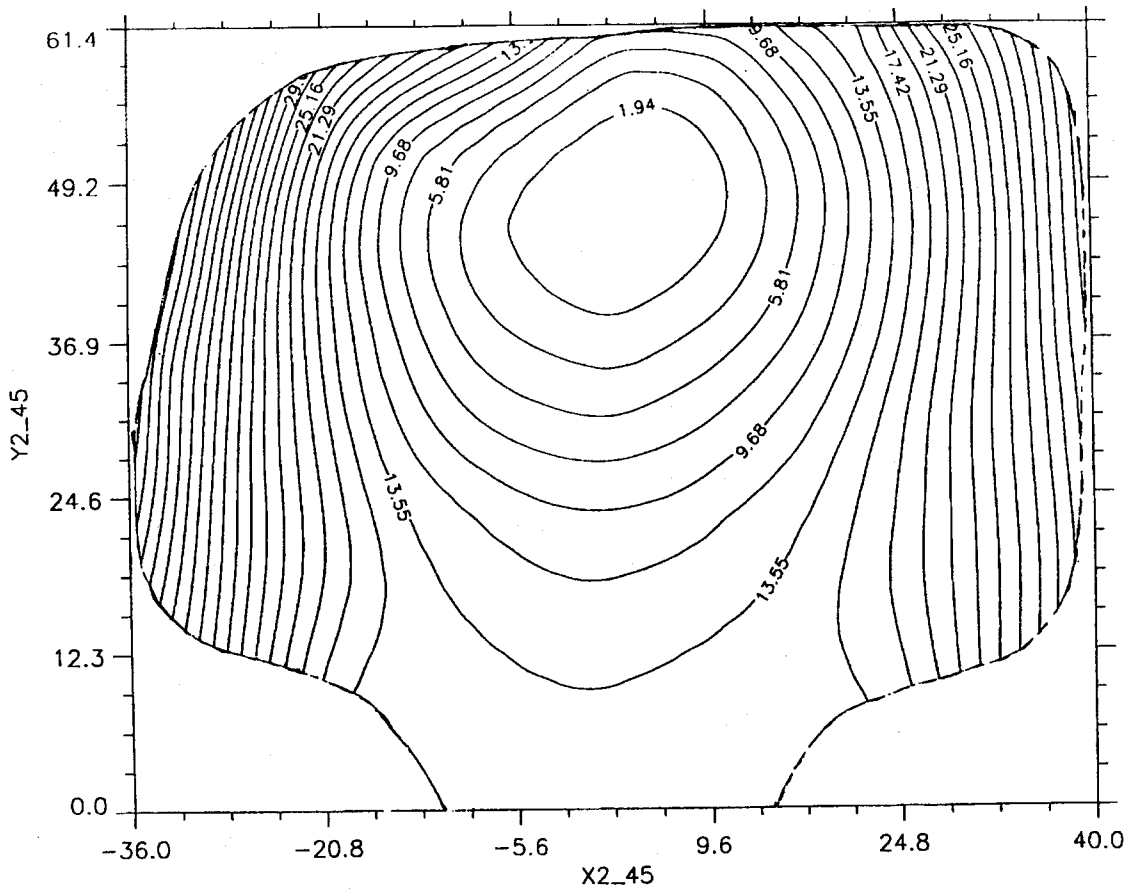

Fig. 42 v-field displacement contours (μm)
(rail # 2 conformal grinding, 45° oblique slice)

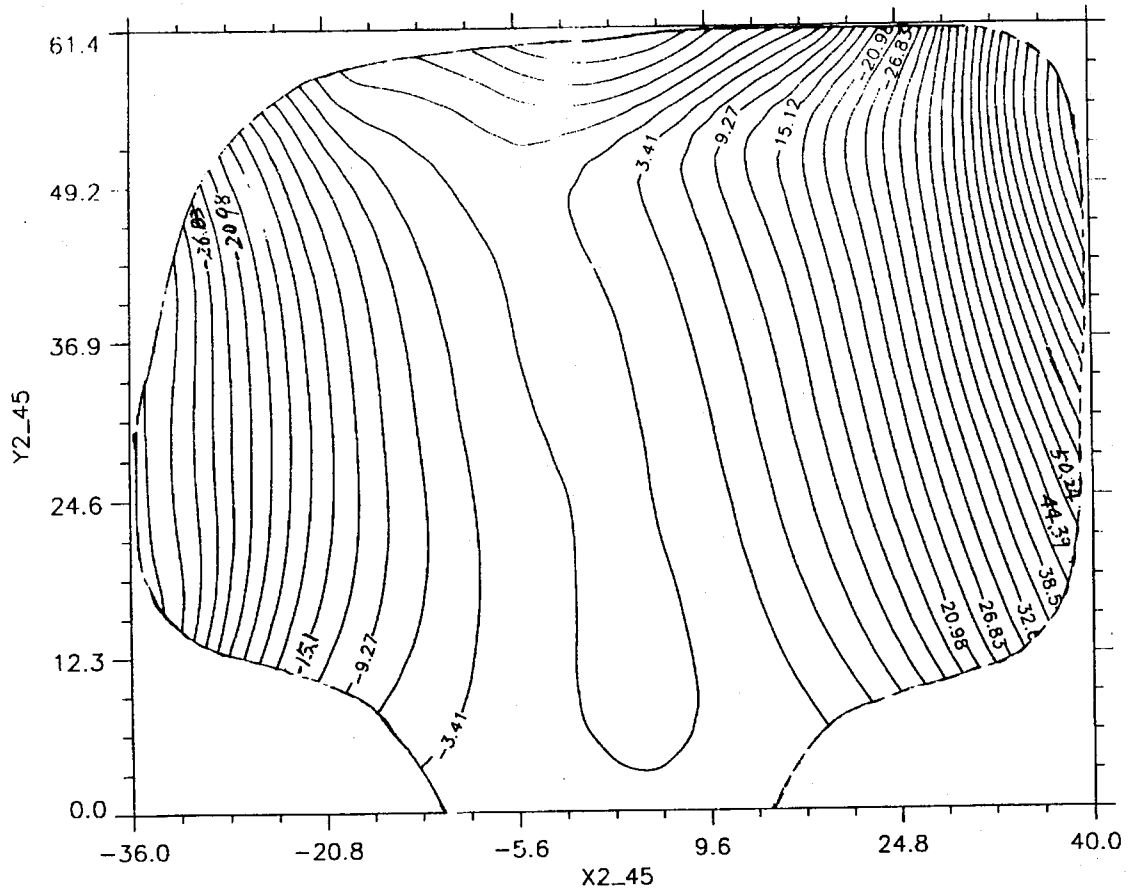

Fig. 43 w-field displacement contours (μm)
(rail # 2 conformal grinding, 45° oblique slice)

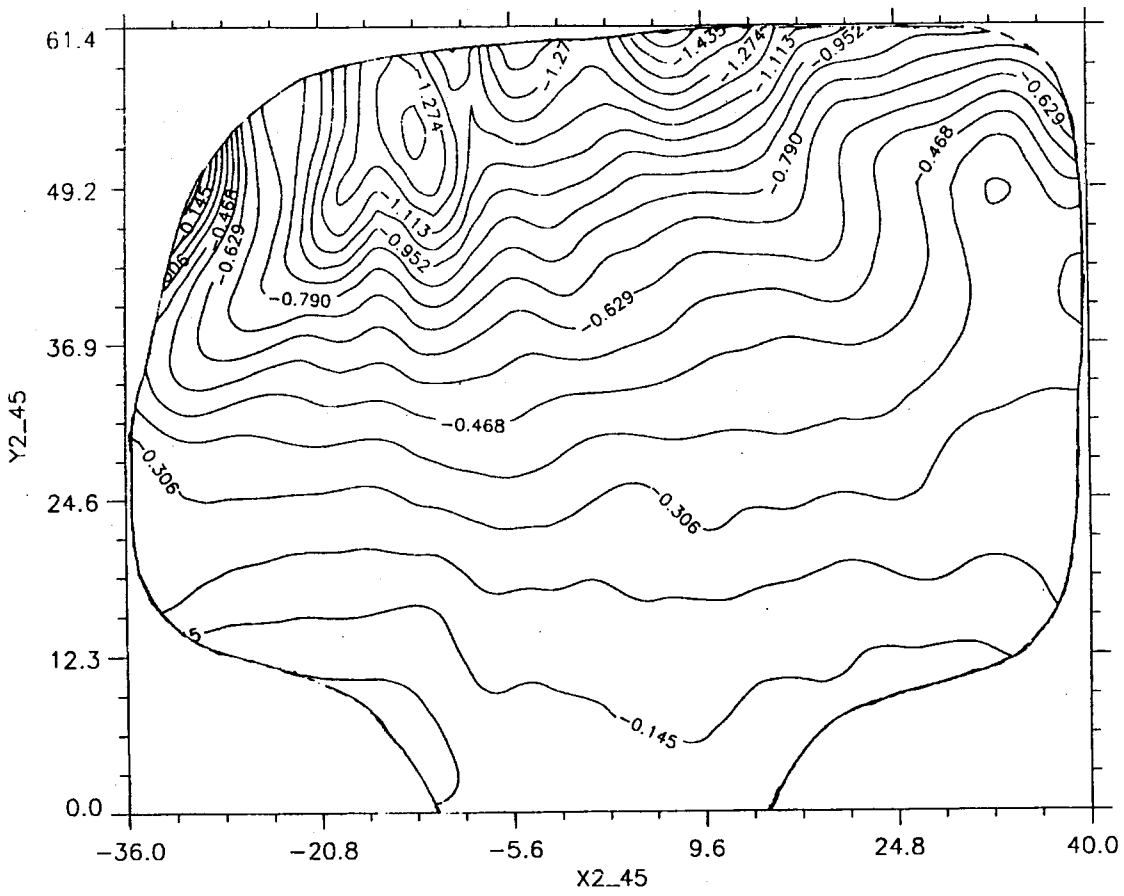

Fig. 44 $\epsilon_{x'}$ (10^{-3})
(rail # 2 conformal grinding, 45° oblique slice)

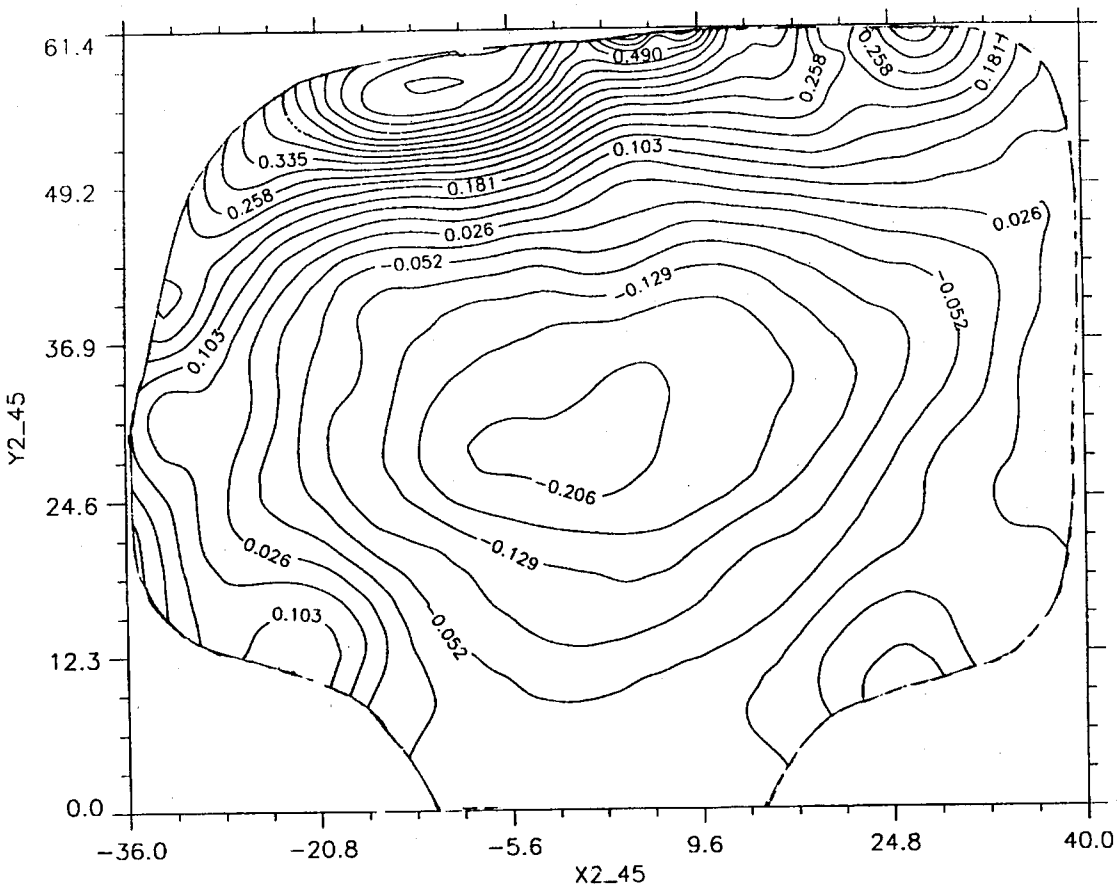

Fig. 45 $\epsilon_{y'}$ (10^{-3})
(rail # 2 conformal grinding, 45° oblique slice)

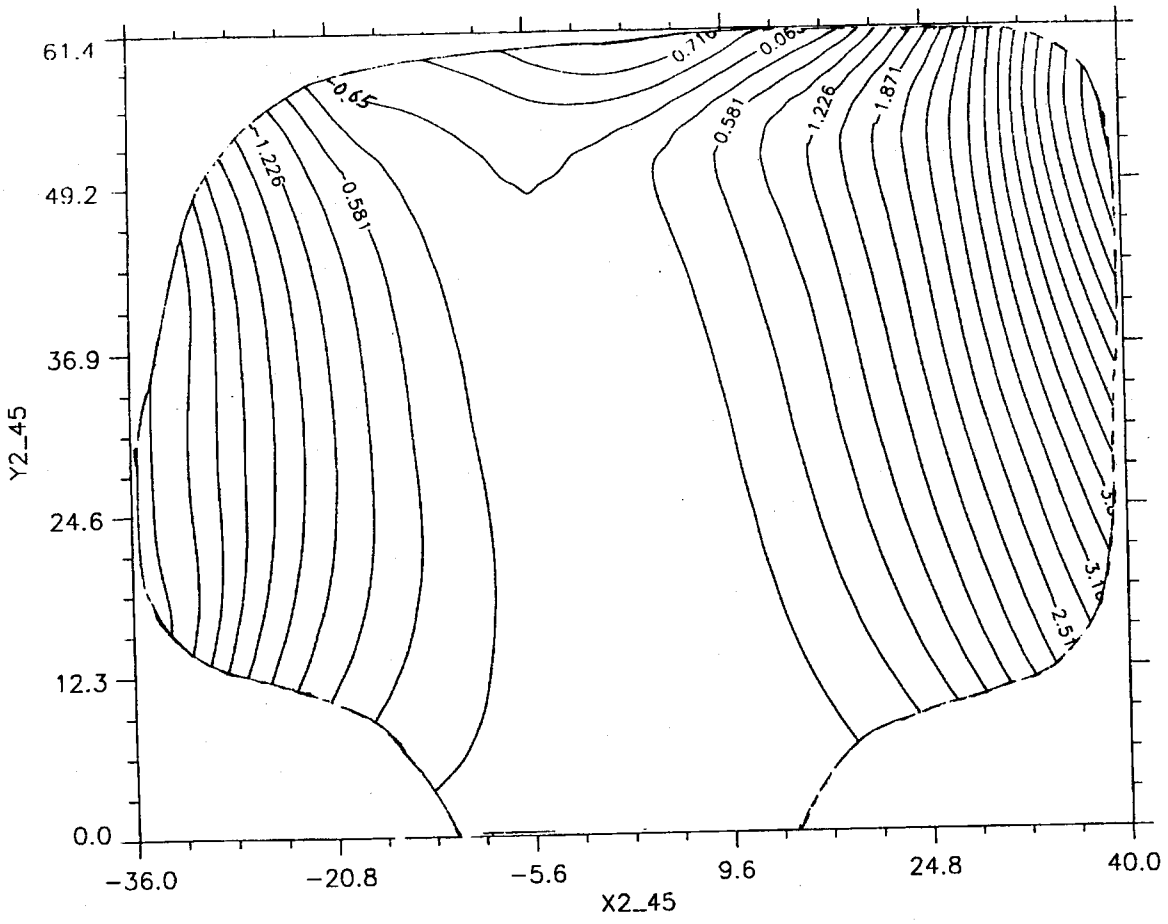

Fig. 46 ϵ_z. (10^{-3})
(rail # 2 conformal grinding, 45° oblique slice)

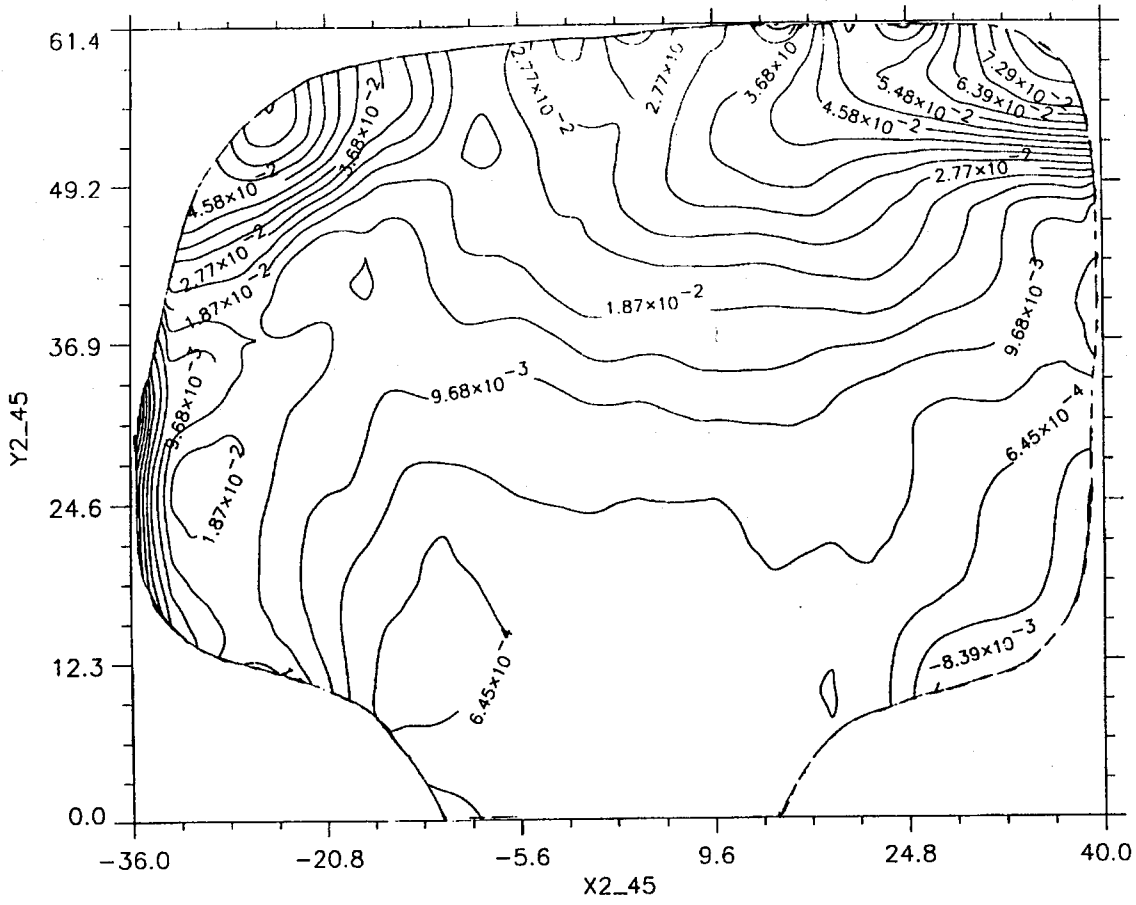

Fig. 47 $\epsilon_{x'y'}$ (10^{-3})
(rail # 2 conformal grinding, 45° oblique slice)

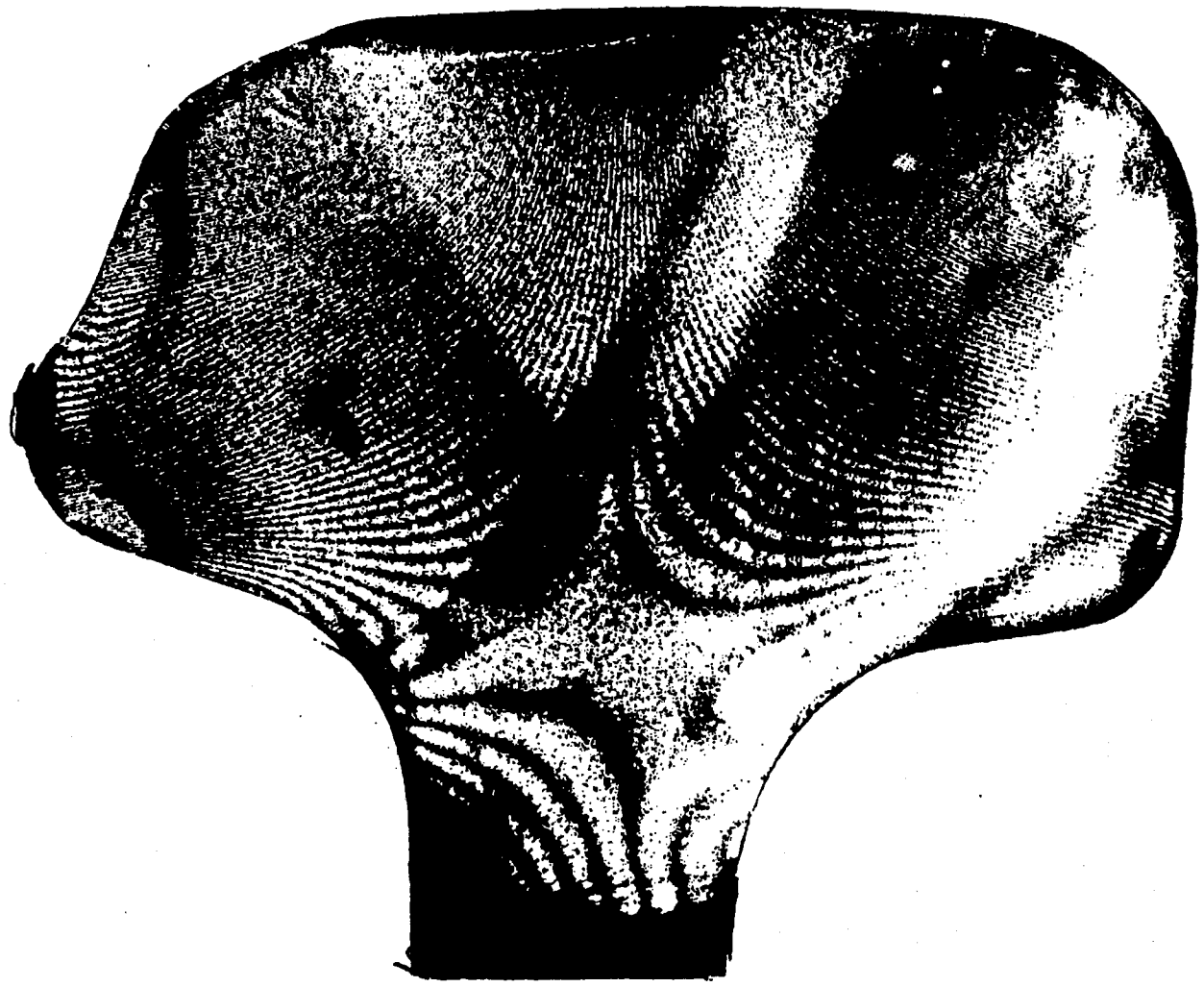

Fig. 48 u-field fringes by moire interferometry
(rail # 4 two-point contact --CFI 136 RE25-1042)

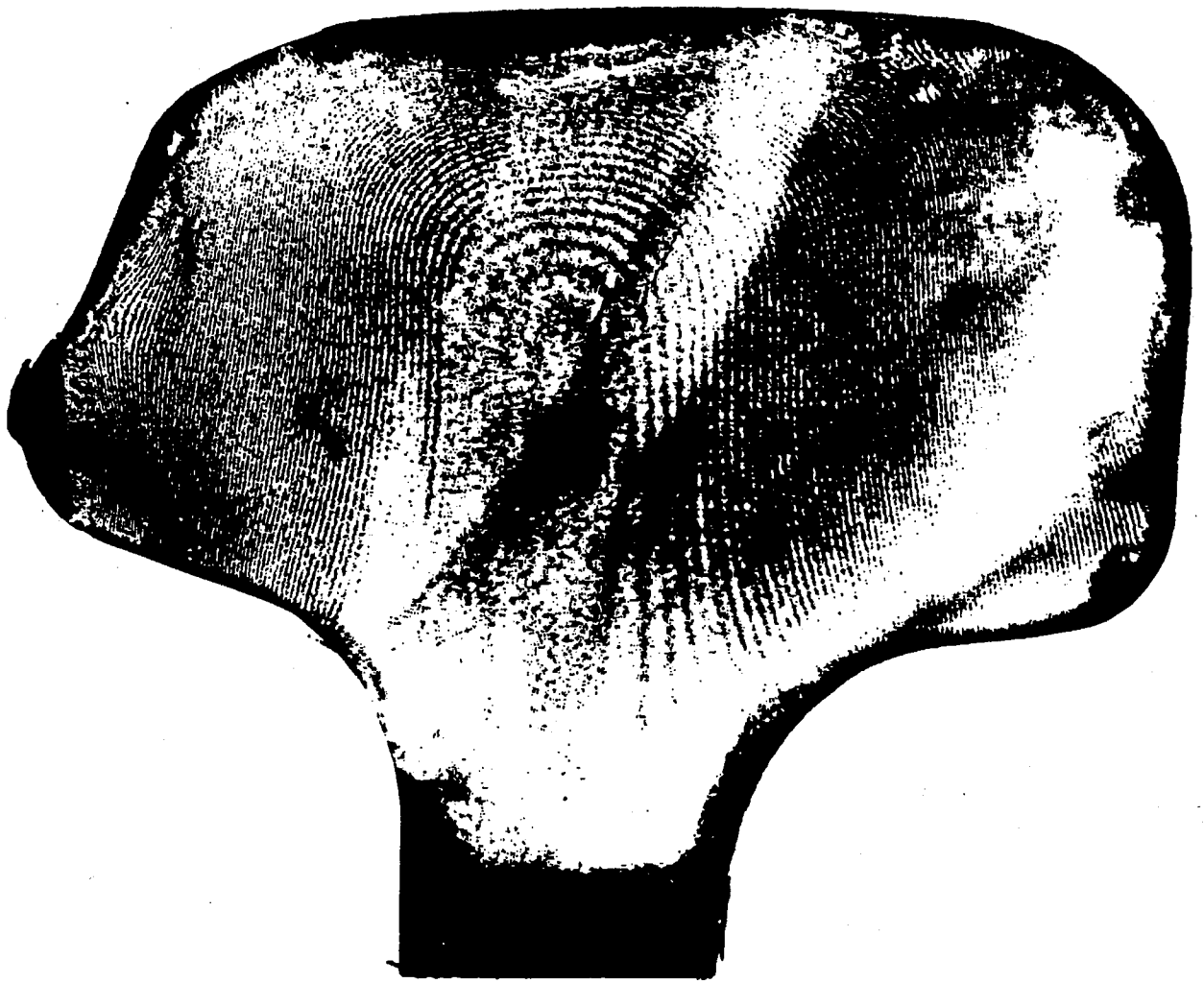

Fig. 49 v-field fringes by moire interferometry
(rail # 4 two-point contact --CFI 136 RE25-1042)

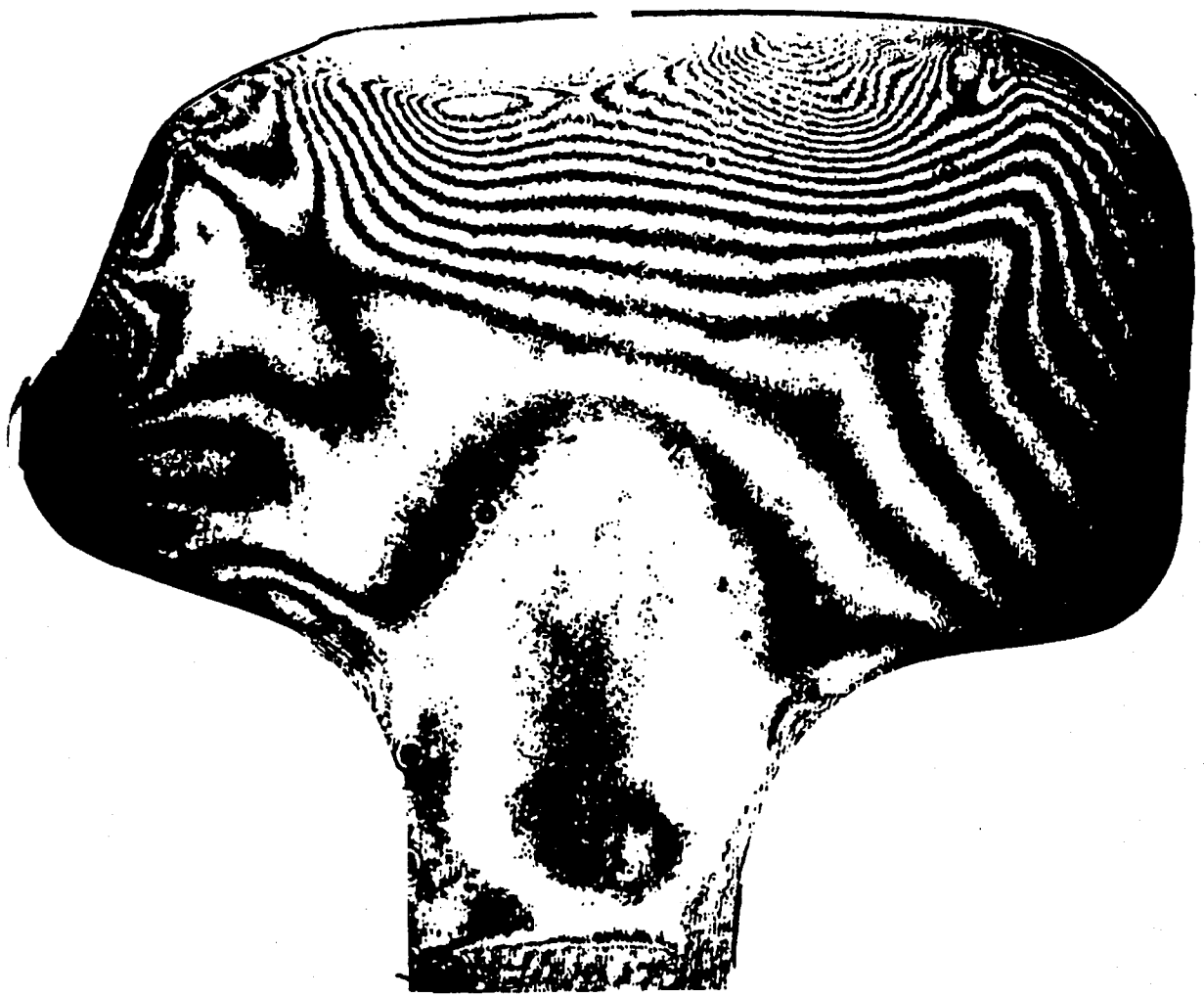

Fig. 50 w-field fringes by Twyman/Green interferometry
(rail # 4 two-point contact --CFI 136 RE25-1042)

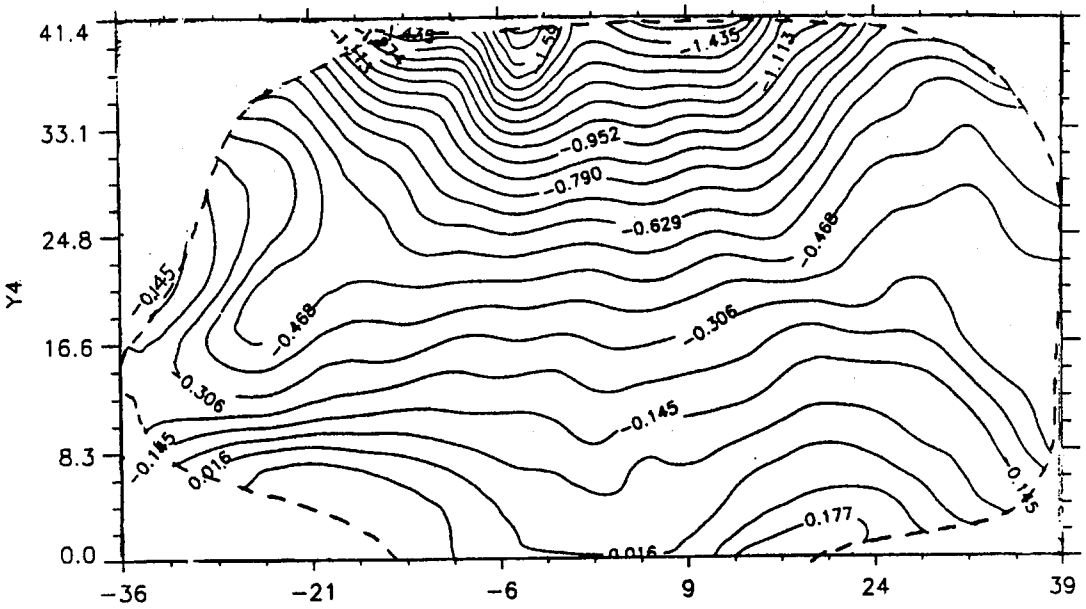

Fig. 51 ϵ_x (10^{-3})
(rail # 4 two-point contact --CFI 136 RE25-1042)

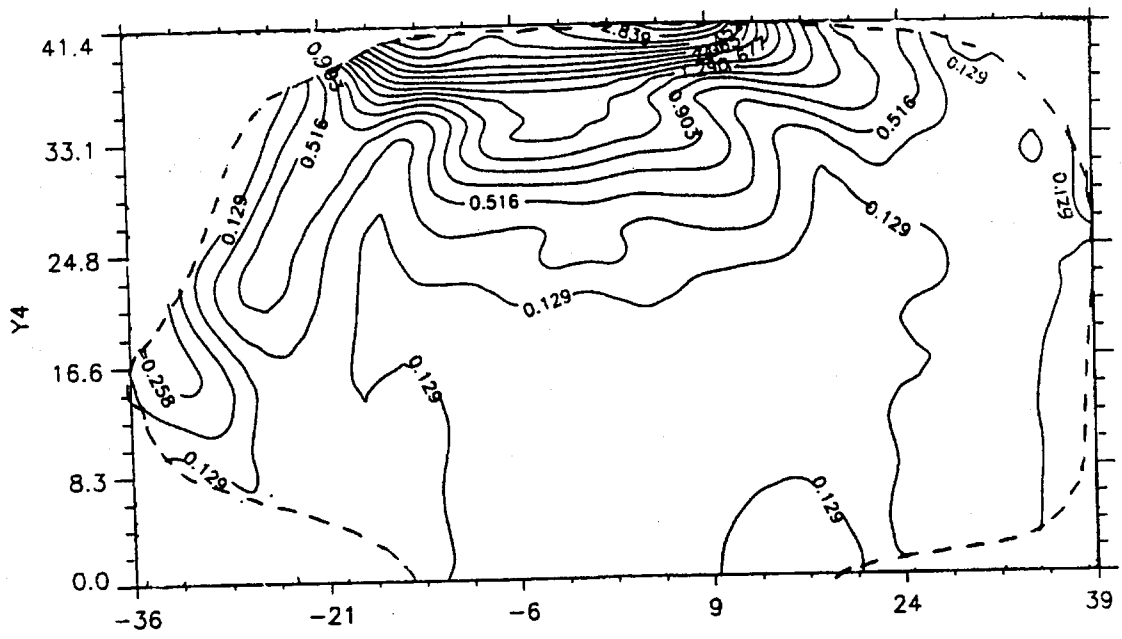

Fig. 52 ϵ_y (10^{-3})
(rail # 4 two-point contact --CFI 136 RE25-1042)

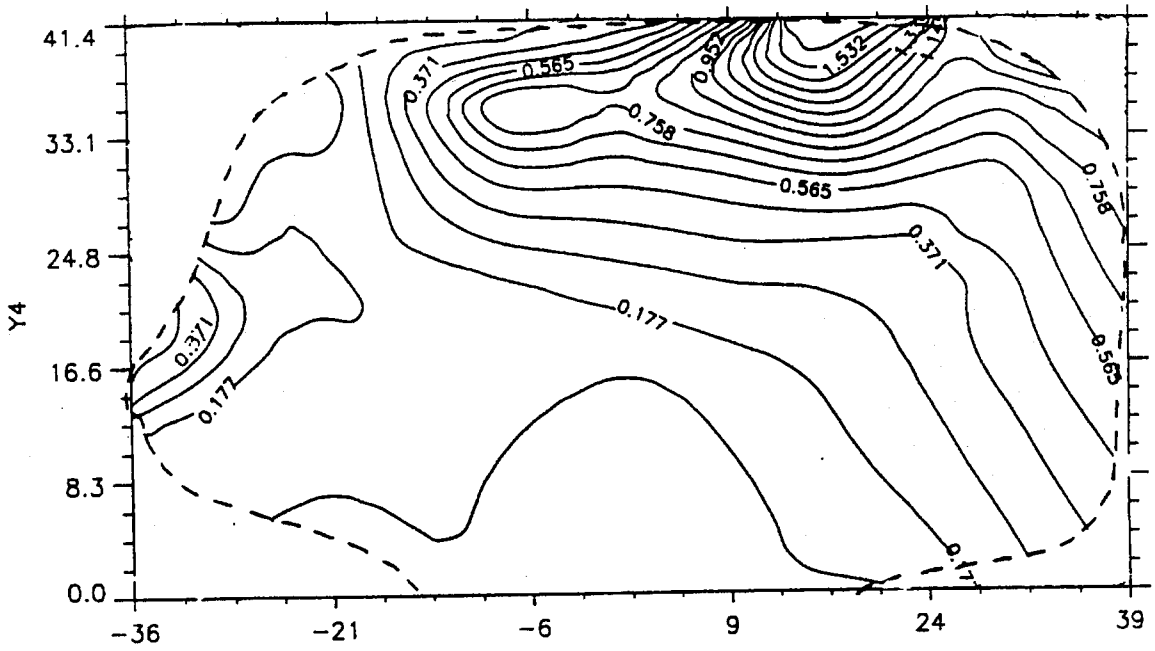

Fig. 53 ϵ_z (10^{-3})
(rail # 4 two-point contact --CFI 136 RE25-1042)

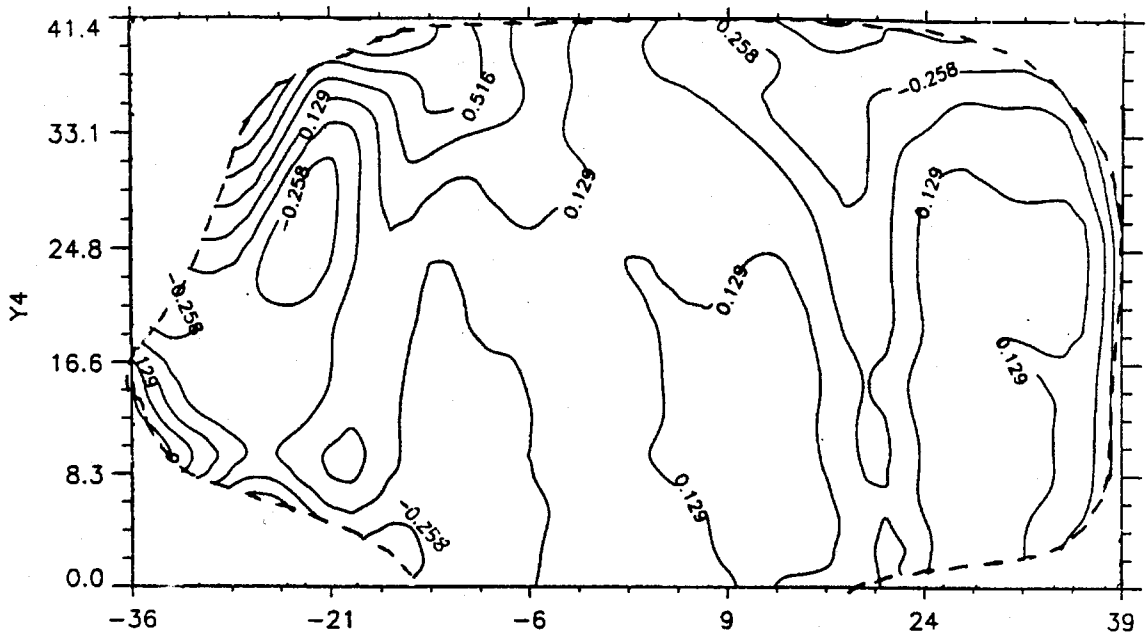

Fig. 54 ϵ_{xy} (10^{-3})
(rail # 4 two-point contact --CFI 136 RE25-1042)

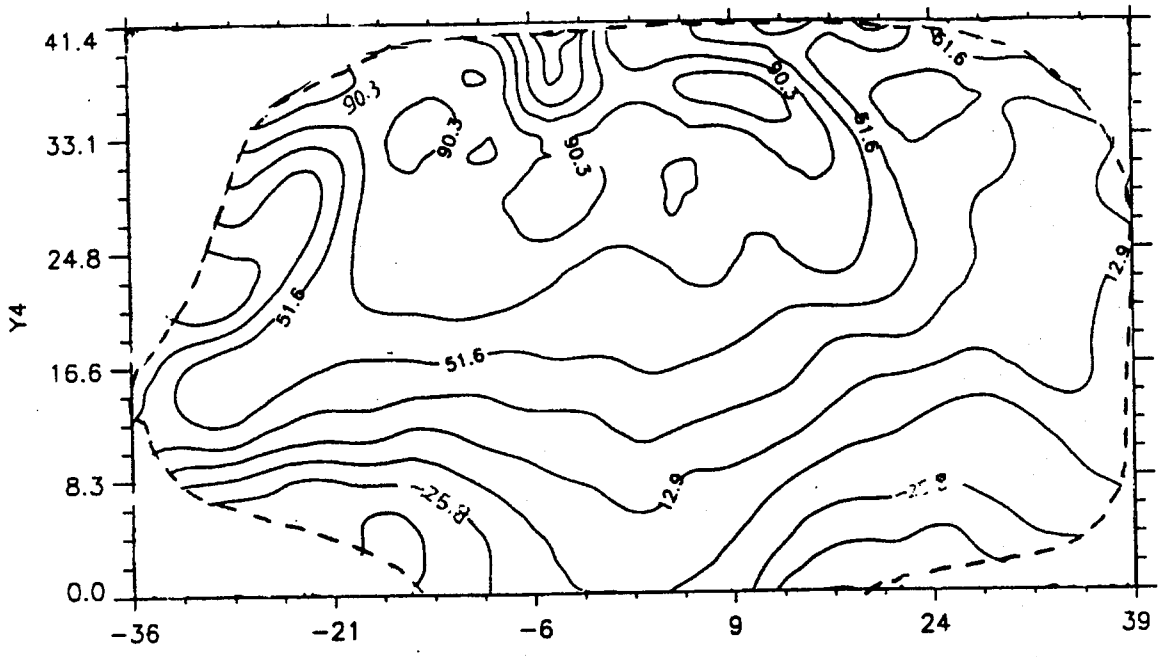

Fig. 55 σ_x (MPa)
(rail # 4 two-point contact --CFI 136 RE25-1042)

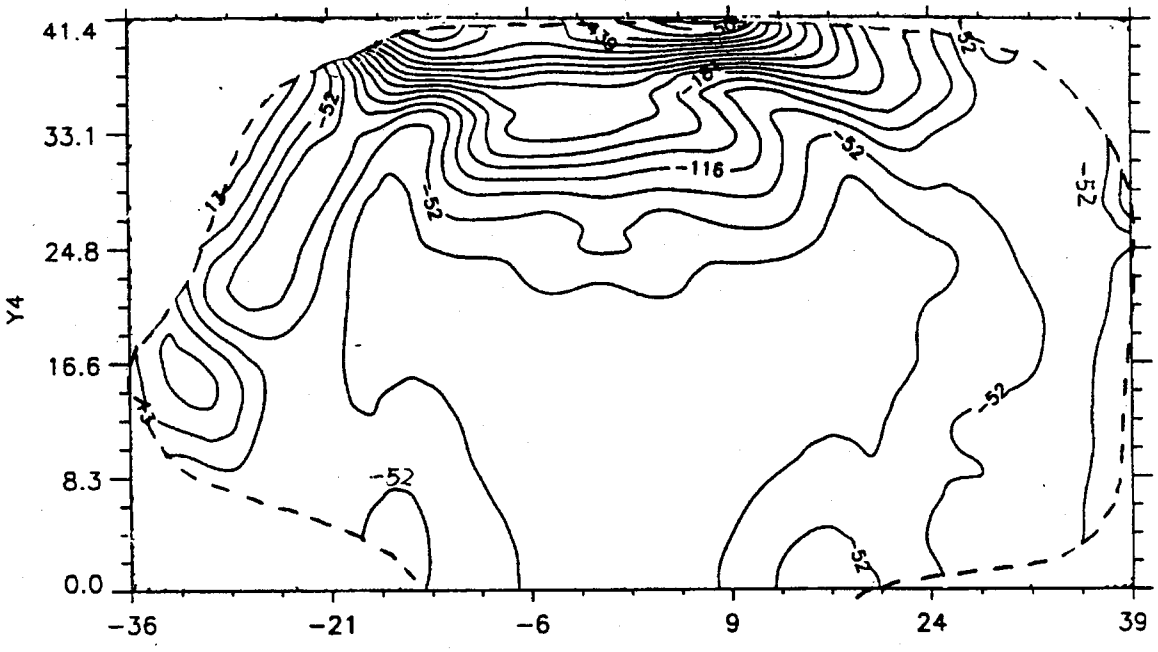

Fig. 56 σ_y (MPa)
(rail # 4 two-point contact --CFI 136 RE25-1042)

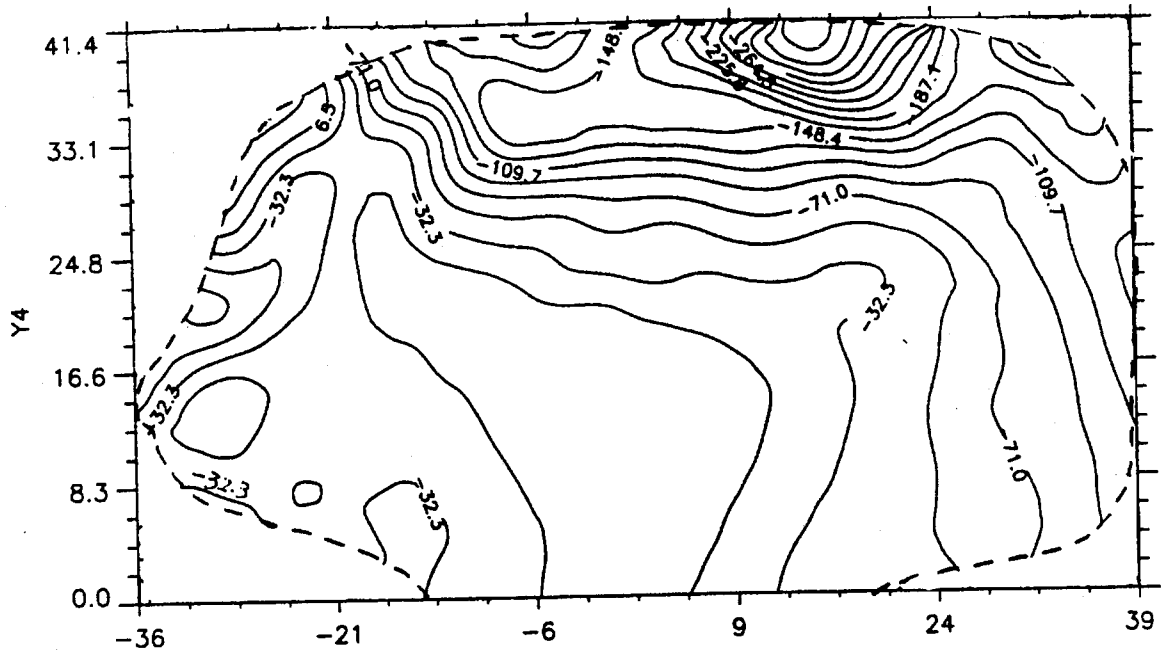

Fig. 57 σ_z (MPa)
(rail # 4 two-point contact --CFI 136 RE25-1042)

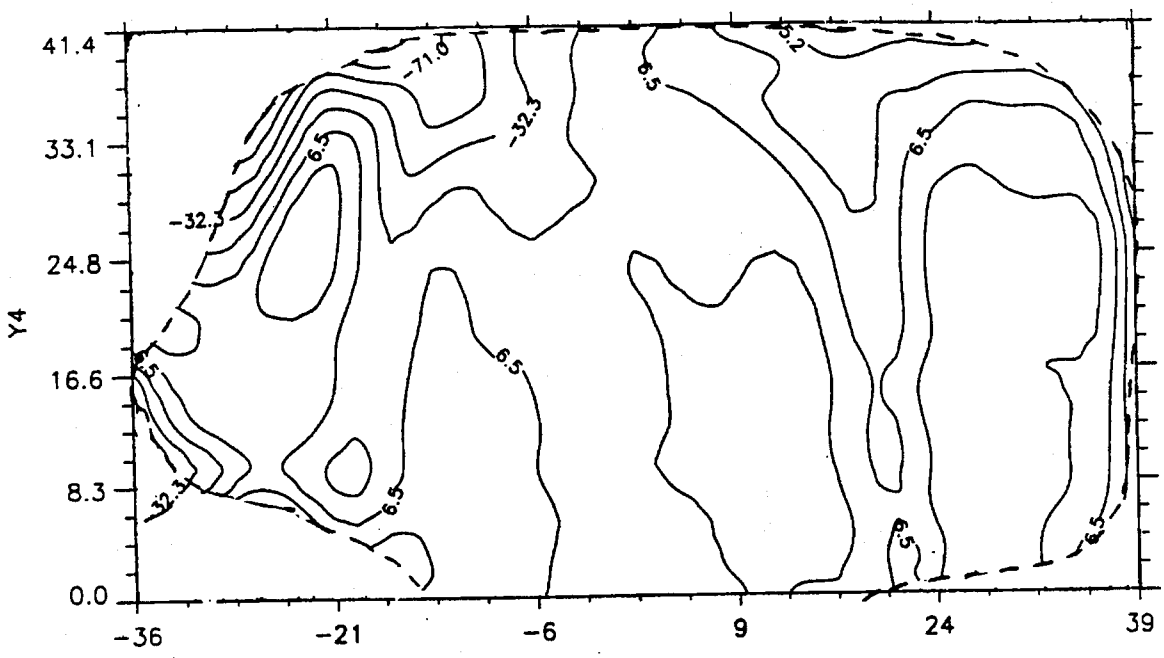

Fig. 58 σ_{xy} (MPa)
(rail # 4 two-point contact --CFI 136 RE25-1042)

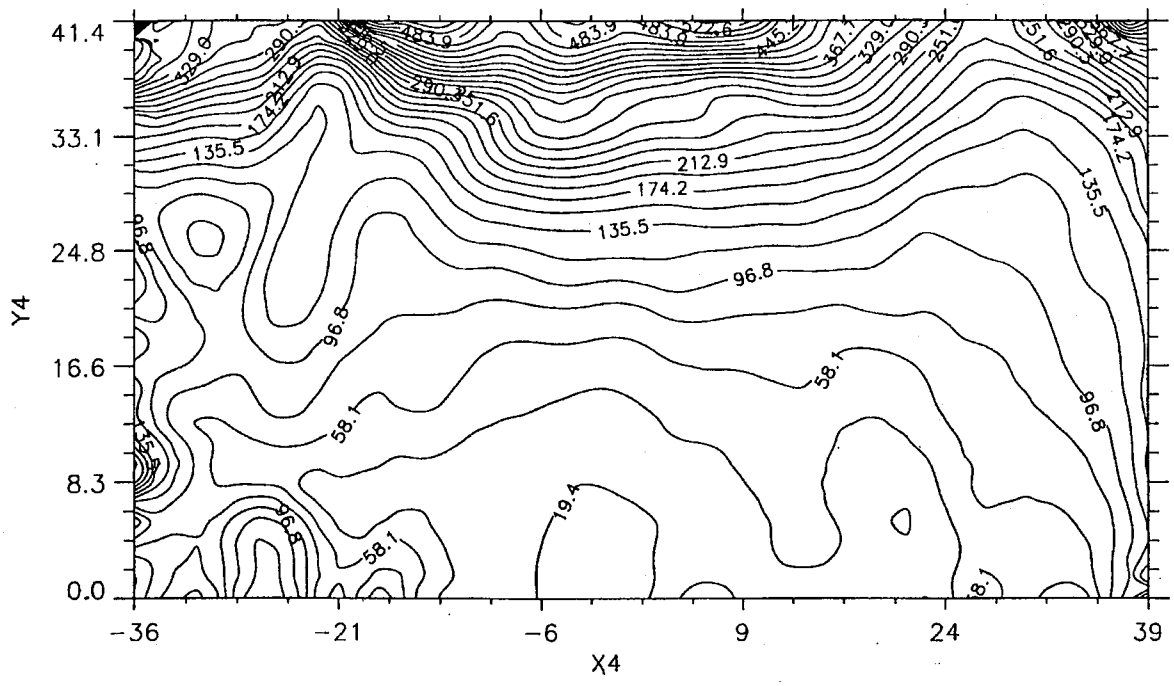

Fig. 59 effective stress σ_e (MPa)
(rail # 4 two-point contact --CFI 136 RE25-1042)

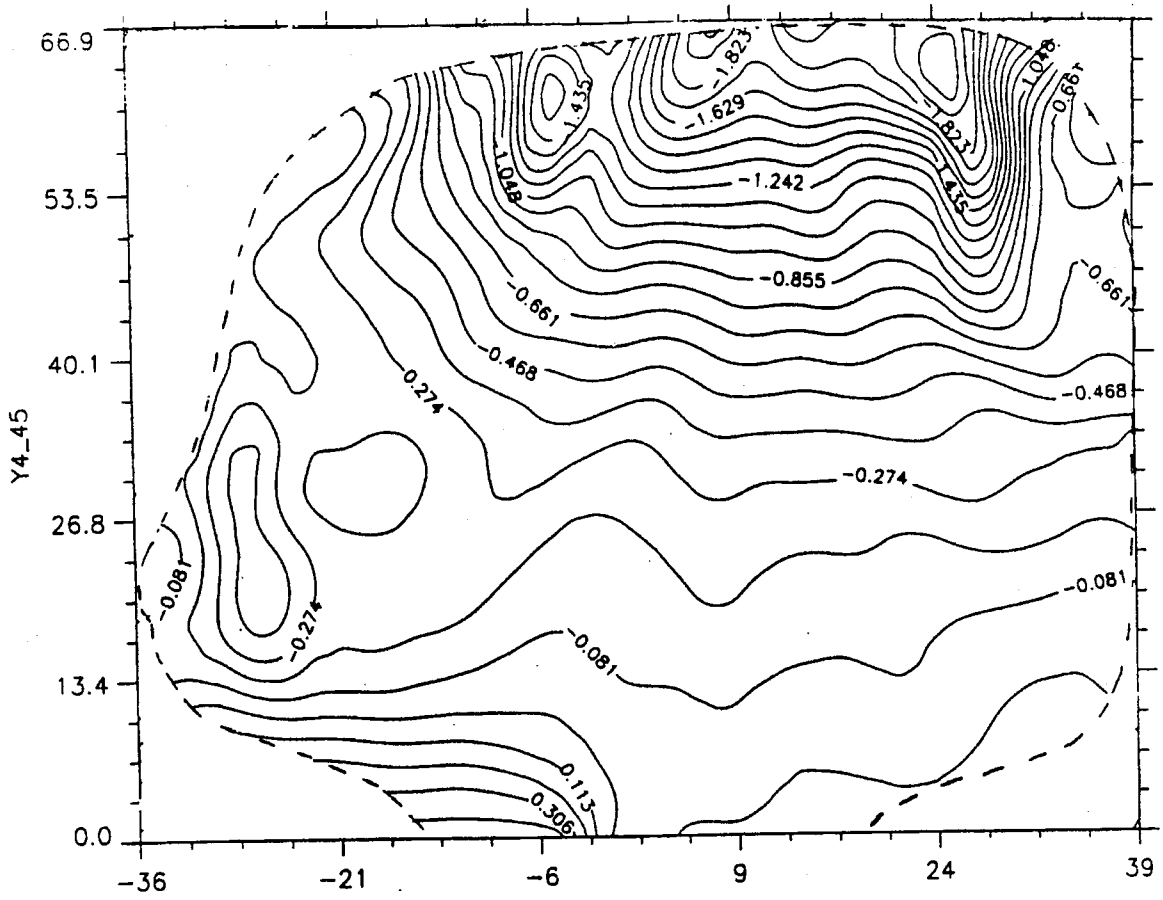

Fig. 60 $\epsilon_{x'}$ (10^{-3})
(rail # 4 two point contact, 45° oblique slice)

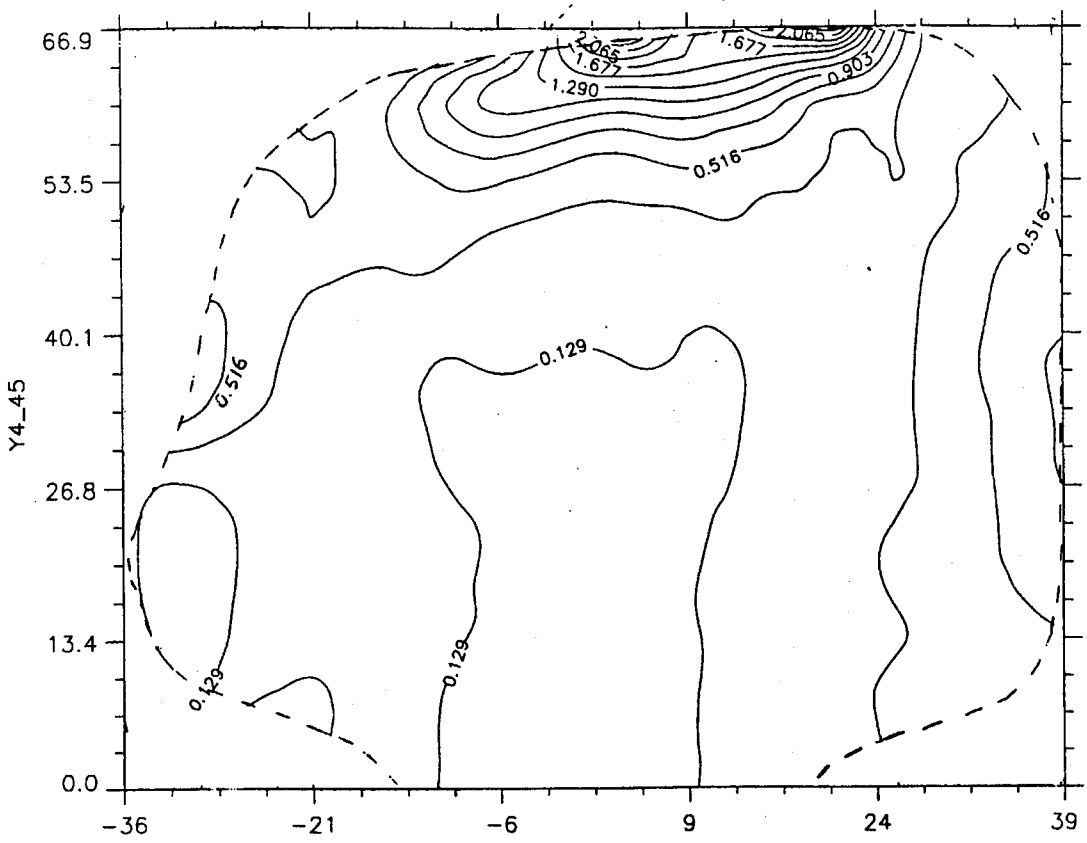

Fig. 61 $\epsilon_{y'}$ (10^{-3})
(rail # 4 two point contact, 45° oblique slice)

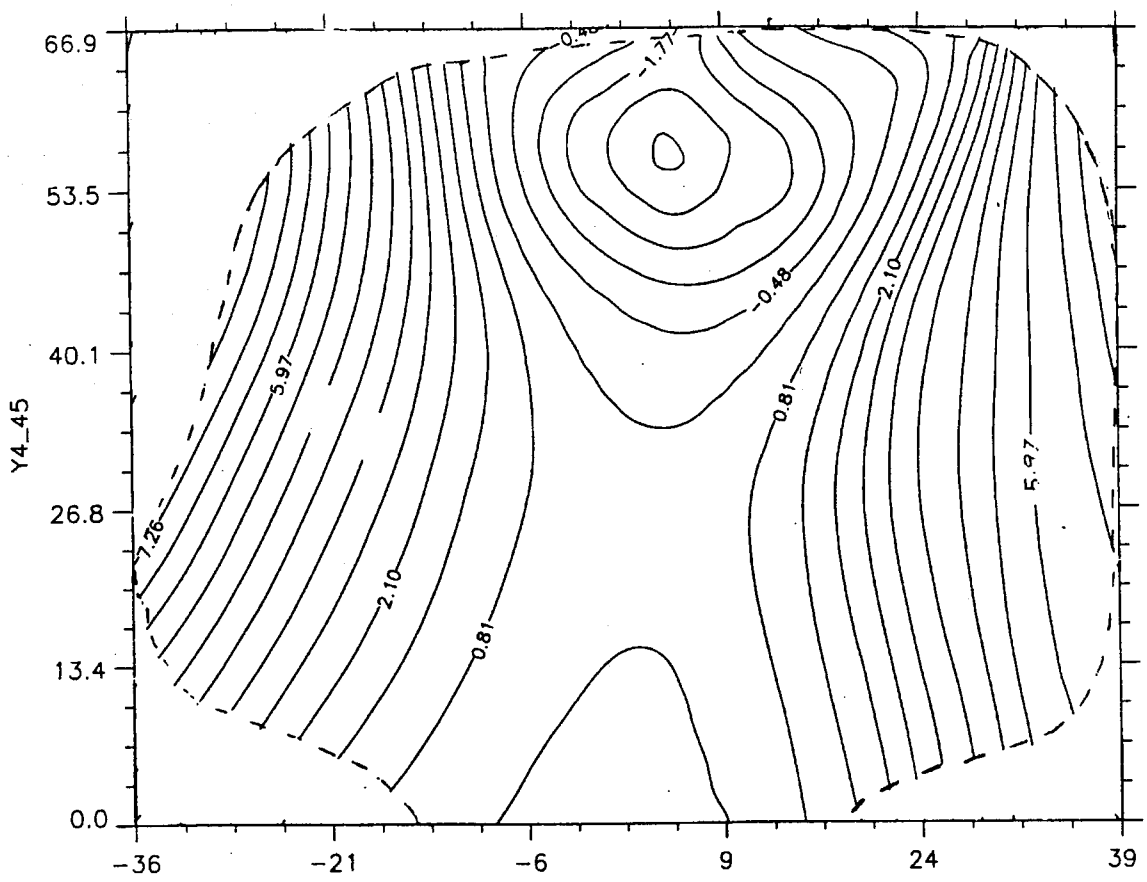

Fig. 62 ϵ_z, (10^{-3})
(rail # 4 two point contact, 45° oblique slice)

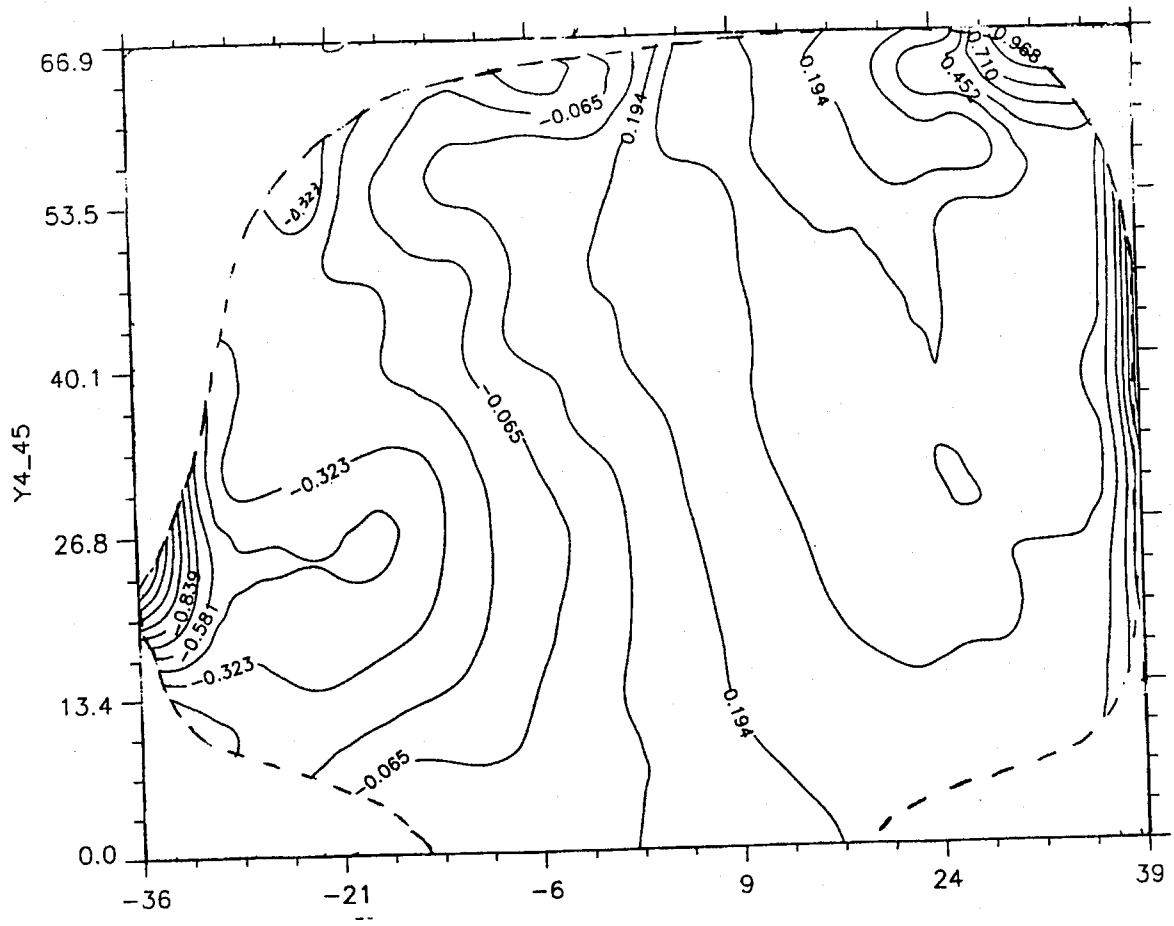

Fig. 63 $\epsilon_{x'y'}$ (10^{-3})
(rail # 4 two point contact, 45° oblique slice)

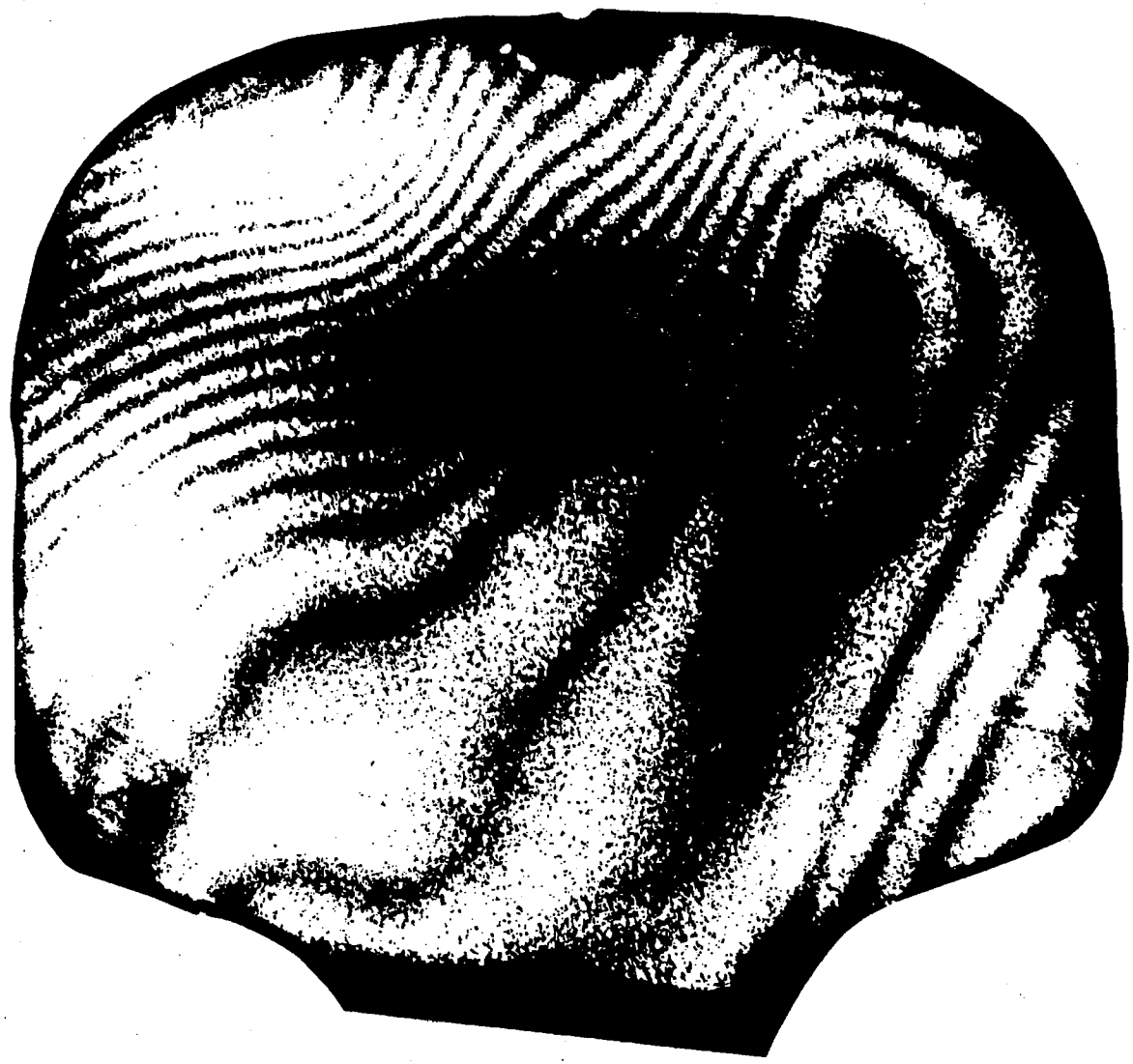

Fig. 64 u-field fringes by moire interferometry
(rail # 5 new CFI, 45° oblique slice)

Fig. 65 v-field fringes by moire interferometry
(rail # 5 new CFI, 45° oblique slice)

Fig. 66 w-field fringes by Twyman/Green interferometry
(rail # 5 new CFI, 45° oblique slice)

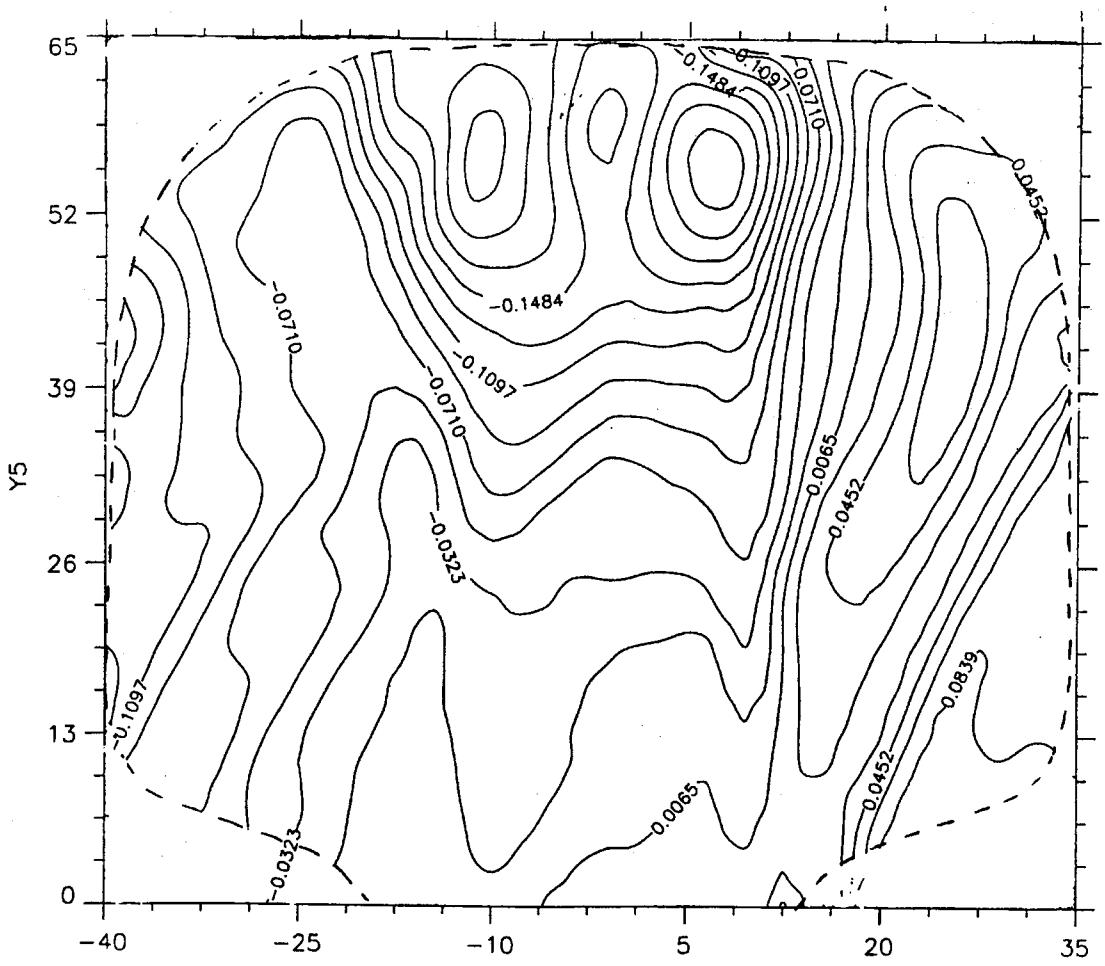

Fig. 67 $\epsilon_{x'}$ (10^{-3})
(rail # 5 new CFI, 45° oblique slice)

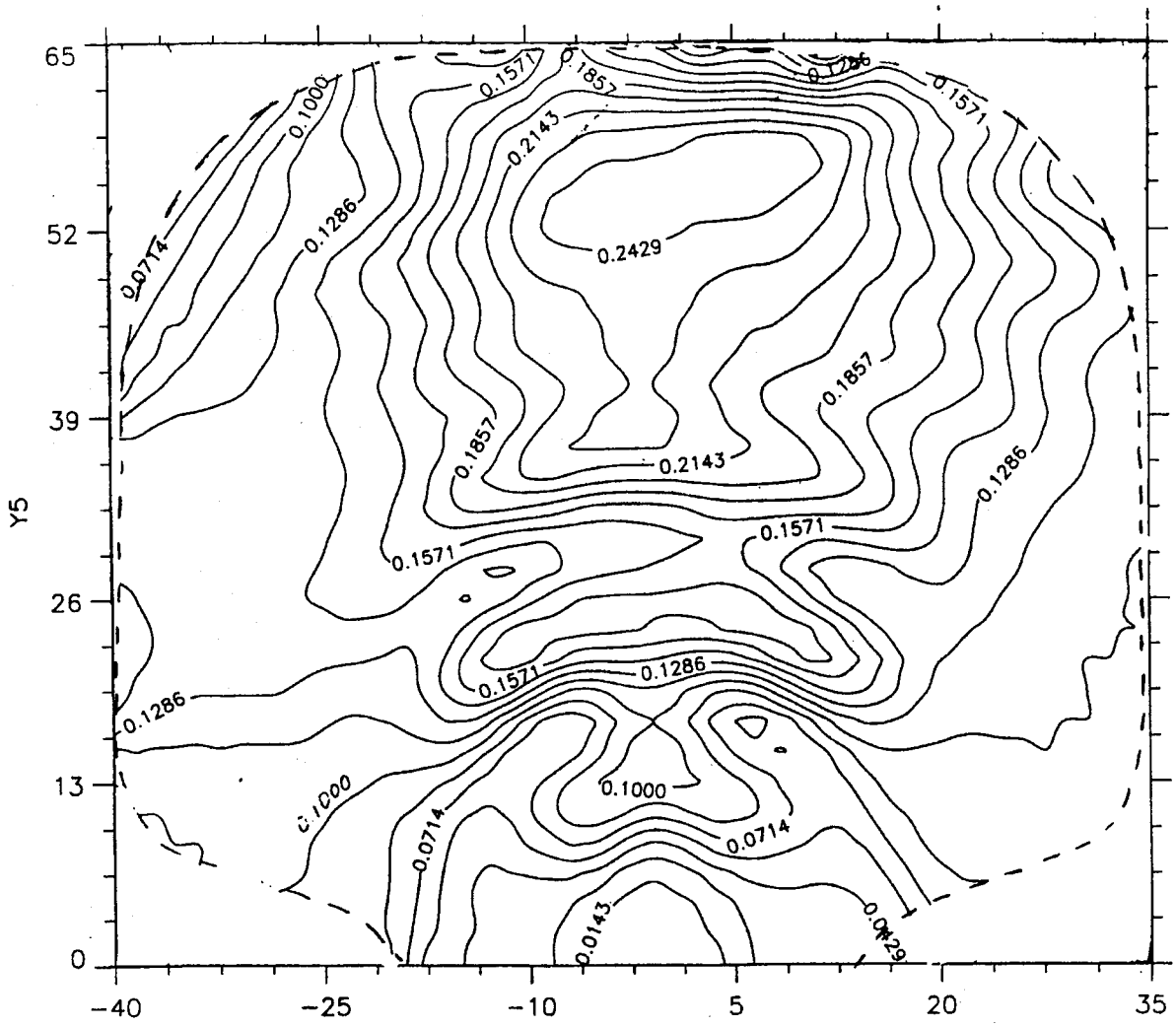

Fig. 68 $\epsilon_{y'}$ (10^{-3})
(rail # 5 new CFI, 45° oblique slice)

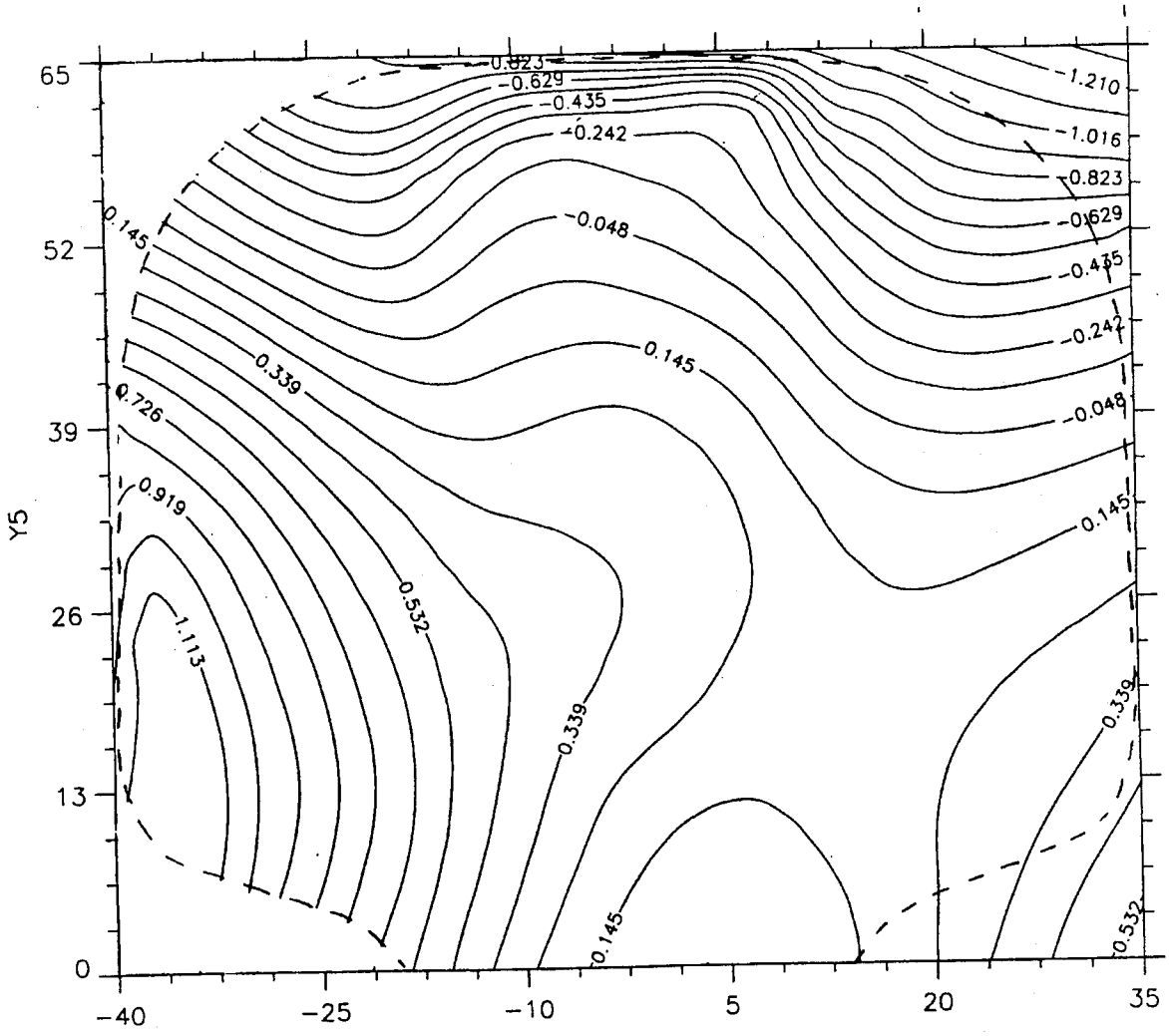

Fig. 69 ϵ_z, (10^{-3})
(rail # 5 new CFI, 45° oblique slice)

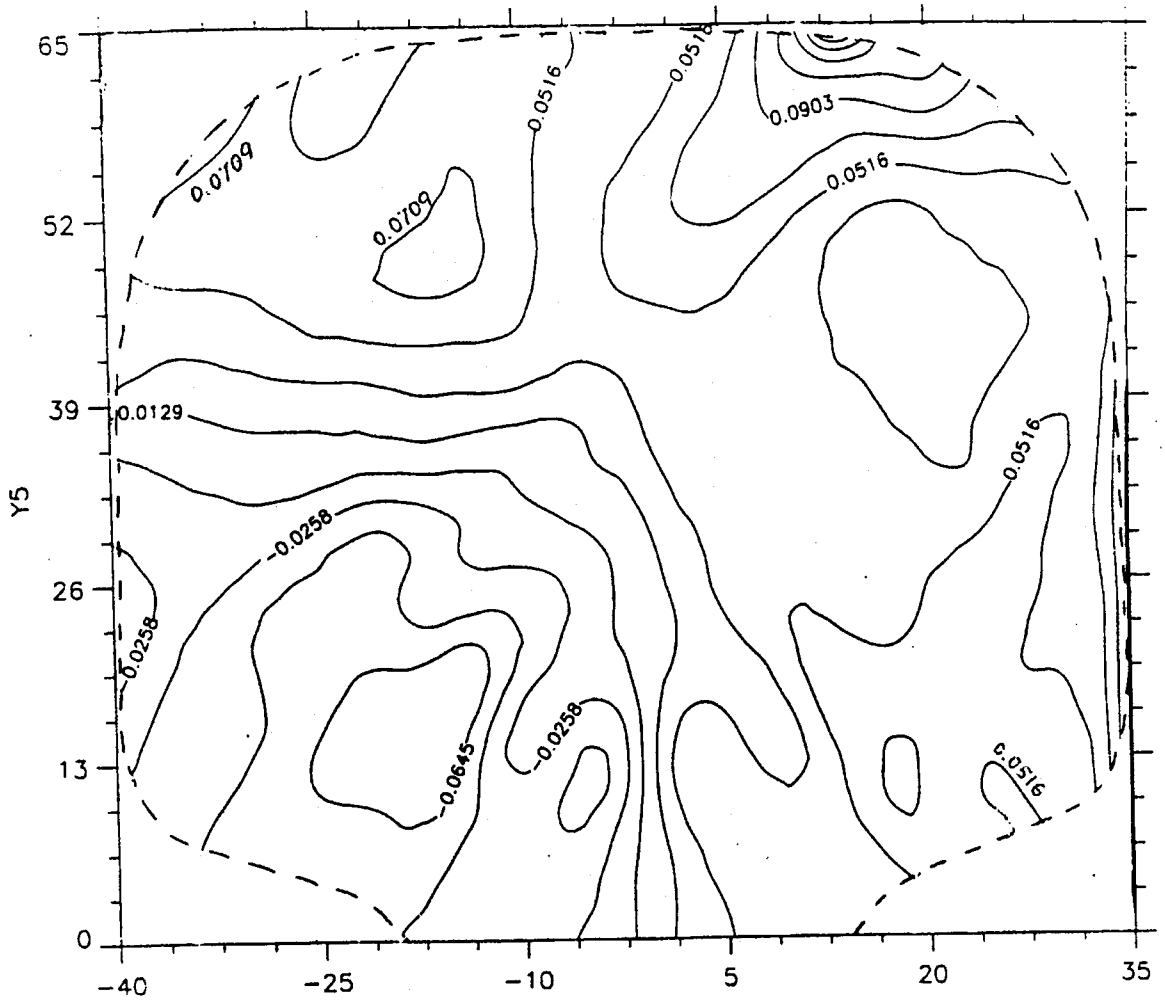

Fig. 70 $\epsilon_{x'y'}$ (10^{-3})
(rail # 5 new CFI, 45° oblique slice)

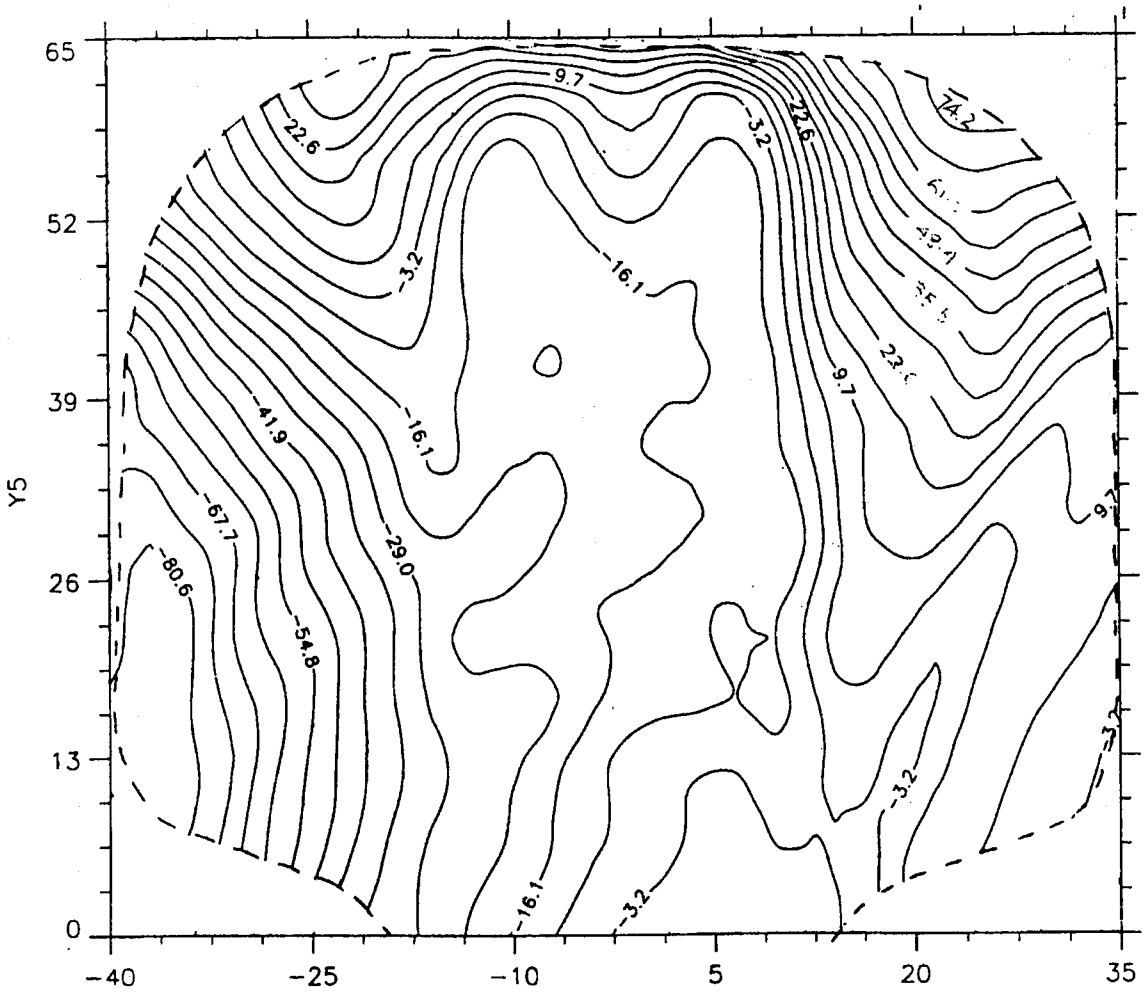

Fig. 71 $\sigma_{x'}$(MPa)
(rail # 5 new CFI, 45° oblique slice)

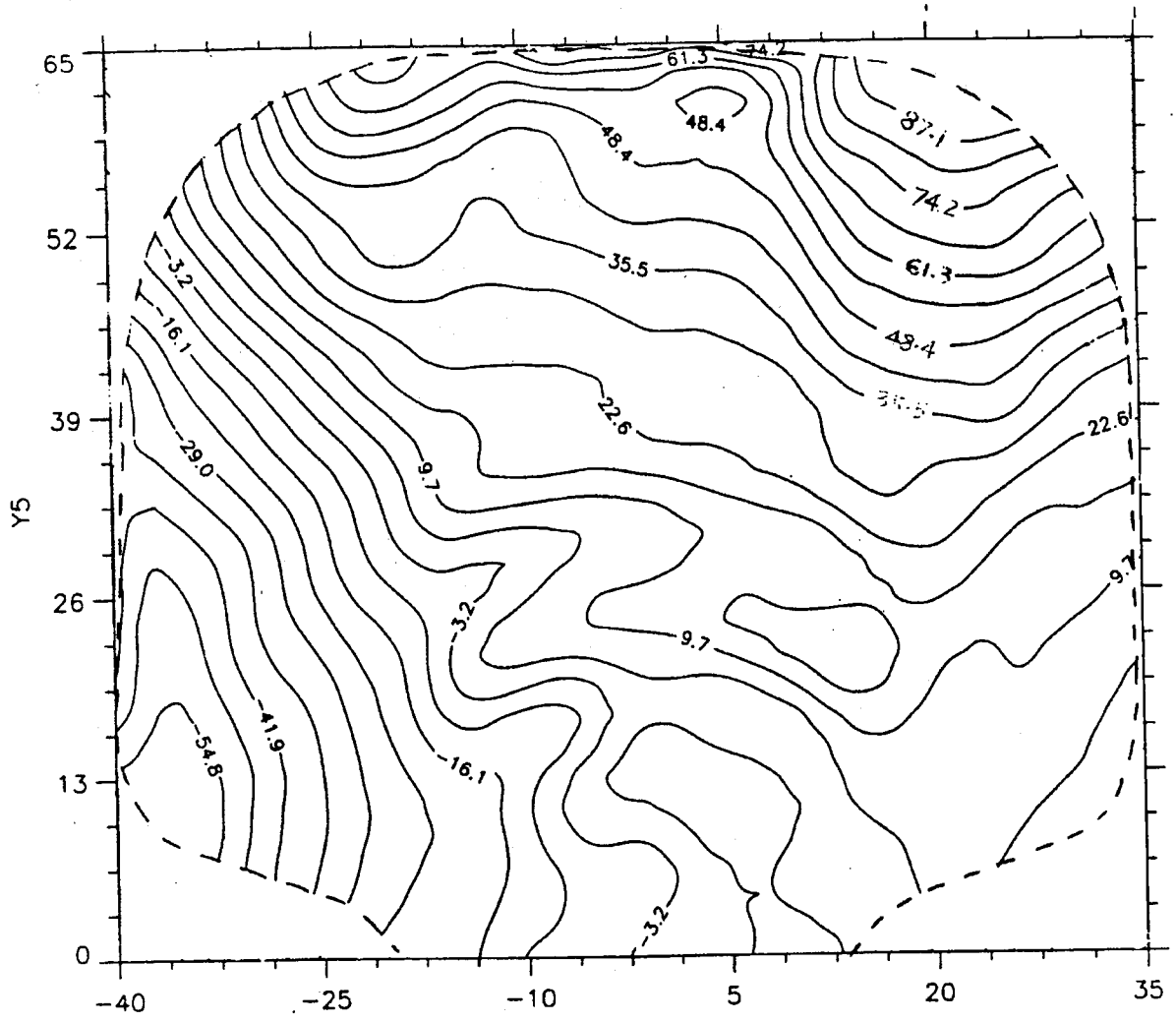

Fig. 72 σ_y, (MPa)
(rail # 5 new CFI, 45° oblique slice)

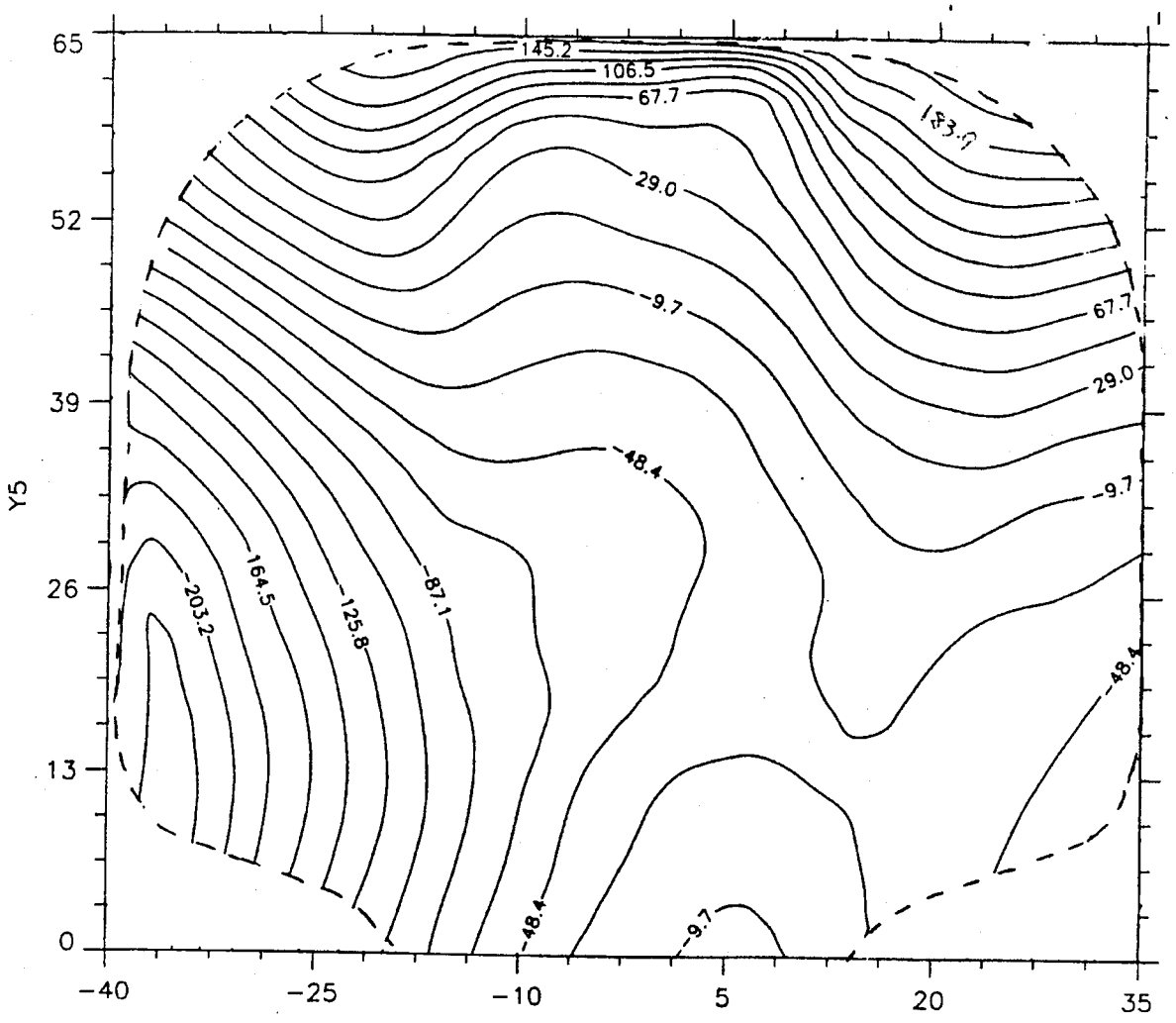

Fig. 73 σ_z, (MPa)
(rail # 5 new CFI, 45° oblique slice)

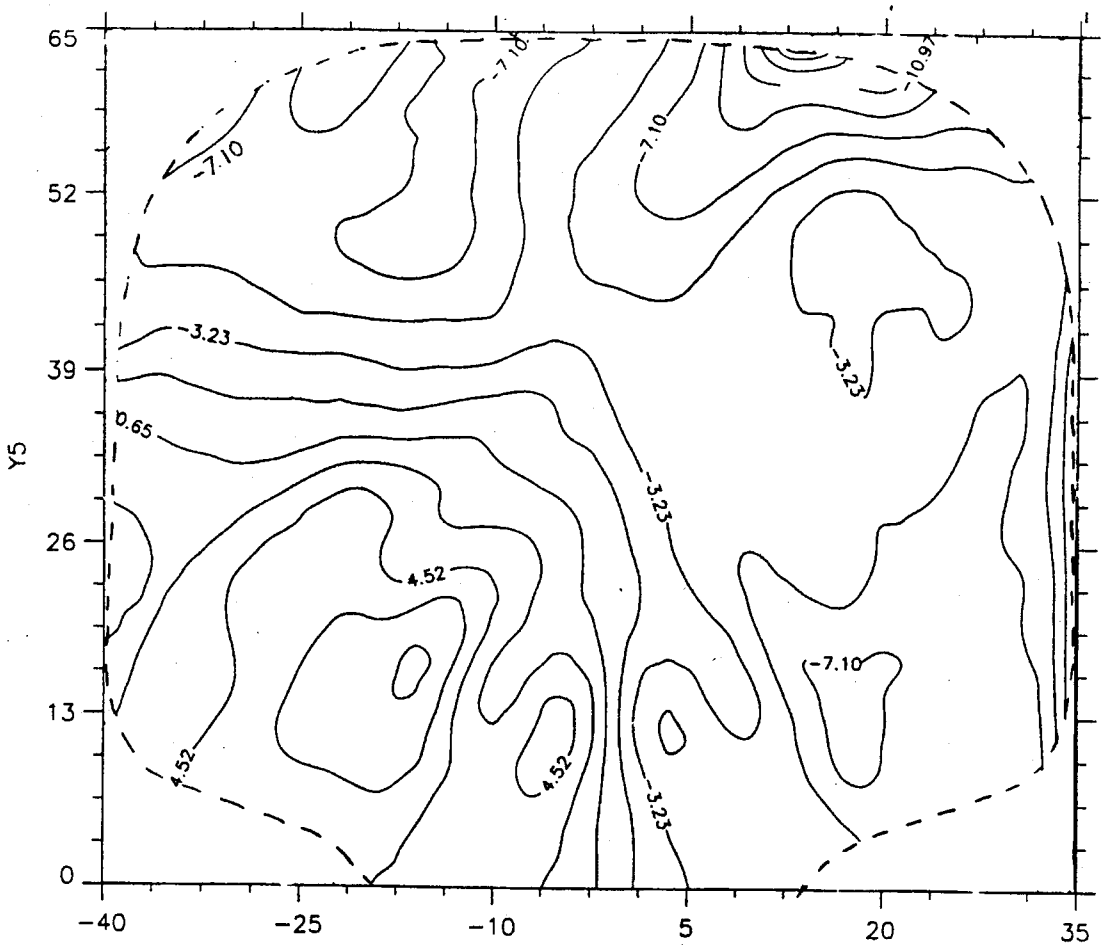

Fig. 74 $\sigma_{x'y'}$ (MPa)
(rail # 5 new CFI, 45° oblique slice)

7. REFERENCES

1. J. J. Groom, "Determination of residual stress in rails," ***Final Report to US DOT No. DOT-TSC-FRA-81-21***, May 1983.

2. J. Magiera, J. Orkisz & W. Karmowski, "Reconstruction of residual stresses in rails from measurement made on vertical and oblique slices," ***Proc. of the 4th International Conference on Contact Mechanics and Wear of Rail/Wheel Systems***, Vancouver, Canada, 1994.

3. R. Czarnek, J. Lee & S. Y. Lin, "Moiré interferometry and its potential for application to residual stress measurement in rails," ***Residual Stress in Rails***, Vol. 1, 153-167, Kluwer Academic Publications: Boston, MA. 1992.

4. Y. Y. Wang & F. P. Chiang, "Experimental study of residual stress in rail by moiré interferometry," ***Final Report. To US DOT***, VNTSC, DOT/FRA/ORD-94/02, DOT-VNTSC-FRA-93-24, 1993.

5. D. McLean, ***Mechanical Properties of Metals***, John Wiley & Sons, Inc.: New York, N.Y. 1967.

6. J. Orkisz, "Prediction of the actual residual stresses by constrained minimization of energy," ***Residual Stresses in Rails,*** Vol. 2, Theoretical and Numerical Analysis, edited by O. Orringer et al, 101-124, 1992.

7. A. B. Perlman, J. E. Gordon & O. Orringer, "Effect of grinding strategy on residual stress in rail head," ***Rail Quality and Maintenance for modern railway operation***, edited by J. J. Kalker et al, 297-306, 1991.

8. X. F. Shen, "Whole field measurement of residual stresses in rail," ***M. S. Thesis***, State University of New York/Stony Brook, 1995.

APPENDIX

Whole Field Measurement of Residual Stresses in Rail

A Thesis Presented

by

Xiaofeng Shen

to

The Graduate School

in Partial fulfillment of the Requirements

for the Degree of

Master of Science

in

Mechanical Engineering

State University of New York

at Stony Brook

April 1995

February 1995

State University of New York
at Stony Brook
The Graduate School

Xiaofeng Shen

We the thesis committee for the above candidate for the Master of Science degree, hereby recommend acceptance of the thesis.

Fu Pen Chiang
Advisor and Leading Professor
Department of Mechanical Engineering

James Tasi
Professor
Department of Mechanical Engineering

Peisen Huang
Asistant Professor
Department of Mechanical Engineering

This thesis is accepted by the Graduate school.

Graduate School

Abstract of the Thesis

Whole Field Measurement of Residual Stresses in Rail

by

Xiaofeng Shen

Master of Science

in

Mechanical Engineering

State University of New York

at Stony Brook

1995

It is well known that the presence of residual stresses in rails effects the life expectancy of the rail. The need to minimize the presence of residual stresses in rails requires a detailed description of distribution of the residual stress. The whole field distribution of residual stresses in both the head and the base of the rail is investigated by a non-dissection method. The residual stresses are relieved by an elevated temperature. The relieved residual deformations are detected by moire interferometry. The technique to deposit a high temperature resistance grating on the rail slice is developed. The

proper annealing profile is obtained. The effect of cutting on redistribution of residual stresses in rails is determined. And the experimental result of residual stresses distribution is compared with our former result gained from a dissection method.

TABLE OF CONTENTS

LIST OF TABLES

LIST OF FIGURES

LIST OF FIGURES (cont.)

Acknowledgments

I would like to take this opportunity to thank Dr. Fu-Pen Chiang for suggesting the topic for this thesis and for his guidance throughout the duration of my research.

I would like also to express my appreciation for Dr. Yinyang Wang's cooperation throughout the whole investigation, and for Dr. Lipski of Department of Physics of SUNY-SB of his effort in helping me doing the metal coating.

The work was supported by DOT/RSPA/Vople National Transportation System Center. The author wishes to thank Dr. Oscar Orringer of the Center and Dr. Roger Steel of the Association of American Railroads for their encouragement throughout the investigation and supply of the specimens.

1 Introduction

The failure rate of rails is believed to be greatly influenced by the residual stresses. Rail manufacturing processes and the action of train load in service, as well as the thermal stresses create residual stresses in railroad rails. These stresses, acting in conjunction with stresses produced by live loads, can threaten the safety of train operation by increasing the hazard of creation and propagation of fatigue cracks and the possibility of violent brittle breakage. Based on the prior experimental and theoretical research of DOT[14], the rolling contact plastic zone is confined to the rail head. The residual stresses caused by manufacturing processes are localized in both the head and the base parts of the rail. It is believed that the level of residual stresses in the middle part of the rail is relatively low in comparison with the head or base part.

Since recognition of importance of the residual stress on integrity of railroad rails and economics of railways operation there has been observed a constant effort aimed at determination of those stresses and understanding of all the effects they cause. Efforts have been made by many people during the past both experimentally and numerically[1]. Experimentally, one of the most renowned techniques of experimental examinations of the rail residual stress is the Battelle 3D technique[2]. In

view of the fact that its means of releasing residual stresses is cutting the rail into small cubes. Another method which can measure the whole rail is the dissection method. In this method, small grid elements are formed on the surface of the rail slice with a reflection grating fixed on its surface by slots cutting[3][4]. The residual stresses are relieved by the cutting process. Both methods yielded reasonable results. However these methods are destructive and among the most serious arguments raise against these techniques are the total investment in time and expense and the amount of laborious and painstaking work that is required so as to accomplish the final results.

In this thesis, a new experimental approach (**non-dissection method**) for studying residual stresses in rails is presented. This is a non-destructive method. The residual stresses are relieved by an elevated temperature. The results obtained are detected by moiré interferometry(or called grating imterferometry). The results obtained by the non-dissection method is compared with the dissection method which was developed by my colleague[8](see Fig. 1.1). The new method has obvious advantages: It provides moiré fringes throughout the specimen surface without breakage(see Fig. 1.2). Error due to machining process are completely circumvented. As a result a more detailed and accurate analysis can be made.

The main challenge raised in this non-dissection method is the making of a high density grating which can withstand baking at high temperature for long hours. Several ways are tried until the satisfactory procedure for making such a grating is found. This procedure starts with depositing a uniform thin layer of photoresist(a kind of photo-sensitive liquid). This process is often used in micro-electric circuit making. It is difficult to be applied to deposit the whole rail slice. Due to the fact that only the rail head and base are of interest, we study the effect of cutting on redistribution of residual stresses in rails. Based on our experiment on two rail samples of different types, it turns out that judiciously cutting away the web region from both the head piece and the base piece does not effect the distribution of the residual stresses in either pieces.

In our latest experiment, the residual stresses in the head and base pieces of a rail slice are measured using the new non-dissection method.

2 Principles of the Methods

2.1 Relief of Residual Stresses

There are two main groups of techniques to reconstruct the residual stresses[5]. One is destructive and the other is non-destructive. Techniques in the destructive group include hole-boring as commonly applied to metals, composites, and rock; grid elements-grooving which treats the average stress in the grid as the stress of the point at the center of the grid. The basic idea is that the residual stresses will be relieved at the edge where material is removed. These destructive methods can only obtain stresses at the local region of material removal. It is very labor costing and time consuming if a whole field detectioin is desired. More over if we consider the machining induced residual stresses during the boring or grooving, the analyses becomes complicated. Techniques in the non-destructive group include ultrasonic methods of Raleigh surface waves and acoustoelasticity; x-rays; electrical-resistance strain gages; nuclear acoustic resonance, *etc.* These methods detect the irregularity in the material or physical properties which are caused by the residual stresses under the surface of the sample. They are efficient in detecting the residual stresses qualitatively but not so accurate in the measurement level.

The technique we used in our determination of residual stresses in rail is different from all the above techniques. It takes the advantage of the annealing property of metal substances. The annealing process is a well used process by metal products manufacturers.—The residual stresses confined in a piece of metal will be relieved after the metal piece is subjected to elevated temperature for a certain amount of time.

2.2 Reconstruction of Residual Stresses

Many electrical and photomechanical techniques can be used to measure the residual stresses like strain gages, brittle coatings, speckle and moiré. Strain gages are not efficient to measure the whole field stresses, and neither the brittle coatings nor speckle technique yield the accuracy for measuring minute residual stresses. In this experiment, we choice moiré interferometry as our means of measuring the deformation of steel substrates caused by the annealing process. In order to resolve small strains, comparable with those found in situations involving creep or residual stress, the technique of moiré interferometry does offer adequate sensitivity[6].

2.3 Moiré Interferometry

2.3.1 Experimental Method

The word '*moiré*' is the French name for a fabric known as watered silk, which exhibits patterns of light and dark bands. This moiré effect occurs

whenever two similar but not quite identical arrays of equally spaced lines or dots are arranged so that one array can be viewed through the other. These arrays are the fringe patterns that can be measured to decide the deformation of the specimen surface.

Moiré interferometry is a high-sensitivity optical methods of measuring in-plane deformation of solid bodies[6]. Two-beam interference is applied to produce the resulting array of alternating light and dark fringes as shown in Figure 2.1. The two beams are produced by a single coherent light source and emerge from the mirror arrangement, used to orient the beams. The distance p between fringes is determined from Eq.(2.1) and (2.2)by

$$p = \lambda / (2\sin\theta) \tag{2.1}$$

The fringe gradient is representative of a spatial frequency f given by

$$f = 1 / p = 2\sin\theta / \lambda \tag{2.2}$$

where f is expressed in terms of lines/mm.

The two intersecting beams are used to produce high-frequency gratings which are employed as the specimen gratings in moiré interferometry. Fig.2.2 illustrates the experimental setup used in this investigation. A collimated and coherent laser beam is split into two beams with one impinging on the specimen and the other on the mirror. The beam propagating to the mirror is also reflected onto the specimen. Therefore,

there are two plane waves illuminating the specimen grating. The incident angle of the two beans are so arranged that their ±1 diffraction orders form the grating of the two diffractions along the Z direction. When the specimen grating is deformed, the wave fronts of the two diffraction beams are warped. It is the interference of these two diffraction beams that results in the forming of the moiré fringe pattern. A compound lens is used to collect diffraction beams to form an image of the specimen. Since the frequency of the interference is very high (1000 to 3000 lines/mm), production of the gratings is far from routine. An excellent vibration isolation table is required to maintain stability of the optical elements during the exposure interval. Also, forming the image of the grating on the film plane requires a very-high-quality process lens. In our experiment, cross grating is printed on the surface of the rail specimen so as to measure the displacement both in u and v coordinate directions. The specimen is mounted on a rotation stage which is rotatable about the Z-axis. The specimen is aligned in such a way that the fringes representing one displacement field, for example the u-field, are recorded first, the specimen is then rotated 90 degrees to allow the formation of the v-field fringes for recording. The rotation stage is controlled by a stepping motor with a minimum step being 0.01 degrees. This rotation stage is also used to perform rotation mismatch when the sign of strain needs to be determined.

With moiré interferometry, the frequency of the grating is usually in the range from 1000 to 3000 lines/mm, whereas with mechanical moiré, the frequency rarely exceeds 80 lines/mm. The light frequency we use in our experiments is 1200 lines/mm.

2.3.2 Analysis of Experimental Results[7]

The strain components are calculated using,

$$\varepsilon_{xx} = \frac{P}{S_{xx}} \tag{2.1}$$

$$\varepsilon_{yy} = \frac{P}{S_{yy}} \tag{2.2}$$

$$\gamma_{xy} = \left(\frac{1}{S_{xy}} + \frac{1}{S_{yx}} \right) P \tag{2.3}$$

where p is one half of the pitch of the specimen grating, and S_{ij}($i,j = x,y$) are fringe spacing along x and y axes, that is, the distances between two intersected points of the fringes on the x and y axes, respectively. Since the pitch of a grating is the inverse of its frequency, p is equal to 0.417um for our case.

The signs of the strains are determined by the mismatch fringe patterns. According to reference[7], when a small rotation is imposed on the reference grating, the moiré fringes will rotate along the same direction if

the normal strain components are positive, and in the opposite direction if negative. As for the shear strain, if the crossed fringe spacing (*Sxy* or *Syx*) becomes smaller when the reference grating is rotated, the shear strain has the same sign as the rotation; if the crossed fringe spacing becomes larger, the shear strain has the opposite sign. The rotation mismatch is easily achieved by simply rotating the specimen in our experimental set up.

3 The Effect of Cutting on Redistribution of Residual Stresses in Rails

When considering the formation of the residual stresses in rails, we assumed that they are localized in the base and the head regions of the rail. A rail that is roller straightened at the mill and then subjected to wheel contact loads may have residual stress in the web region as well. The straightening process creates plastic deformation in the rail base as well as in the rail head. The rolling of wheels of railroad cars may extend the plastic zones into the web region. In the previous studies, only rail heads were investigated [3][8][9]. Several questions need to be answered such as, whether or not the residual stresses are localized; whether or not the plastic zones are contained in the rail base and the rail head only, and *etc.*

An ideal issue would involve annealing an entire cross-sectional slice of a rail and determine the resulting residual stress distribution. However, the practical difficulty of printing a fine grating of 1200 lines/mm on an irregular shape specimen of about 180×155 mm in dimension is quite substantial. An alternating is to cut a cross-sectional slice into two pieces, one containing the rail head and one containing the rail base, and proceed to cutting the web region away from the pieces. If the resulting moiré fringes due to initial imperfection are not disturbed by the cutting, it is

reasonable to conclude that there is no appreciable residual stress in the web and the cutting does not redistribute the residual stress in either the rail head or the rail base. Two types of rails (one is KSC and one is 5A) are tested.

The cross-sectional slices were cut from the rails that had experienced rolling cycles as well as straightening from the mills. One of the surfaces of the rail slice was polished. Epoxy gratings were replicated onto the head and the base regions. The whole slice was then cut into two pieces at the center of the web and were placed into moiré interferometer respectively. No irregular fringes were observed at this stage except two broad fringes created by misalignment or grating imperfection. These initial fringes are present in almost all moiré interferometry investigation. It indicated that the cutting of the slice at the center of the web did not cause noticeable redistribution of the residual stresses in the rail head or in the rail base. A series of sequential cuttings were performed thereafter on both the separated rail head and the base. Fig.3.1 depicts a schematic of the sequence cuttings. After each cut, the rail head and the base were brought back into the interferometer and the resulting fringe patterns were carefully compared to the one before the cutting to see if there were any changes. Cutting was stopped when an obvious change of fringe distribution was observed. Fig.3.2 shows sample patterns of rail KSC at different cutting stages. Similar results were obtained from rail 5A.

The results of the investigation indicate that the residual stresses are localized in the head and the base regions of the rail. A whole slice can be separated into two pieces containing the head and the base respectively. Judiciously cutting away the web region from the two pieces does not effect the distribution of the residual stresses in either the rail head nor the rail base. In this particular study, the limiting distance is 63mm for rail KSC and 60mm for rail 5A from the top of the rails for the head pieces and 55mm for both rails KSC and 5A from the bottom of the rails for the base pieces.

The result of this study has been sent to the Journal of Experimental Techniques for publication[13].

4 Making of High Temperature Resistant Gratings on Steel Substrates

For normal(room temperature) application of moiré interferometry, a reflective surface grating is cast onto the component's surface using a replication material, such as silicon rubber or epoxy resin from a master grating. Since both silicon rubber grating and epoxy grating will be destroyed over 300 °F which is much lower than the required annealing temperature for steel, new technique need to be introduced to make high temperature resistant gratings on steel substrates. In our application, the grating should be able to survive 10 hours of baking at temperature 900 °F or 100 hours of baking at temperature 800 °F.

Processes to produce high temperature resistant grating has been developed by several other research groups [10][11][9] *etc.* The procedure developed in our laboratory has successfully withstand baking at 900 °F for 30 hours or at 800 °F for 100 hours after which the fringe pattern is still illustrative to the details. The fundamental of this technique is printing high density grating on photoresist by Two-Beam Interference.

The procedures of making high temperature resistant gratings on steel substrates is as stated in the following sections.

4.1 Surface Polishing

The surface of the components is first prepared to a polished finish. This is carried out with as gentle a mechanical working procedure as possible so as to minimize work-induced stresses. The surface of a substrate is polished by steps of 400 and 600-grit sand paper. The surface is then finally finished by 1um polishing paste.

There are inevitable stresses introduced, even if polishing is carried out at a slow rate and under well lubricated conditions, but according to Dr. Colin Forno's measurements using X-ray diffraction on his carefully polished specimens [10] which have then been incrementally etched suggest that, although such stresses may be high, they are confined to a surface layer only a few micrometers thick[12]. During the polishing, attention should also be paid to avoid the rounding off of the edge of the surface.

4.2 Metal Layer Deposition

A thin layer of Chromium about 40nm is evaporated on the steel substrate first. The second layer is Aluminum and the thickness is about 30nm. Chromium serves as an adhesion between Aluminum coating and the steel substrate. It could also protect the substrate from oxidization at a high

temperature. Aluminum has good anit-oxidization ability at temperature below 1,000 °F and remains shinning through out the baking.

4.3 Photoresist Deposition

Next, the substrate with Chromium and Aluminum coatings is coated with photoresist[15], followed by a bake at 120 °F for 20 min. The whole operation of photoresist deposition had to be done under a safety light. To achieve a uniform thin layer the method of spinning at high speed is used. If the component is circular, then it is possible by spinning to achieve the ideal condition of a completely uniform and very thin layer of photoresist. Unfortunately, most test components are seldom circular and the resulting spun layer of resist may vary in thickness by several micrometers, especially around the edges. However, acceptable results has been made on both the rail head and base by carefully control the process of spinning and spraying. Still, the edge effect has not been fully overcome.

4.4 Grating Making

The resist layer on the component is then exposed to a 1200lines/mm intensity pattern(this is the standard spatial frequency for moiré interferometry.) for 2 min using the set up described in last chapter. The light field is 5″ in diameter. A blue Argon laser is used with wave length of light 488nm and the power output of the laser is set at 500mw. For the

production of a crossed grating, which is needed if all in-plane strain components are required, the specimen has to be double exposed after rotating it through an angle of 90 degrees.

After the exposure, the specimen is developed. The developer [16] is diluted with 2 parts of water. It has to be noted that the developer should be kept fresh. It is no good to use overnight developer. The developing time is about 1 min. After the developing, the specimen is rinsed in water and then blown with a hair dryer to dry. During the developing, a Robby laser observation arrangement is designed to trace the diffraction the growing grating exhibits. When the diffraction is observed, by experience, to be strong enough, the specimen must be taken out from the developer to avoid over development. Since the developer of the photoresist exhibits an alkaline behavior, it will etch off the Aluminum. Therefore an Aluminum grating is formed onto the surface of the rail slice. The residual photoresist is washed off with alcohol.

4.5 An Improved Way of Grating Making

The grating making procedure mentioned in 4.4 directly etches off Aluminum to form the grating. The process, based on our experience, is difficult to control. The quality of the Aluminum grating varies greatly with the quality of the Aluminum coating. Also, the Aluminum coating peels off easily in the dilution of developer and water. Once the attempt to

make such a grating is failed, the steel substrate need to be polished again and coated with the heat resistant metal once more. It is not only time consuming but also expensive. An alternative way which is proved better than this is developed in our laboratory lately.

4.5.1 Grating Mold Preparation

In this process, the steel substrate is coated with photoresist after it is polished. Then a 1200 lines/mm grating structure is printed on the photoresist use the same Two-Beam interference technique. If the resist coating is developed at this stage the surface will exhibit amplitude modulation of 1200 lines/mm. Purpose of the resist grating is to form a mold for a subsequent thin layer of a heat resistant metal. Several attempt can be made before a satisfactory photoresist grating is obtained.

4.5.2 Coating with Heat Resistant Materials

Two layers of different heat resistant and anit-oxidizing metals are applied by vacuum deposition. Providing the layers are sufficiently thick(normally 50 nm each), they will retain its molded shape when the resist is eliminated during the heating process. During the annealing process followed, the resist decompose and eventually vaporize through any cracks or holes in the metal films at temperature above 300 °F, leaving the molded grating attached to the substrate. The metals are "keyed" onto the component and act as a fixed grating. The remained grating is still

shinning after the annealing process(30 hours of baking at 900 °F). This process need to polish the steel substrate and perform the vacuum deposition only once. It is a more efficient way of making high temperature resistant grating than the other mentioned in this thesis. However, the choice of the components of the two metal layers is crucial to the success of this method.

5 Establishment of Heat Treatment for Relief of Residual Stress in Rails

Former experiments was done in our laboratory on a rail head specimen subjected to stress relief at 900 °F for 10 hours. The DOT(Department of Transportation) has proposed two temperature-time profiles of heat treatment for rail stress relief: (1) 800 °F for 100 hours; and (2) 900 °F for 10 hours. According to DOT's requirement, we conducted laboratory experiments on pieces of rail head specimen to establish the minimum elevated-temperature holding time required to produce an acceptable degree of stress relief.

Two specimen were carefully measured. Both of them were heated at 900 °F for more than 30 hours, with periodic interruption and cooling to room temperature for interim measurements at the times indicated in Table 1. As shown in Table 1, the number of fringes between two pre-made marks on each specimen surface are counted at each interim. For rail sample #1, the number of fringes merely increases after 15 hours of baking; for rail sample #2, the number of fringes merely increases after 10 hours of baking. Prediction could be made that the residual stresses have almost been relieved after 20 hours of baking at 900 °F, since no significant fringe density changes, if any, have been observed for both samples after

20 hours of baking no matter how long the baking lasts thereafter. In the following investigation, the temperatuer-time profile we use is as shown in Fig. 5.1.

6 Position Recovery of Specimen After Annealing Process

Since the specimen need to be heated in a furnace to reach temperature as high as 900 °F, it has to be removed from the optical arrangement and put back precisely to the original place for deformation measurement. Moiré interferometry is very sensitive to displacement in the spatial field. Any minute rotational mismatch(displacement) will lead to significant change in the deformation fringe pattern thus cause severe error to the experiment result.

A clamping device (see Fig.6.1) is specially designed for the position recovery of the rail specimen on the rotation stage after annealing process. It contains a supporting base with the contacting surface ground flat; a position pin; a clamping bar to fix the specimen. The lower side of the specimen is also ground flat. When the specimen is rested on the supporting base, the two grounded surface are perfectly contact. Then the specimen is slowly moved towards the position pin with a finger until it is firmly against the pin. The specimen is then fixed by the clamping bar. After the interferometer is adjusted to a null field with the non-heat-treated specimen, the specimen is taken off and then put back in the same way.

The null field remains.—It claims that the position recovery device performs well.

7 Experimental Procedure

7.1 Specimen Preparation and Grating Making

The rail slices studied are provided by Dr. Roger Steel of the Association of American Railroads. A 10mm thick vertical slice is cut off from the central part of the rail that has experienced rolling cycles (see Fig.7.1). The rail head and base are cut off as the subjects of the study. Both of them are carefully grounded followed by slow hand lapping to avoid introducing additional residual stresses or rounding off the edges. The polish is done till a mirror like surface is achieved.

The polished rail head and base are then coated with cross gratings of 1200 lines/mm using the improved method of high temperature resistant grating making techniquewhich is described in 4.4.

7.2 Relief of Residual Stresses by Annealing Process

Both of the rail head and base are subjected to the annealing process. They are baked in a furnace with a programmable temperature controller at 900 °F for 20 hours (see Fig. 5.1) and cooled down to room temperature in the furnace without interference.

7.3 Experimental Results and Data Analysis

When the specimens of rail head and rail base are cooled down to room temperature after the annealing process, they are brought back to the interferometer with their former position carefully recovered. The resulting fringe pattern for the u-field deformation is taken. The specimen is then rotated 90 degrees and the fringe pattern for the v-field deformation is taken. Figures 7.2 and 7.3 show the fringe pattern of the rail head and base.

The strain calculation is easier and more accurate for the non-dissection method. The continuous fringes obtained by the non-dissection method are digitized and differentiated numerically. The strain components of ε_{xx}, ε_{yy} and γ_{xy} are calculated by,

$$\varepsilon_{xx} = p \frac{\partial N_x}{\partial x} \tag{7.1}$$

$$\varepsilon_{yy} = p \frac{\partial N_y}{\partial y} \tag{7.2}$$

$$\gamma_{xy} = p \left(\frac{\partial N_x}{\partial y} + \frac{\partial N_y}{\partial x} \right) \tag{7.3}$$

where N_x and N_y are fringe orders of the u and v field fringe patterns respectively.

Figure 7.4 and 7.5 show the contour maps of strain components ε_{xx}, ε_{yy} and γ_{xy} for the rail head and base obtained by non-dissection methods.

8 Results and Discussions

8.1 Residual Stresses in Rail

The residual stresses in the rail head and base have been successfully obtained by the non-dissection method. For the particular rail shown in Fig.7.2 and Fig. 7.3, from the symmetric patterns of the deformation contour in both u and v field of the base, conclusion can be drawn that rail manufacturing makes the major contribution to the residual stresses formation in the rail base. Similarly, rail manufacturing plays the major role in the formation of the residual stresses for the most part of the rail head, except in the regions near the upper bound of the rail head where stress concentrations occur (see Fig. 7.3 and Fig. 7.4). The strain level is much higher in the rail head than in the rail base, which may be because that the rail head is more bulky and produce more residual stresses when it is cooling down. This infers the significance of the manufacturing induced residual stresses in rail. In future, the presented system will be applied for determining the stress field σ_x , σ_y , σ_z by analyzing obliquely cut sample.

8.2 Problems in the Heat Resistant Grating Making Stage

The non-dissection method proved to be successful and easily fulfilled. Although making of a high temperature resistant grating costs many efforts and needs a powerful laser with short light-wavelength output, this method is strongly recommended to obtain accurate results. The mismatch of the thermal coefficients of expansion of the grating and the substrate does not effect the resulting fringes since the differences of the thermal coefficients between steel and heat resistant metal layers are small and the thickness of the metal layers are as thin as about 50 nm.

Due to the irregular shape of the rail head and upper speed limit of the rotary stage, the uniformity of the photoresist layer is difficult to achieve. One solution to it is to make the surface of the specimen extremely flat and carefully avoid the round off at the edge during polishing.

Chromium will react with photoresist at high temperature and reduce the reflectivity of the specimen. Substitute metal which would not react with photoresist at high temperature need be selected if a detailed fringe pattern is required.

Table 1

The number of fringes between two pre-made marks on each specimen surface are counted at baking interims. For rail sample #1, the number of fringes merely increases after 10 hours of baking; for rail sample #2, the number of fringes merely increases after 5 hours of baking. The Baking temperature for both samples is 900 °F.

	Rail sample #1	Rail sample #2
Total hours of Baking	# of fringes	# of fringes
5	34	63
10	37	63
15	38	63
20	38.5	63.5
30	38.5	64
40	39	64

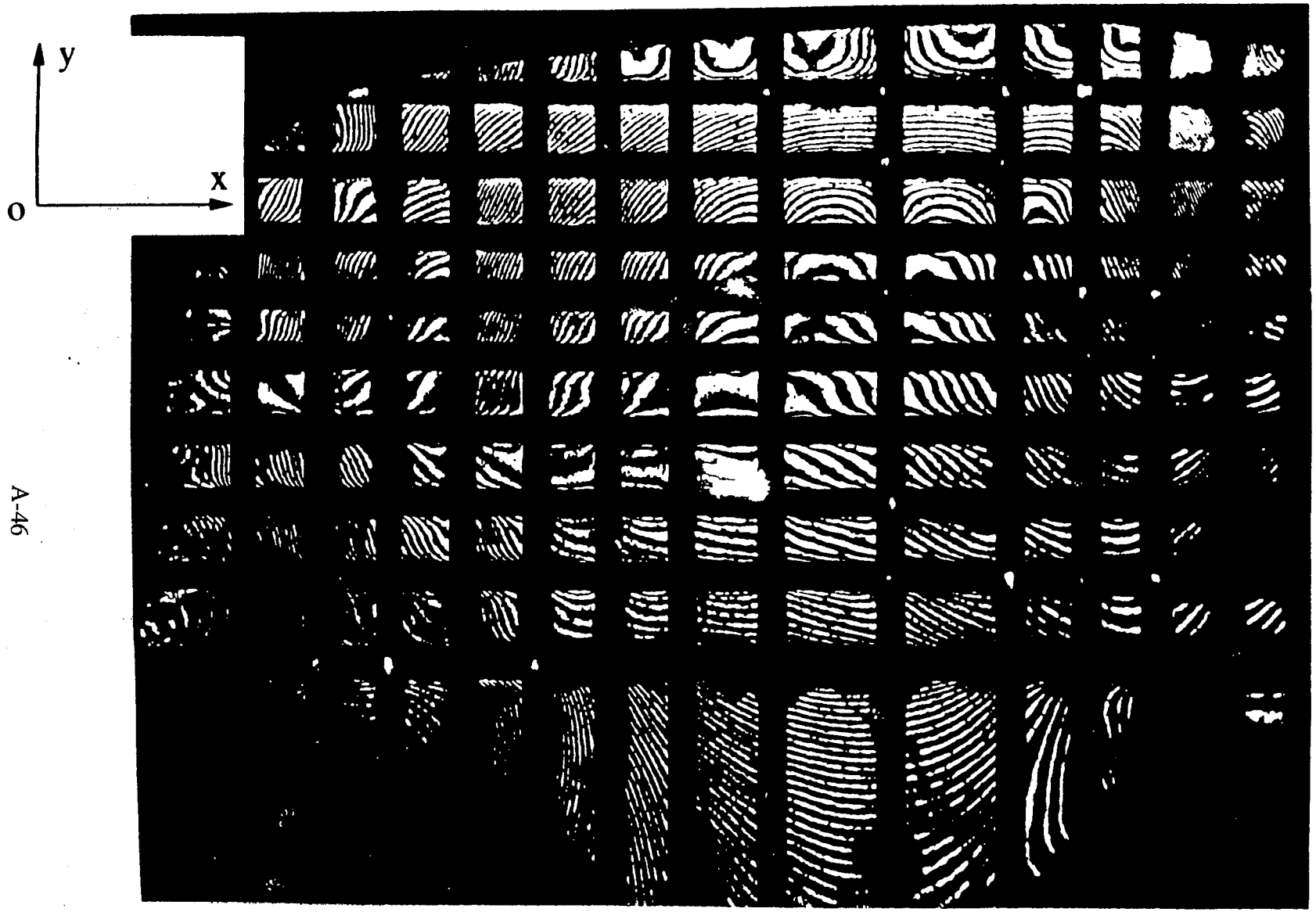

Fig. 1.1 U-field fringes obtained by the dissection method.

Fig. 1.2 The preliminary result of U-field fringe pattern obtained by the non-dissection method.

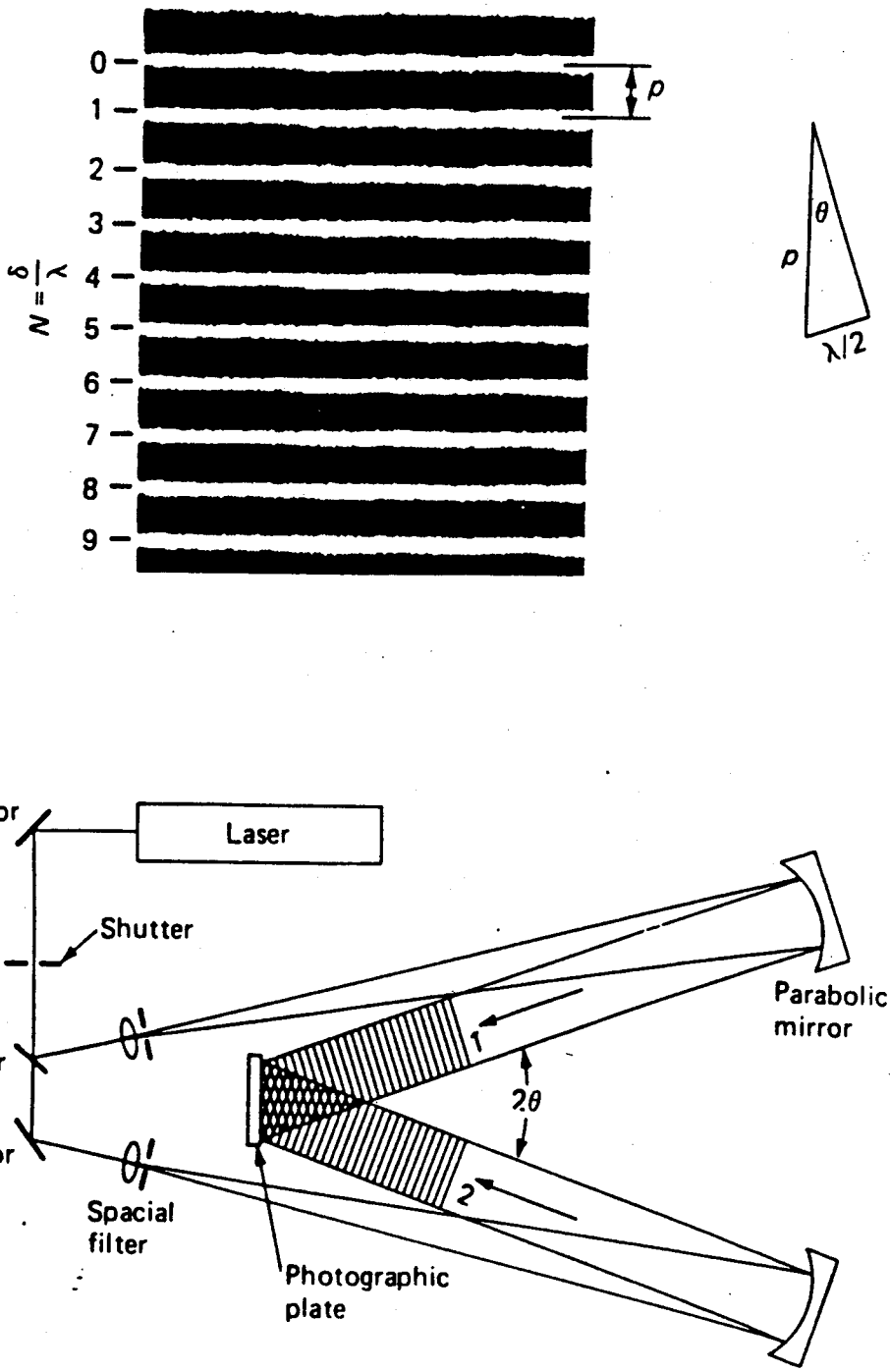

Fig. 2.1 Interference fringe pattern produced by intersecting wavefronts (Courtesy of D. Post), and optical arrangement used to produce high-frequency moiré gratings.

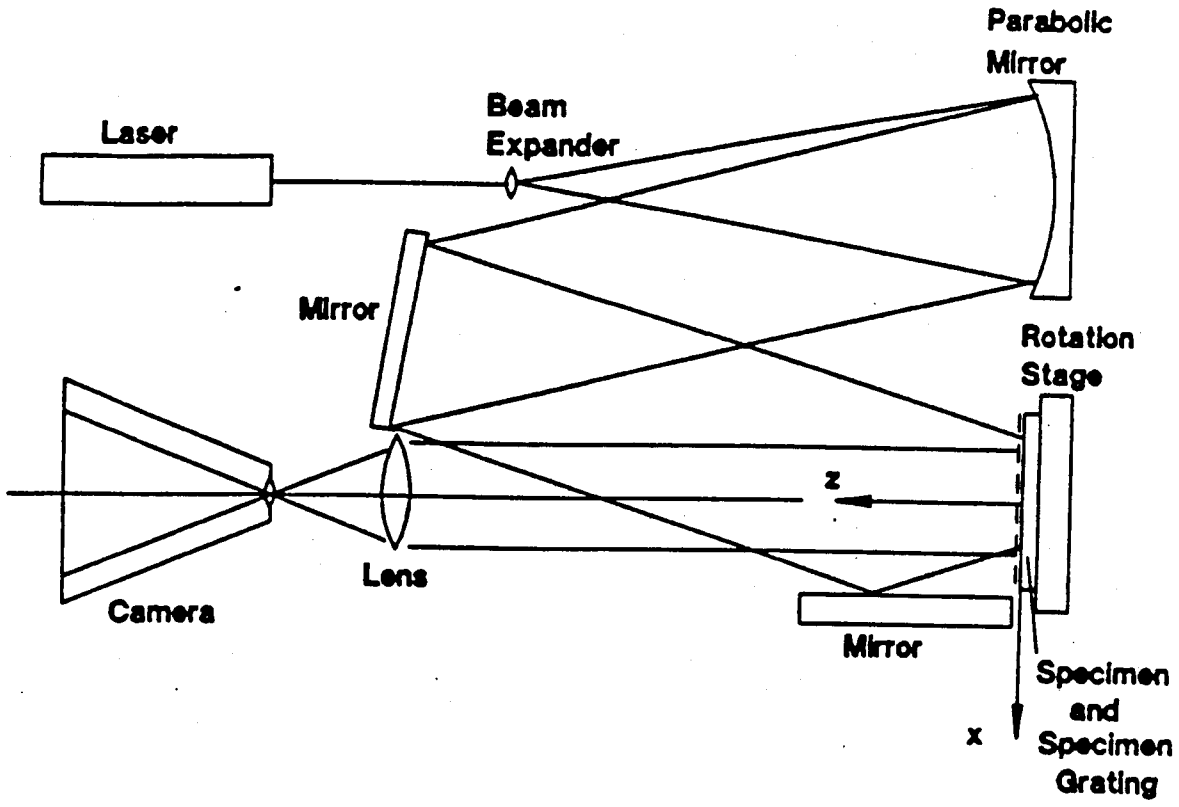

Fig. 2.2 The experimental setup of moiré interferometry for our study.

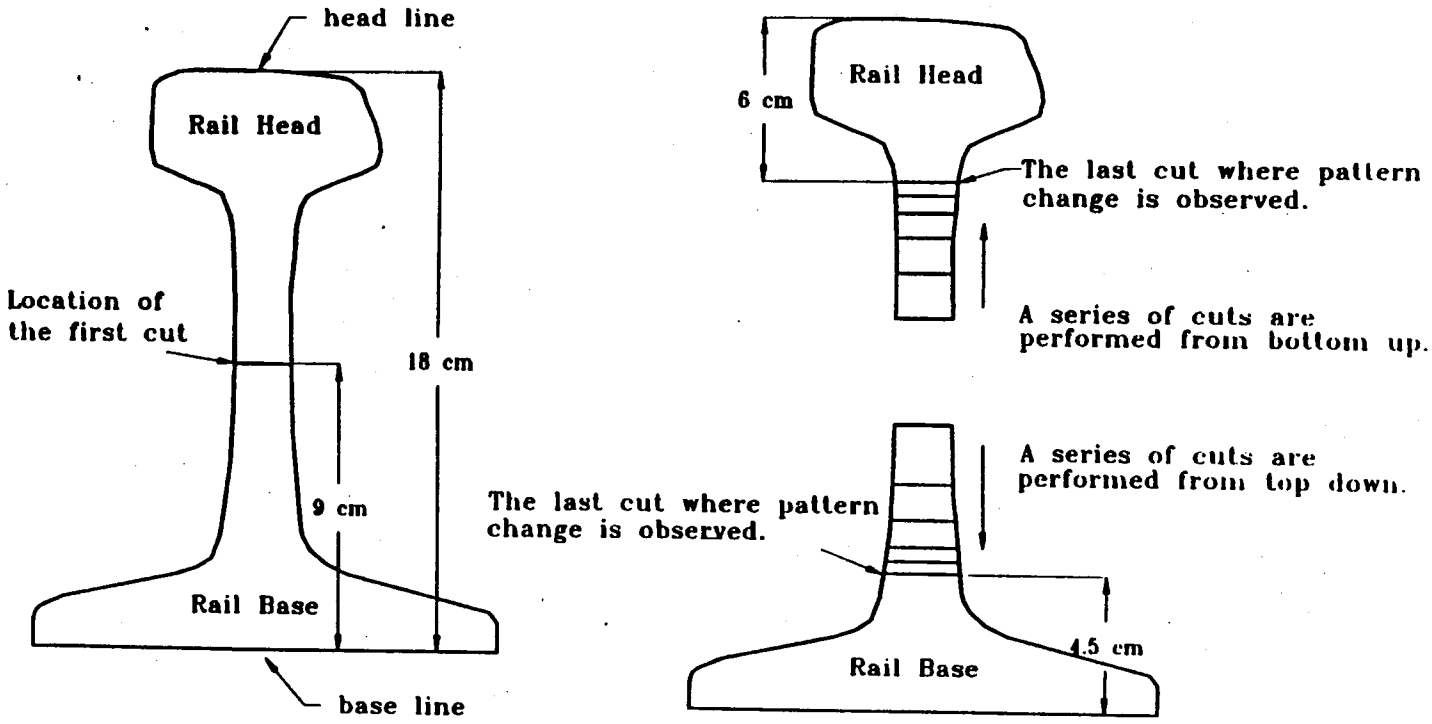

Fig. 3.1 Schematic of a series of cutting of a rail.

(a) A head piece before cutting.

(b) A head piece after a cutting at the center of the web.

(c) A head piece after the cutting when pattern change is observed.

(d) A base piece before cutting.

(e) A base piece after a cutting at the center of the web.

(f) A base piece after the cutting when pattern change is observed.

Fig. 3.2 Patterns of a head and base pieces of a rail slice. (a) to (f)

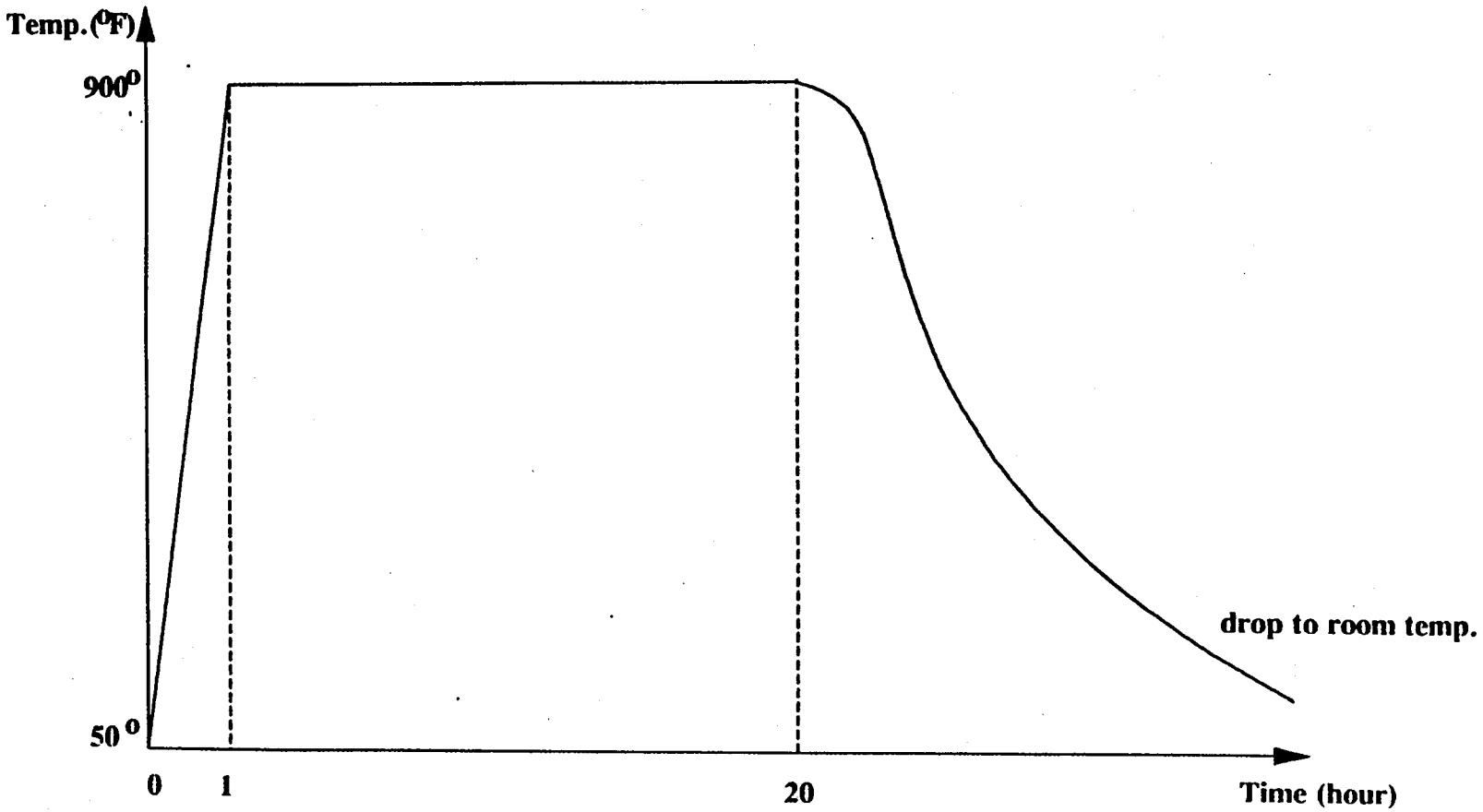

Fig. 5.1 Time-Temperature Profile of the Annealing Cycle.

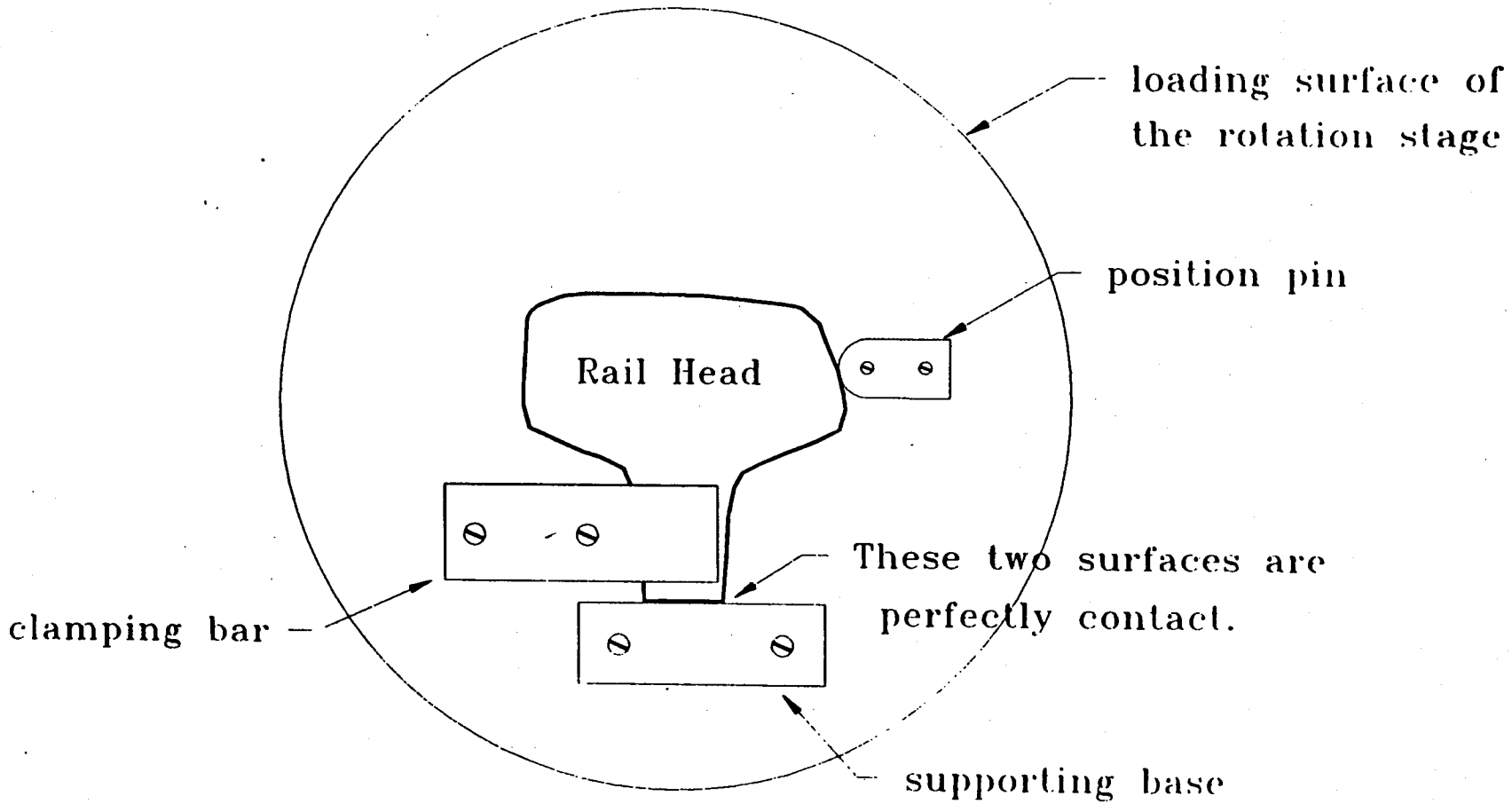

Fig. 6.1 The clamping device for position recovery of specimen.

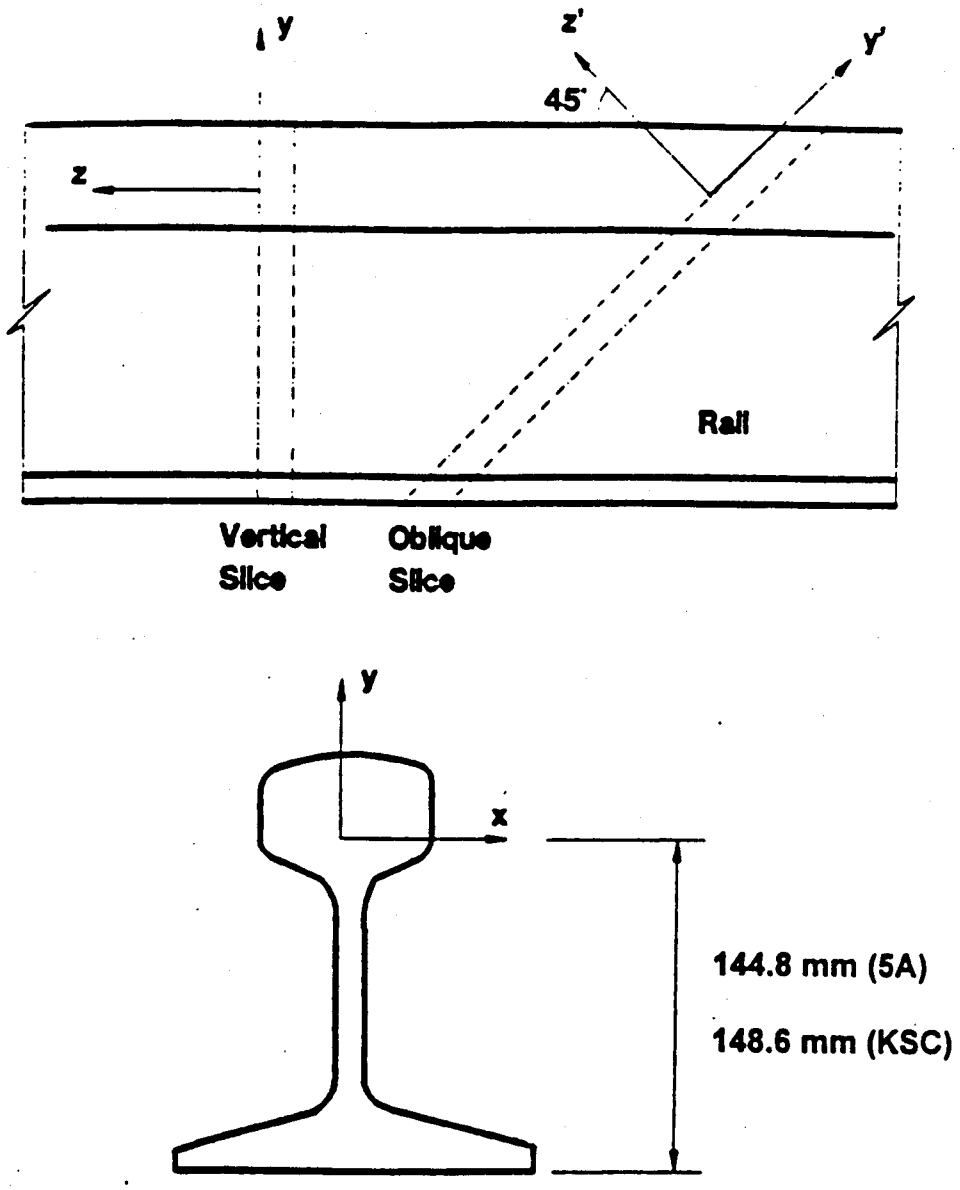

Fig. 7.1 Orientation of the rail slices.
The oblique slice is used in further studies.

Fig. 7.2 Fringe pattern of the rail base.

(a) U-field

(b) V-field

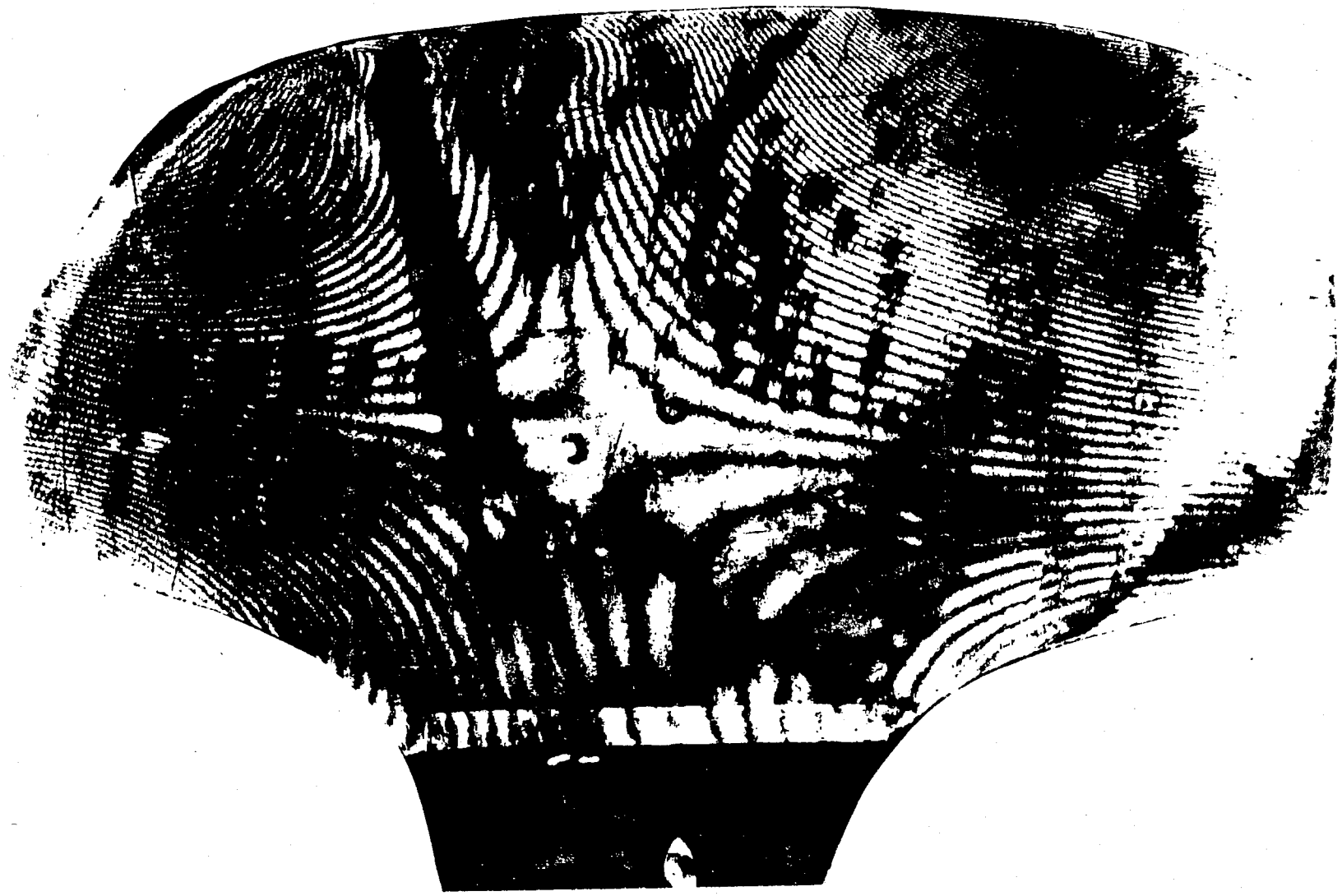

Fig. 7.3 Fringe pattern of the rail head.

(a) U-field

(b) V-field

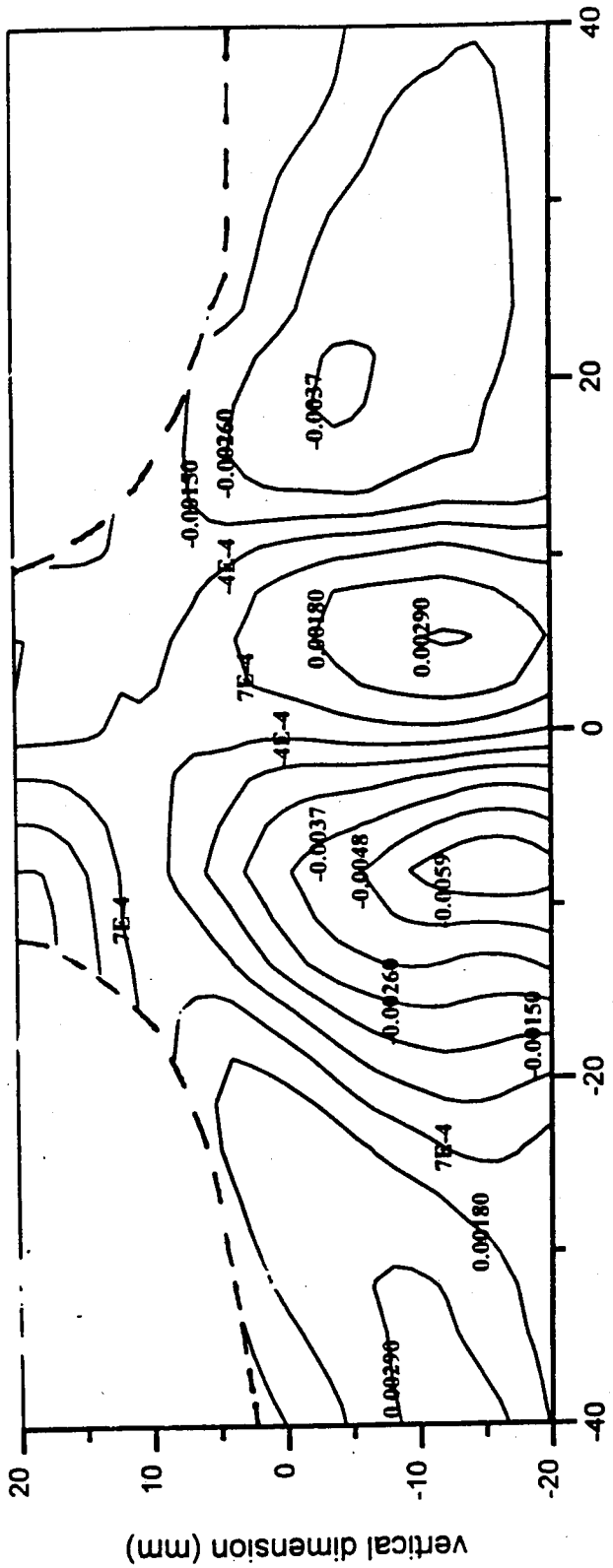

Fig. 7.4 Contour maps of strain components for the rail base.

(a) ε_{xx} (%)

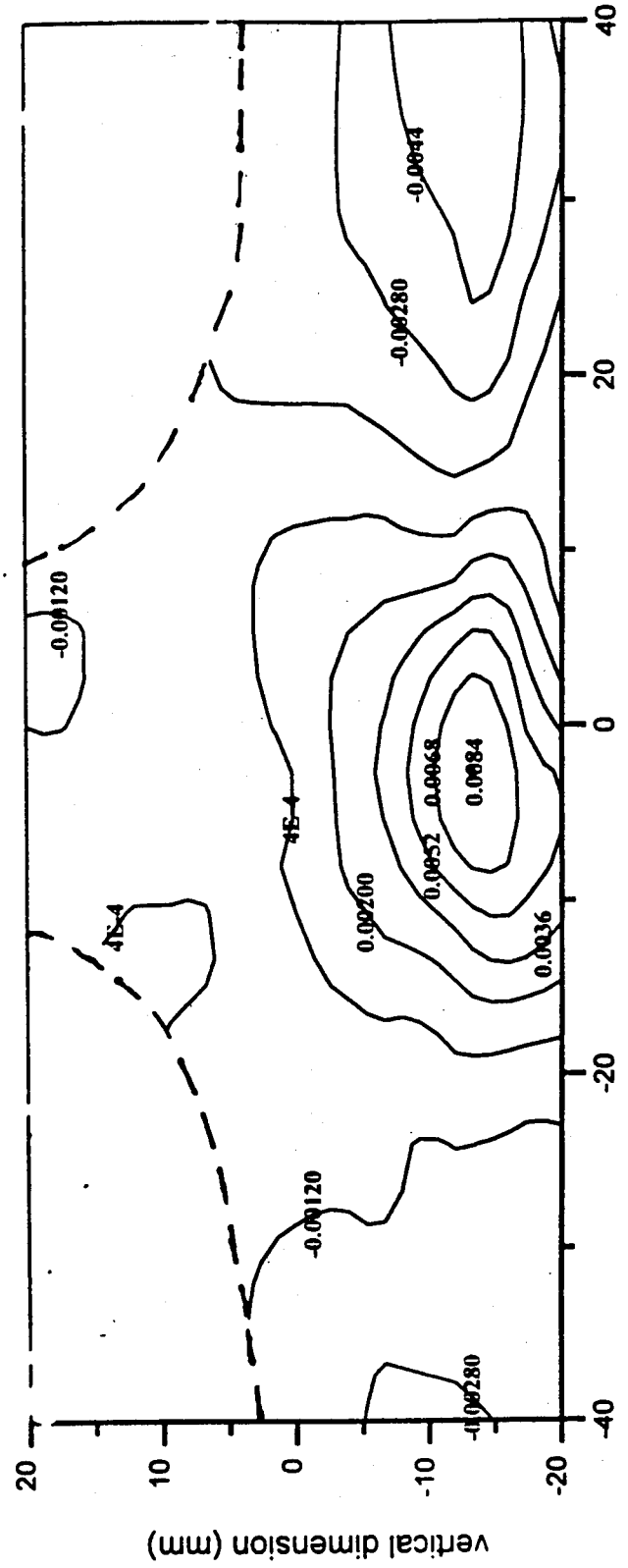

(b) ε_{yy} (%)

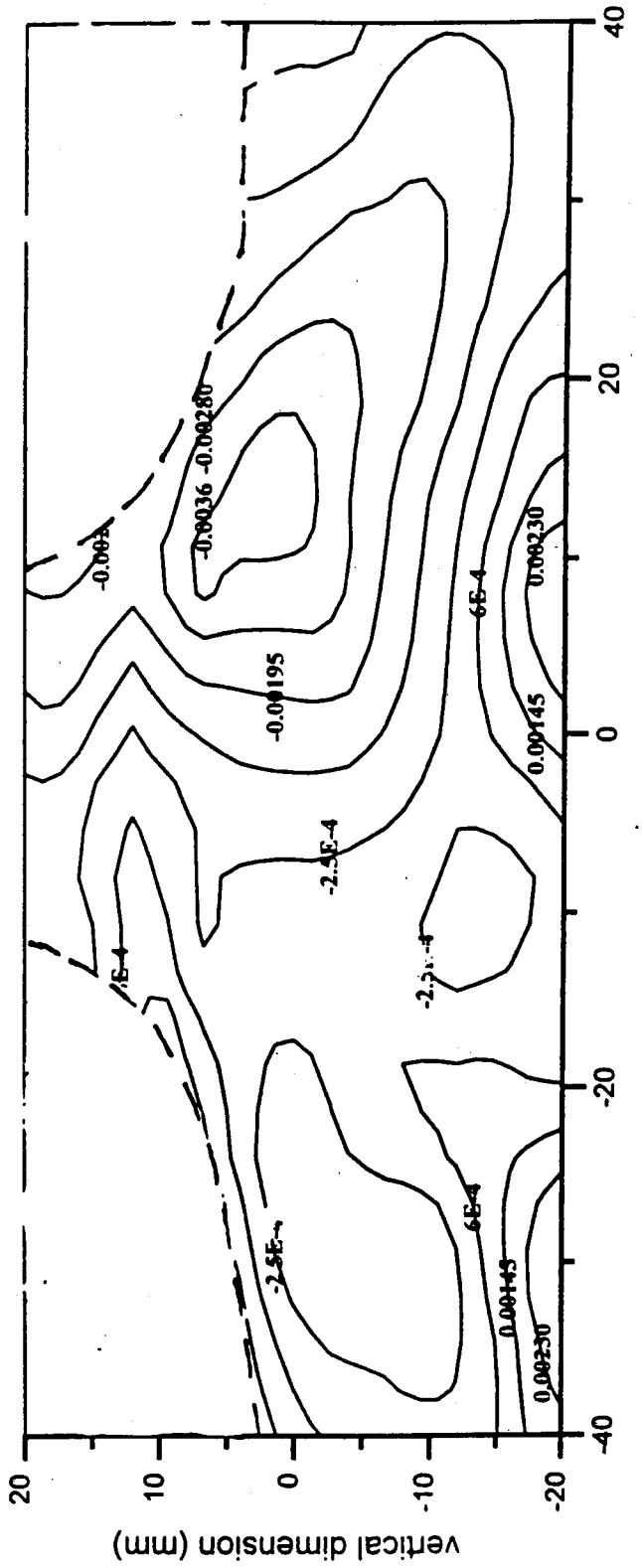
vertical dimension (mm)
20
10
0
-10
-20
-40
-20
0
20
40
horizontal dimension (mm)
-0.0036
-0.00280
-0.00195
-2.5E-4
6E-4
0.00145
0.00230

(c) γ_{xy} (%)

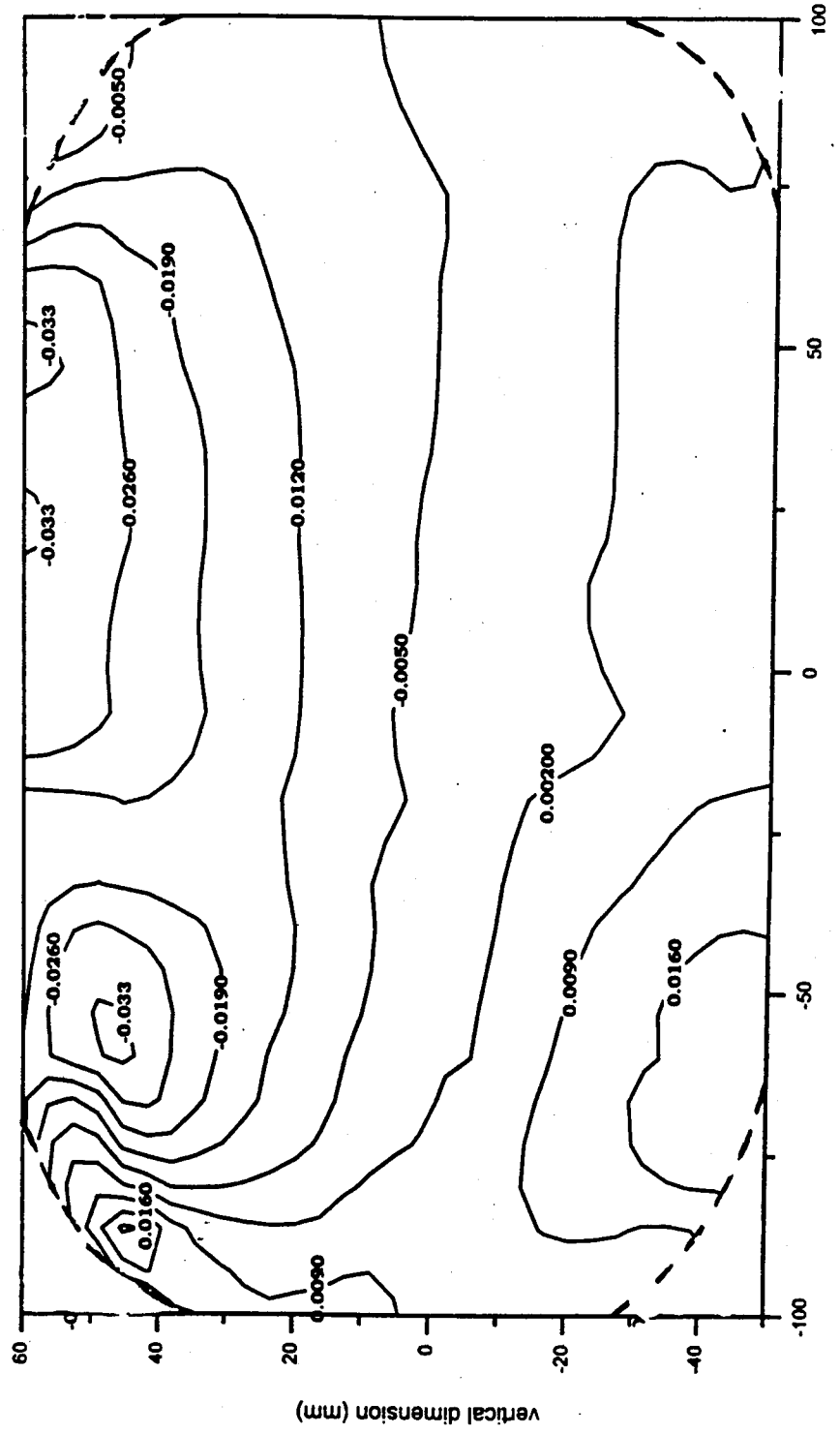

Fig. 7.5 Contour maps of strain components for the head.

(a) ε_{xx} (%)

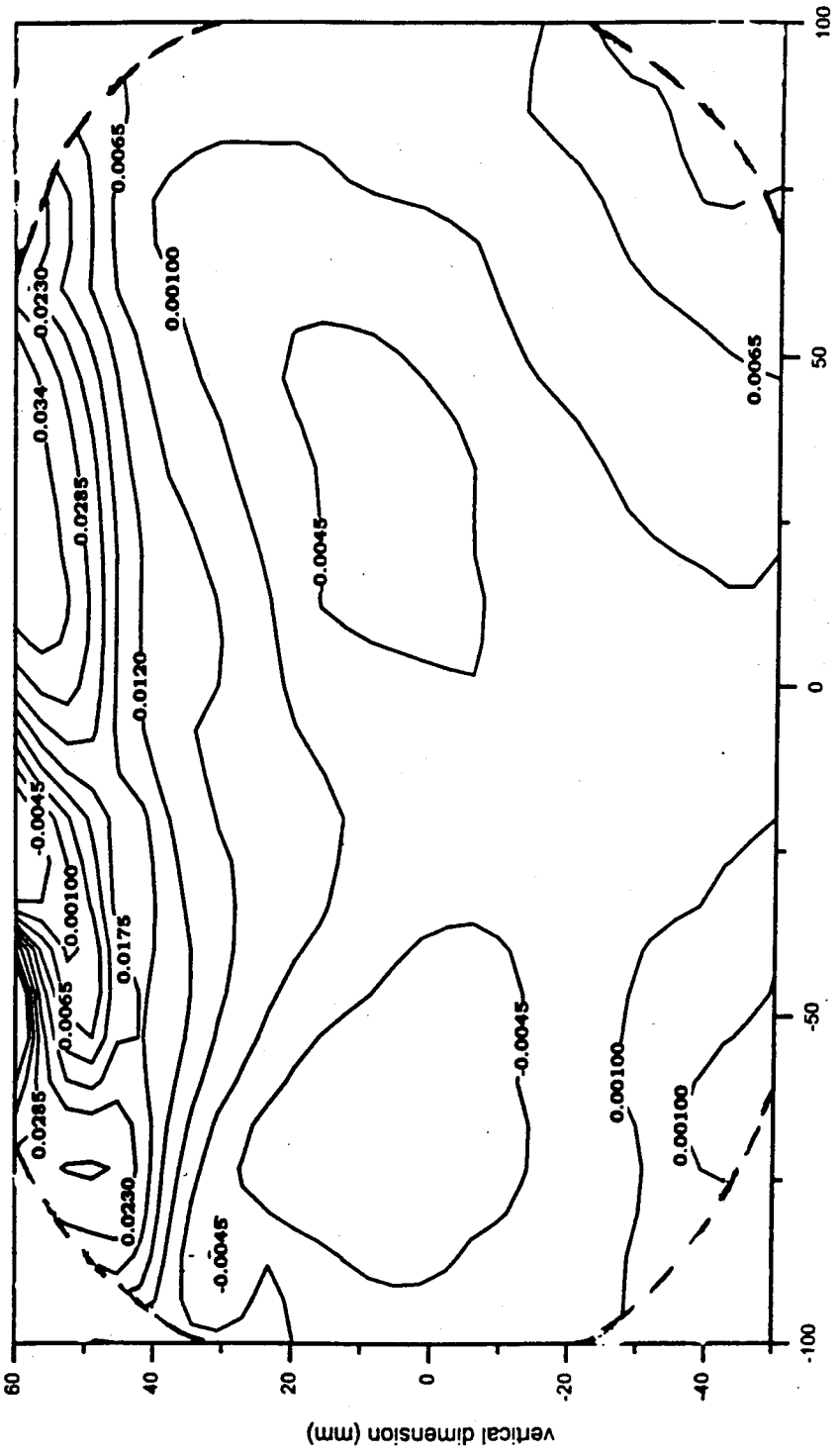

(b) ε_{yy} (%)

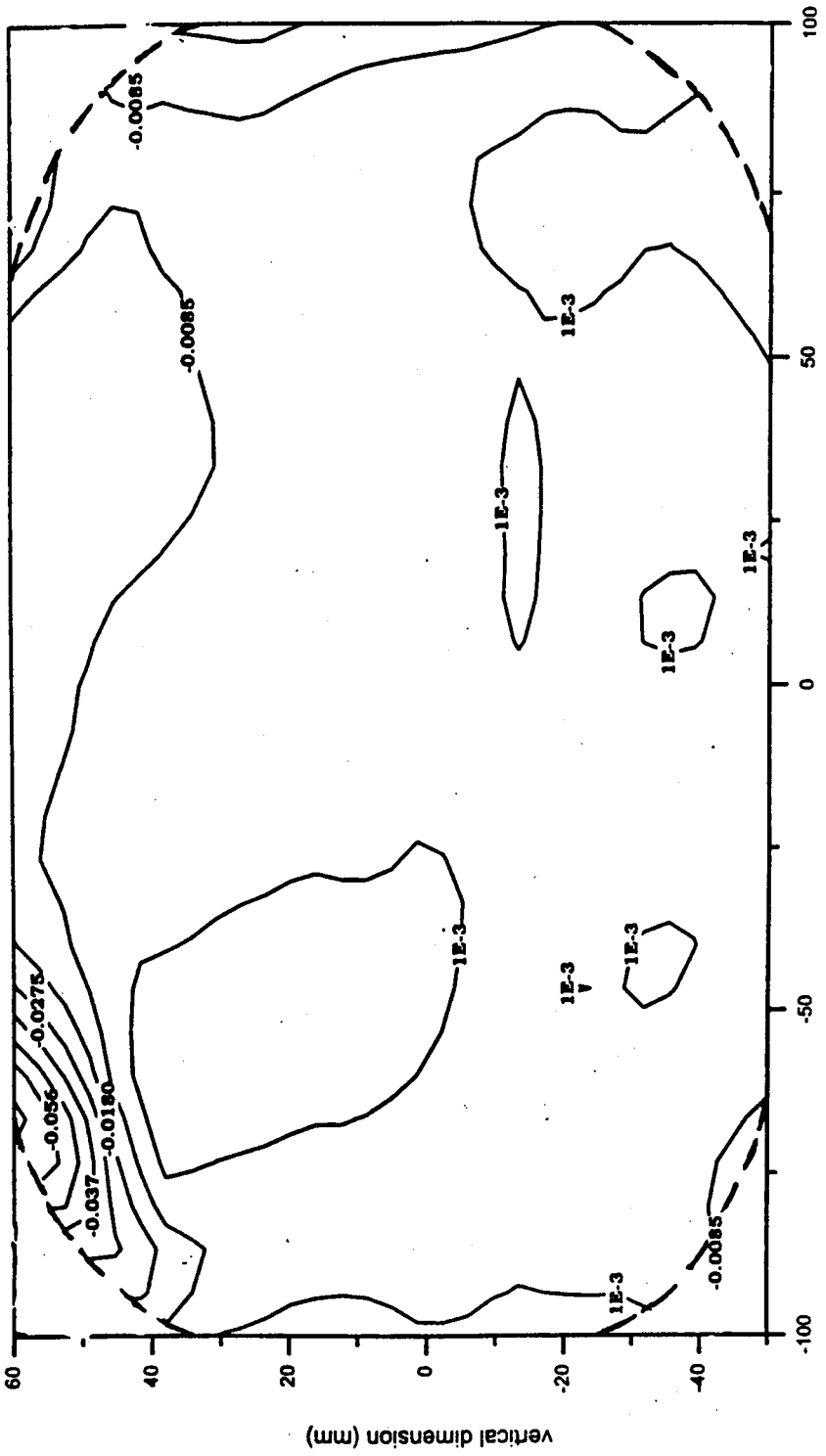
-0.0085
-0.0085
-0.0275
-0.056
-0.037
-0.0180
1E-3
1E-3
1E-3
1E-3
1E-3
1E-3
1E-3
-0.0085
60
40
20
0
-20
-40
-100
-50
0
50
100
vertical dimension (mm)
horizontal dimension (mm)

(c) γ_{xy} (%)

References

[1] J. Magiera. J. Orkisz. "Experimental-numerical analysis of 3D residual stress state in railroad rails by means of oblique slicing technique". Proc. of SPIE Conference :Interferometry '94", Warsaw 1994.

[2] C.H. Cundiff, R.C. Rice, "Comparative evaluation of several alternative methods for measuring rail residual stress", Residual Stresses in Rails; Effects on Rail Integrity and Railroad Economics, O. Orringer et al., Vol. I, pp. 121-142, Klawer Acad. Publ., Dordrecht, Boston, London 1992.

[3] Czarnek R., J. Lee, S.Y. Lin, "Moire interferometry and its potential for application to residual stresses measurement in rails", Residual Stress in Rails, vol.I, 153-167, Klawer Acad. Publ., 1992.

[4] Salbut L., M. Kujawinska, J. Kapkowski, "Automatic analysis of residual stresses in rails in the modified Moire interferometry system", Proc. SPIE 2004, 1993.

[5] Robert E. Rowlands, "Residual Stresses", Handbook on Experimental Mechanics. A. S. Kobayashi ed., Society for Experimental Mechanics, Inc., Englewood Cliffs, 1987.

[6] D. Post, "Moire Interferometry", Handbook on Experimental Mechanics, A. S. Kobayashi ed., Society for Experimental

Mechanics. Inc.. Englewood Cliffs. 1987.

[7] F.P. Chiang. "Moire methods of strain analysis". Chap. 6. Manual of Experimental Stress Analysis. 3rd ed.. A.S. Kobayashi. Ed.. Society for Experimental Stress Analysis, Bookfield Center. CT 1978.

[8] Y. Wang, and F.P. Chiang, "Experimental study of three dimensional residual stresses in rails by Moire interferometry and dissecting method", Wear, 1994.

[9] Y. Wang. X.F. Shen, and F.P. Chiang, "New experimental approach for studying residual stresses in rails", The 4th Inter. Conference on Contact Mechanics and Wear of Rail/Wheel systems, Vancouver, Canada, 1994.

[10] A. Kearney, and C. Forno, "High temperature resistant gratings for Moire interferometry", Experimental Techniques, 9-12,1993.

[11] M. Kujawinska, et al, "Automatic analysis of residual stresses in rails using grating interferometry", Personal communication.

[12] J.C. Middleton, personal communication, British, Steel, Swindon Laboratories, Rotherham, 1993.

[13] Y. Wang, X.F. Shen, and F.P. Chiang, "The effect of cutting on redistribution of residual stresses in rails", submitted to Experimental Techniques. 1995.

[14] U. S. Department of Transportation.

[15] J1818 photoresist, made by Shipley Co..

[16] Developer 351, made by Shipley Co..